The development of a measuring technique for the UV-C distribution emitted from low pressure mercury lamps

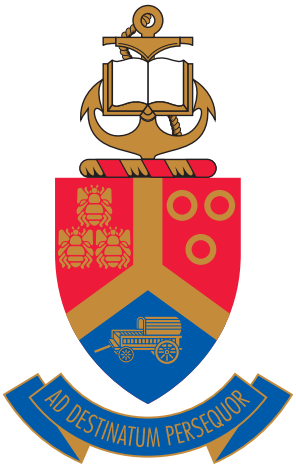

by

Mkabela Macdufe

Submitted in partial fulfilment of the requirements for the degree

Magister Scientiae

in the Department of Physics

in the Faculty of Natural and Agricultural Sciences

University of Pretoria

Pretoria

February 2019

Supervisor:	Prof. W.E. Meyer
Co-supervisors:	Mr. P.J.W. Du Toit
	Mr. R.H. Sieberhagen

Declaration of originality

1. I, Mkabela Macdufe, understand what plagiarism is and am aware of the University of Pretoria's policy in this regard.

2. I declare that this dissertation, which I hereby submit for the degree *Magister Scientiae* at the University of Pretoria, is my own original work and has not previously been submitted by me for a degree at this or any other tertiary institution. Where other people's work has been used (either from a printed source, Internet or any other source), this has been properly acknowledged and referenced in accordance with departmental requirements.

3. I have not used work previously produced by another student or any other person to hand in as my own.

4. I have not allowed, and will not allow, anyone to copy my work with the intention of passing it off as his or her own work.

Signature: .....
Mkabela Macdufe
Student number: 16394403

Date: February 2019

Acknowledgements

I am grateful to all those with whom I have had the pleasure to work with during this project. Special mentions goes to my supervisor Prof WE Meyer, co-supervisors Mr PJW du Toit and Mr R Sieberhagen and the rest of the staff in the Photometry and Radiometry department at National Metrology Institute of South Africa (NMISA). Each of the members of my supervisors has provided me professional guidance and taught me a great deal about scientific research.

Financial support

This work is based upon research supported by NMISA. Any opinion, findings and conclusions or recommendations expressed in this material are those of the author(s) and therefore the NMISA does not accept any liability in regard thereto.

Abstract

The development of a measuring technique for the UV-C distribution emitted from low pressure mercury lamps

by

Mkabela Macdufe

Supervisor:	Prof. W.E. Meyer
Co-supervisor:	Mr. P.J.W. Du Toit
	Mr. R.H. Sieberhagen
Degree:	*Magister Scientiae*
Keywords:	Calibration, measurement uncertainty, ultraviolet (UV), ultraviolet-C (UV-C), UV germicidal irradiation, radiometry, spectral irradiance, signal-to-noise ratio, relative uncertainty, uncertainty budget

The measurement of spectral irradiance in the ultraviolet (UV) region of the electromagnetic spectrum has higher uncertainties largely due to a low signal-to-noise ratio (SNR). UV-C radiation emitted by low pressure (LP) mercury (Hg) lamps is very important in a wide range of applications including disinfection of air and surfaces of microorganisms. This study investigates some measurement aspects to be considered when calibrating LP Hg lamps. The aim is to characterise the spectroradiometer system and improve measurement techniques for calibrating this lamp for use as a source standard for disseminating the unit of spectral irradiance in the UV-C spectral region.

The research question is answered through an experiment that includes a direct measurement of a LP Hg lamp against a deuterium (D_2) standard (STD) lamp. The measurements showed that the alignment of the LP Hg lamp should be a primary concern as this aspect contributed 15 % to the combined uncertainty. Ambient temperature changes are known to influence some components used in

the measurement of spectral irradiance. In this regard, the study indicated that the LP Hg lamp may be operated at lower temperatures to achieve maximum light output. The lamp has a calculated temperature coefficient of $-2{,}5 \pm 0{,}01$ %/°C at an ambient temperature of 21,3 °C. During measurements, a short-term drift of a measurand can be an obstacle to lamp spectral irradiance calibration. The cause is frequently heat build-up and temperature changes in the components of a spectroradiometer. The spectroradiometer had a higher measured short-term drift of 5 % when irradiated with a LP Hg lamp compared to 1 % when irradiated with a D_2 STD lamp. Apart from a higher measured drift, the lamp's light output was more stable over time when monitored with UV enhanced silicon (Si) detectors: 1,6 % for a LP Hg lamp and 0,11 % for a D_2 STD lamp.

The LP Hg lamp had a calibrated total UV irradiance of 1,12 W/m^2 from 230 nm to 400 nm wavelengths. The expanded uncertainty was 8 % which is lower than 11 % uncertainty that the National Metrology Institute of South Africa (NMISA) is accredited for. This showed that even though the spectroradiometer system had a higher measured short-term drift when irradiated with a LP Hg lamp, the lamps can be used as a source standard for calibrating clients' instruments. Further research must be conducted to identify and characterise other measurement aspects that could have significant uncertainty contributions.

Contents

List of figures xi

List of tables xv

1 Introduction 1

1.1 Background 1

1.2 Definition of metrology 2

1.2.1 Categories of metrology 2

1.2.2 The metre convention 4

1.2.3 Basic traceability chain 4

1.3 Research problem 6

1.3.1 Objectives 6

1.4 Overview of the dissertation 7

1.4.1 Chapter 1 7

1.4.2 Chapter 2 7

1.4.3 Chapter 3 7

1.4.4 Chapter 4 7

1.4.5 Chapter 5 7
1.4.6 Chapter 6 8
1.4.7 Chapter 7 8
1.4.8 Chapter 8 8

2 Light and electromagnetic radiation 9

2.1 Behaviour of light 10
2.1.1 Reflection 11
2.1.2 Refraction 11
2.1.3 Diffraction 12
2.1.4 Transmission 12
2.1.5 Absorption 12

3 Radiometry 13

3.1 Radiometric background 13
3.1.1 Terminology and units 15
3.2 Basic principles of radiometry 20
3.2.1 Inverse square law 20
3.2.2 Point source approximation 20
3.2.3 Lambertian surfaces 21
3.2.4 Lambert's cosine law 22
3.3 Source based radiometry 22
3.4 Interpolated spectral data 23
3.4.1 Cubic spline interpolation 23

4 Instrumentation **25**

4.1 Spectral irradiance lamps 25

4.1.1 FEL tungsten lamp standards 25

4.1.2 Deuterium lamp standards 28

4.1.3 Argon mini-arcs 30

4.1.4 Low pressure mercury lamps 31

4.1.5 Wavelength standard source 32

4.2 Monochromator system 34

4.2.1 Input optics 34

4.2.2 Double grating monochromator 35

4.3 Detectors 40

4.3.1 Photomultiplier tubes 41

5 Traceability of UV-C spectral irradiance measurements **44**

5.1 Introduction 44

5.2 Traceability chain 46

5.3 Key comparisons 47

5.3.1 CCPR k1-a 47

5.3.2 CCPR k1-b 48

6 Spectral irradiance calibration **50**

6.1 Introduction 50

6.2 Measurement setup 50

6.3 Characterisation 54

6.3.1 Noise characterisation 54
6.3.2 Wavelength calibration 56
6.3.3 Alignment of spectral irradiance lamps 61
6.3.4 Inverse square law approximation 65
6.3.5 Short term drift 68
6.3.6 Spectroradiometer temperature dependence 70
6.4 Calibration 80
6.4.1 Pre-calibration procedure 80
6.4.2 Calibration procedure and measurements 80

7 Uncertainty budget **87**
7.1 Introduction 87
7.1.1 Description of uncertainties 87
7.1.2 Types of uncertainties and distributions 87
7.1.3 Standard uncertainty 88
7.1.4 Sensitivity coefficients 88
7.1.5 Uncertainty contribution 88
7.1.6 Combined standard uncertainty 89
7.1.7 Expanded uncertainty 89
7.2 Wavelength calibration uncertainty budget (UB) 89
7.2.1 Measurement model 89
7.2.2 Uncertainty estimates 90
7.2.3 Sensitivity coefficients 90

7.2.4 Uncertainty contributor, combined and expanded uncertainties 93

7.3 Uncertainty analysis for spectral irradiance 95

7.3.1 Measurement model 95

7.3.2 Sources of uncertainties 95

7.3.3 Calculating sensitivity coefficients 96

7.3.4 Combined and expanded uncertainty 97

8 Conclusion **101**

A List of acronyms **A–1**

B Calibration certificates of standards lamps **B–3**

C Publications **C–9**

Published in The Proceedings of the South African Institute of Physics Conference 2017 pages 204 to 209 - Characterization of the spectral irradiance lamps at NMISA C–10

Accepted for publication in Test and Measurement Conference 2018 - Characterization of a spectroradiometer system for ambient temperature dependence C–16

References **R–1**

List of Figures

1.1 The organizations and their relationships associated with the Meter Convention [Czichos [2011]]. 3

1.2 The traceability chain for measurements [Czichos [2011]]. 5

2.1 Reflection and refraction of light. 11

3.1 A typical configuration of radiometric measurement system [Grum and Becherer [1979]]. 14

3.2 A figure illustrating how irradiance on a surface element is measured per unit area dA of that element [Duda [1983]]. 16

3.3 The radiance L from the incident flux ϕ measured on an element of surface area dA at an angle θ [Duda [1983]]. 17

3.4 The solid angle at the center of the sphere is the surface area enclosed in the base of the cone divided by the square of the sphere radius [Zalewski [1995]]. 18

3.5 The inverse square law of point sources emitting irradiance E at a distance d from the surface of area dA at an angle θ [Ashdown and Eng [2002]]. 19

3.6 A diagram illustrating the diffuse reflectance of a Lambartian surface [Ryer [1997]]. 21

4.1 The setup for realizing the current of the quartz tungsten halogen (QTH) lamp using the calibrated 0,1 Ω ballast resistor. Digital voltmeter (DVM) 1 measured the input electrical lamp voltage and DVM 2 measures the current passing through the standard resistor [Walker *et al.* [1987]. 27

4.2 The deuterium lamp electrical input power connection [Kostkowski [1997]]. 29

4.3 Diffraction by a plane grating. The sign convention for the angles α and β is shown by the + and – signs on either side of the grating normal [Palmer and Loewen [2005]]. 36

5.1 The traceability chain at NMISA of the spectral irradiance unit traceable to the high temperature blackbody (HTBB) at Physikalisch-Technische Bundesanstalt (PTB). 46

6.1 The measurement setup for disseminating the spectral irradiance unit in a source based radiometry at NMISA. 51

6.2 The background signal levels measured at 800 V, 1000 V and 1200 V photo multiplier tube (PMT) supply voltages with the monochromator set to 8 nm bandwidth. The signal was measured as voltage from the PMT detector. The QTH standard lamp was used to illuminate the monochromator, with the baffle closest to the lamp covered. 56

6.3 The light signal levels measured at 1000 V PMT supply voltage with 2 nm, 4 nm and 8 nm monochromator bandwidth. The monochromator was illuminated with the QTH standard lamp. 57

6.4 The wavelength stepper positions $\bar{y}$ plotted as a function of wavelength in air λ_{air} (Table 6.3). The linear fit equation was $y = 599,5\lambda_{air} - 151888,6$ with the coefficient of determination $R^2 = 0,99$. The markers were the λ_{air} stepper positions. This linear equation was used as the monochromator reference equation. 60

6.5 The output of the Hg pencil discharge lamp monitored with a UV enhanced silicon detector. 61

6.6 The measured $S(\lambda)$ of the spectroradiometer when illuminated with the QTH STD lamp due to a change in angular position of the lamp around vertical axis. The measurements were performed at wavelengths of 450,5 nm and 441,5 nm. 63

6.7 The measured spectral output voltage of the spectroradiometer when illuminated with the LP Hg lamp at 255 nm wavelength from different lamp orientations around its vertical axis. 64

6.8 The measured spectral output voltage of the spectroradiometer when illuminated with the D_2 STD lamp due to a change in orientation around its vertical axis. The measurements were performed at 255 nm and 350 nm wavelengths. 64

6.9 Investigating the applicability of the point source approximation of the QTH standard lamp using the measured spectral output voltages at different distances. The measurements were performed at 450,5 nm and 441,5 nm wavelengths. The markers are measured results and the line is the model. 67

6.10 The spectral output voltage signal measured at different distances to approximation a point source of the LP Hg lamp. The measurements were performed at 255 nm wavelength. 67

6.11 The point source approximation of the D_2 spectral irradiance STD lamp was performed at 255 nm and 350 nm wavelengths. 68

6.12 The spectroradiometer measured $S(\lambda)$ short term drift when irradiated with a QTH lamp measured over 30 minutes. 69

6.13 The spectroradiometer measured $S(\lambda)$ short term drift when irradiated with a D_2 lamp measured over 40 minutes. 69

6.14 The meassured spectroradiometer $S(\lambda)$ short term drift when irradiated with a LP Hg lamp measured over a period of 20 minutes. 70

6.15 The apparent spectral irradiance $E(\lambda)$ measurement system. The setup makes use of a lamp substitution method and was used to investigate the measurement system's and the lamp's dependence on temperature. All the equipment was isolated from the air flow of the room air-conditioner. 72

6.16 The PT100 probes mounted on the surface of the PMT detector to measure its temperature. 73

6.17 The measurement system dark spectral output voltage $S(\lambda)$ dependence on temperature measured at 1000 V PMT supply voltage and 8 nm monochromator bandwidth. The measurements were performed from low to high temperatures. 75

6.18 Dependence of the measured $S(\lambda)$ from the LP Hg UV-C lamp on the temperature T. The observed decreasing linear dependence of $S(\lambda)$ on T had the straight line function $S(\lambda) = -1{,}5$ mV/°C·$T+$ 99,9 mV, where T is measured in °C. 75

6.19 The light output of the LP Hg lamp measured as current dependence on ambient temperature. The light output was measured with a UV-E Si detector after the lamp had warmed-up for 120 minutes. The linear model was I=-0,259 (μA/°C)$\times T$+16 μA with $R^2 = 0,99$. T was measured in °C. 76

6.20 The stability of the LP Hg UV-C lamp measured at 23 °C room temperature for three consecutive days, five hours per day with the UV-E Si detector. 77

6.21 The temperature dependence of the measurement system when corrected for the temperature dependence of the LP Hg lamp. . . . 77

6.22 The spectroradiometer measured $S(\lambda)$ dependence on temperature when illuminated with a QTH lamp. The monochromator wavelength was set at 280 nm to achieve maximum $S(\lambda)$. 78

6.23 The calculated SNR of the QTH lamp at both signal levels. 79

6.24 The D_2 STD lamp spectral irradiance values were verified against the values of the QTH standard lamp. QTH ref indicates the reference spectral irradiance values of the QTH lamp. D2 ref and D2 clac indicates the reference and calculated spectral irradiance values of the D_2 lamp. 81

6.25 The calculated spectral irradiances of the LP Hg lamp calibrated against the responsivity determined with the D_2 STD lamp. The reference spectral irradiances of the QTH and deuterium standard lamps are also plotted. 82

6.26 The stability of the QTH STD lamp measured with the UV-E Si detector during the period t of the standard verification. The relative uncertainty was 0,13 %. 83

6.27 The light output of the D_2 STD lamp measured with the UV-E Si detector during the period t of the calibration. The calculated relative uncertainty was 0,11 %. 84

6.28 The light output of the LP Hg lamp monitored with the UV-E Si for 30 minutes. The calculated relative uncertainty was 1,6 %. 84

6.29 The repeatability of the D_2 STD lamp and LP Hg lamp. The repeatability was expressed as a percentage of the relative standard deviation of the mean (relative standard deviation of the mean (RSDM)) as a function of wavelength. 86

Appendix B The calibration certificate of the deuterium standard lamp calibrated at PTB. B–4

Appendix B The calibration certificate of the QTH lamp calibrated at Gigahertz Optik GMBH. B–7

List of Tables

2.1 The harmful effects of UV radiation on human beings and their applications. 10

3.1 The inverse square law point source approximation 21

5.1 The mean uncertainties for NPL in the Consultative Committee of Photometry and Radiometry (CCPR) k1-a key comparison for measured irradiance when compared to CENAM [Woolliams *et al.* [2006]]. E_{NPL} was the spectral irradiance measured by National Physical Laboratory (NPL). 48

5.2 The averaged key comparison reference value (KCRV) uncertainties $u(E_{KCRV})$ for the CCPR k1-b comparison piloted by the PTB national metrology institute (NMI) are given below [Sperfeld [2008a]]. 49

6.1 The QTH lamp calculated signal-to-background ratio (SBR) and SNR values at a PMT supply voltage of 1000 V and a monochromator bandwidth of 8 nm. 57

6.2 The mercury lines for wavelength calibration. 59

6.3 The monochromator's wavelength calibration results. The acronyms and symbols used are as follows: λ_{air} is the wavelength in ambient air calculated using Equation 6.9, $y1$, $y2$ and $y3$, are the stepper positions corresponding to the wavelength peaks measured from set 1, 2 and 3 respectively, $\bar{y}$ is the average of the stepper positions $y1$, $y2$ and $y3$. experimental standard deviation (ESD) is the standard deviation of the three sets, and experimental standard deviation of the mean (ESDM) is the experimental standard deviation of the mean calculated by dividing the ESD with the square root number of sets measured (n=3). $\bar{y} - \bar{y_0}$ is the shifted stepper motor positions calculated by subtracting the initial stepper motor value at the 253,6665 nm Hg line from $\bar{y}$. 59

6.4 The verification of the wavelength calibration measured results. The headings of the measured and calculated data are: λ_{air} is the ambient air wavelength calculated using NMISA ambient conditions (Table 6.2), λ_{set1}, λ_{set2}, and λ_{set3} are wavelengths of mercury lines measured in set 1, set 2 and set 3. $\bar{\lambda_{ver}}$ was the average of three sets, and the difference was calculated by subtracting $\bar{\lambda_{ver}}$ from λ_{air}. 62

6.5 The $\Delta S(\lambda)/\Delta d$ calculated as a percentage change for all lamps. The wavelengths are indicated on the table headings. 62

6.6 The change in measured $S(\lambda)$ calculated as a percentage due to changing the orientation of the lamps. 65

6.7 The temperature readings measured at different settings of the room air-conditioner, with the PT100#1 and #2 probes positioned as shown in Figure 6.16 and PT100#3 probe placed next to the monochromator. 74

6.8 The temperature coefficients of the measurement system (MS) plus LP Hg lamp and measurement system only determined for ambient temperatures. The associated measurement uncertainty (MU) of the temperature coefficients were 1,2 % calculated using Equation 6.15. 79

6.9 The literature PMT temperature coefficients. 79

6.10 The relative uncertainties of the pencil, D_2, QTH and LP Hg lamps in terms of stability when monitored with the UV-E Si detector. . . . 83

6.11 The signal, current, and voltage short term stability of the deuterium spectral irradiance standard lamp. The headings in this table are defined as follows: Set 1 and 2 are the two measurements of the D_2 lamp, $\bar{x}$ was the average of Set 1 and 2, ESDM was the experimental standard deviation of the mean calculated by dividing the square root of the sum of squares of the standard deviations of light and dark measurements (before and after for the lamp signal) by the total number of measurements n (current n=9868, voltage n=9869, and signal n=539) and percentage uncertainties were calculated as a fraction of the ESDM to $\bar{x}$. . . . 85

6.12 The percentage difference between the experimental and theoretical electrical current and voltage input to the D_2 spectral irradiance STD lamp. 85

6.13 The change in measured ambient temperature and humidity recorded throughout the calibration. $\bar{x}$ was the average of a total number of measurements (n=114), σ was the standard deviation for n=114, ESDM and uncertainties were defined in Table 6.11. . . 85

7.1 The change in refractive indexes of air after changing ambient parameters (temperature, pressure, and humidity) with the uncertainties of the P&R laboratory. n_{air} was the refractive index of air calculated using the nominal P&R ambient conditions, Δn_T, Δn_p and $\Delta n_{\%RH}$ were the changes in refractive index of air caused by a change in temperature, pressure and relative humidity. The ambient temperature was changed by $\pm$2 °C, pressure $\pm$ 11,5 mmHg (1,75 %) and relative humidity was changed by $\pm$15 %RH. 91

7.2 The calculated ambient air wavelengths using Equation 6.9 and the refractive index in Table 7.1. 91

7.3 The values of the sensitivity coefficients calculated from Equations 7.12, 7.13 and 7.14. 93

7.4 The monochromator wavelength calibration uncertainty contributors. 94

7.5 The sensitivity coefficients for translation and orientation relative uncertainties (Table 6.5 and 6.6). 97

7.6 The uncertainty contributors from the deuterium STD and the LP Hg lamps. 98

7.7 Uncertainty contributors of the equipment used during calibration. . 99

7.8 The spectral irradiance total uncertainty calculated for a level of confidence of 95,45 %. 100

Chapter 1

Introduction

1.1 Background

The focus of this study is on the calibration and characterisation of lamps emitting UV radiation. UV radiation is of importance in air and surface disinfection applications. The International Commission on Illumination (CIE) [CIE [2003]] divides the UV region into four bands: vacuum UV (100 nm - 200 nm), UV-C (200 nm - 280 nm), UV-B (280 nm - 315 nm) and UV-A (315 nm - 400 nm). UV radiation below 320 nm is actinic, i.e. it causes photo chemical reactions. The UV lamp studied was the LP Hg lamp emitting UV-C radiation. The application of these lamps to air and surface disinfection is known as ultraviolet germicidal irradiation (UVGI) [Kowalski [2010]].

UVGI is electromagnetic radiation that can destroy the ability of microorganisms to reproduce by causing photo chemical changes in nucleic acids. Wavelengths in the UV-C spectral region are damaging to cells because they are absorbed by nucleic acids. The germicidal effectiveness of UV-C peaks at wavelengths of about 260 nm to 265 nm, which is very close to the UV-C Hg peak of 254 nm and corresponds to the peak UV absorption bacterial deoxyribonucleic acids (DNA). The UV-C germicidal effectiveness may vary between species [Webb and Tuveson [1982]].

This study is limited to the measurements of LP Hg lamps used for air disinfection of airborne diseases (reasons are given in Chapter 2). The LP Hg lamp was characterised for some uncertainties and calibrated to determine its suitability as a transfer standard of spectral irradiance unit. The traceability route for this unit

is given in Chapter 5.1.

1.2 Definition of metrology

Metrology is defined as the science and practice of measurements. Metrology has many applications and is vital in meeting the needs of the economy, society and citizens with the aim to provide measurements that are comparable, stable and coherent [Milton [2014]]. [BIPM and OIML [2008]] defined the following terms which will be used frequently in this research:

- Measurand - the quantity intended to be measured.
- Measurement uncertainty - a non-negative parameter characterizing the dispersion of the quantity values being attributed to a measurand, based on the information used.
- Measurement standard - realization of the definition of a given quantity, with stated quantity value, and associated measurement uncertainty, used as a reference.
- Calibration - is an operation that, under specified conditions, in a first step, establishes a relation between the quantity values with measurement uncertainties provided by measurement standards and corresponding indicators with associated measurement uncertainties and, in a second step, uses this information to establish a relation for obtaining a measurement result from an indication.
- Uncertainty budget - statement of a measurement uncertainty, of the components of that measurement uncertainty, and of their calculation and combination.

1.2.1 Categories of metrology

There are different categories of metrology separated by different levels of complexity and accuracy [Czichos [2011]]. This research was based in scientific metrology, which involves the calibration, measurements and organization and development of measurement standards.

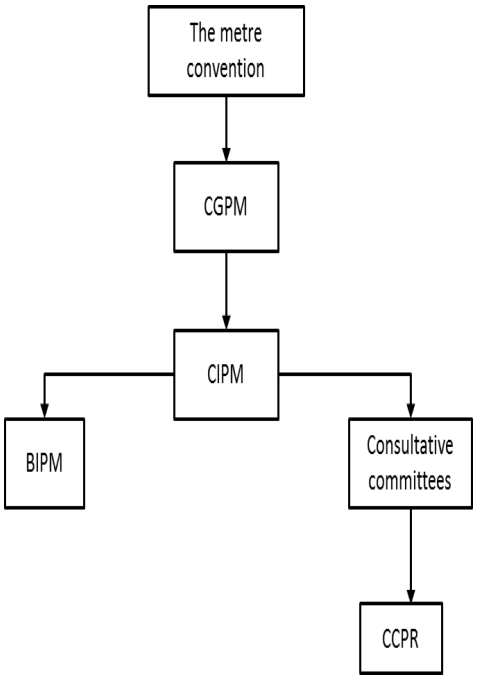

Figure 1.1: The organizations and their relationships associated with the Meter Convention [Czichos [2011]].

1.2.2 The metre convention

The Metre Convention was established in 1875 by 17 member states [Howarth *et al.* [2008]]. The Metre Convention remains the basis of all international agreements on units of measurements (Figure 1.1). The General Conference on Weights and Measures (CGPM) is the committee with representatives from the Metre Convention and meets every four years to approves and updates the International System of Units (SI) with results from fundamental research.

CGPM appoints up to 18 representatives from its structures to the International Committee for Weights and Measures (CIPM) which is supported by the consultative committee (CC) and the International Bureau of Weights and Measures (BIPM). The CIPM meets annually to undertake preparatory work for technical decisions to be made by the CGPM. The CIPM is supported by 10 consultative committees, and the consultative committee of concern for this study is the (CCPR).

To ensure the international equivalence of measurement standards and to provide for the mutual recognition of calibration and issuing of certificates from national metrology institutes (NMIs), the CIPM has signed a mutual recognition agreement (MRA) in 1999 in support of world trade. The international equivalence of measurement standards is performed through measurements called the intercomparisons by NMIs.

1.2.3 Basic traceability chain

The BIPM as an intergovernmental organization acts together on matters related to measurement science and measurement standards. The mission of the BIPM is to ensure and promote the global comparability of measures, provide consistent international system of units for:

- Scientific discovery and innovation,
- industrial manufacturing and international trade and
- sustaining the quality of life and global environment.

The importance of metrology is achieved through traceable measurements which is the property of a measurement result whereby the result can be related to a reference through a documented unbroken chain of calibrations, each

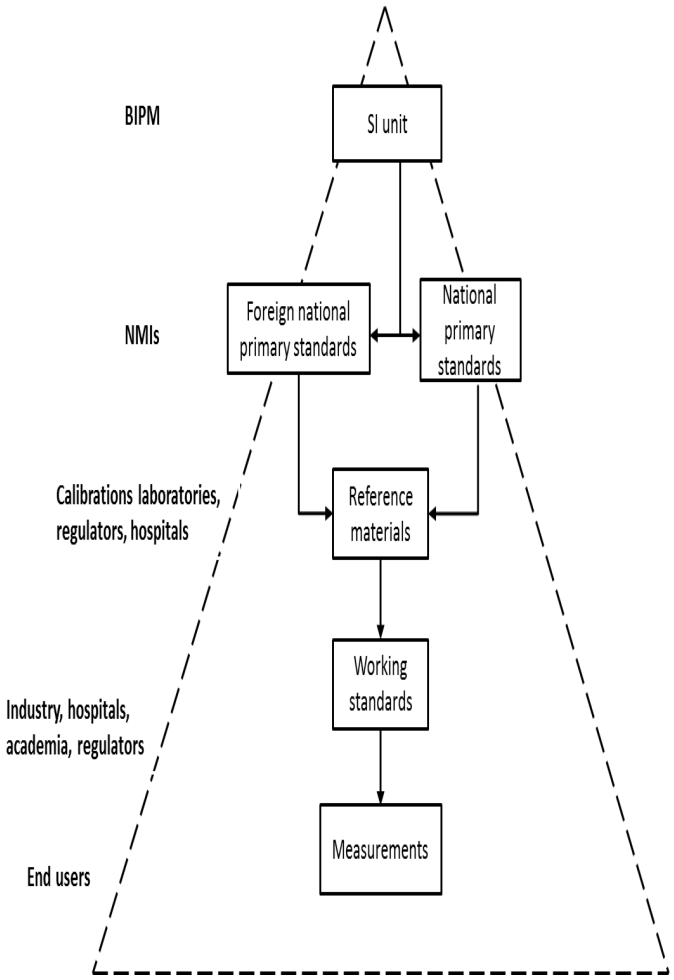

Figure 1.2: The traceability chain for measurements [Czichos [2011]].

contributing to the measurement uncertainty [BIPM and OIML [2008]]. The basic traceability chain in metrology is illustrated in Figure 1.2. The NMIs under the supervision of the BIPM, maintains and disseminates the units of measures to calibration laboratories, hospitals, industries etc. through an unbroken chain of measurements. As can be seen, the uncertainties in measurements indicated by the broken line increases down the traceability chain.

1.3 Research problem

The measurement of spectral irradiance in the UV spectral region is very important for industrial, research, economic and safety purposes. This research develops and investigates the measurements required for the calibration of LP Hg lamps used as spectral irradiance transfer standard for calibrating clients' UV-C detectors and lamps at NMISA. UV-C radiation is known to be germicidal as it disrupts bond DNA in most microorganisms. As a result, the UV-C radiation emitted by LP Hg lamps has been utilized to reduce contamination in hospitals, the pharmaceutical industry, water treatment plants, fresh food products etc. of these microorganisms. It is therefore important that LP Hg lamps be characterised to ensure that they achieve the required germicidal effect.

South Africa is one of the countries in the world with the highest burden of tuberculosis (TB) with the world health organisation (WHO) stating that 0,8 % of the population develops active TB each year. The use of UV-C radiation in air at hospitals' waiting areas can help combat the spread of TB in South Africa. This technology is known as air UVGI. Because exposure to UV-C radiation has harmful effects, there's a need to develop measurement procedures for calibration of germicidal lamps and detectors. This project focused on the characterisation of the measurement system for measuring UV-C spectral irradiance lamps.

1.3.1 Objectives

The aim of this research is to accurately measure and calibrate a LP Hg lamp with the objectives to:

- Investigate spectral irradiance standard lamps that can be used to calibrate LP Hg lamps.
- Characterise practical aspects to be considered when calibrating LP Hg lamps. These practical aspects will be included in the uncertainty budget.

- Verify if a LP Hg lamp is a suitable spectral irradiance transfer standard, through its stability, measurement system short-term drift, repeatability and reproducibility conditions.

1.4 Overview of the dissertation

This section gives a brief overview of each chapter.

1.4.1 Chapter 1

Gives a brief background of the study. It introduces the reader to the concept of metrology followed by the research question, aims and objectives of study.

1.4.2 Chapter 2

This chapter contains a brief summary of electromagnetic radiation (EMR) and the behaviour of light.

1.4.3 Chapter 3

Introduces the concept of light measurement and explains terminology used in radiometry and the basic principles of radiometry that are relevant to this study.

1.4.4 Chapter 4

This chapter describes the components used in spectroradiometry. Only instruments that were used in this project are described: spectral irradiance lamps, monochromator with the integrating sphere (IS) and the PMT detector.

1.4.5 Chapter 5

Chapter 5 gives a detailed description of the traceability route of the UV-C spectral irradiance in source-based radiometry.

1.4.6 Chapter 6

This chapter describes the measurement setup used and its characterisation. Follows hereafter, the calibration procedure is discussed followed by the measurement results.

1.4.7 Chapter 7

Chapter 7 gives the uncertainty budget of the wavelength and spectral irradiance lamp calibration. The calculations and derivation of sensitivity coefficients are shown.

1.4.8 Chapter 8

The dissertation ends with the conclusion of the research questions.

Chapter 2

Light and electromagnetic radiation

Light is EMR or radiant energy within a portion of the electromagnetic spectrum. EMR moves through space as a wave, and can be described by its frequency, that is, the number of whole waves (or cycles) that pass by a point in some amount of time. Visible light is one form of EMR, other forms include radio waves, microwaves, infrared, visible and UV light to x-rays and gamma rays. All the different kinds of electromagnetic radiation differ in their wavelength, and when they are spread out according to their wavelength, the result is an electromagnetic spectrum. Our eyes respond to visible light but detecting the rest of the spectrum requires scientific instruments.

Wavelength and frequency are related by:

$$\lambda = c \times \nu, \tag{2.1}$$

where λ is wavelength of light and ν is a corresponding frequency, and c is the speed of light (2,99$\times$10^{8} m·s^{-1}). The Watt (W), is the rate of energy transfer of one joule (J) per second, the fundamental unit of optical power. Optical power is a function of both wavelength and a number of photons, where each photon carriers an energy that is described by Planck's equation:

$$\begin{aligned} E &= h \times \nu \\ &= h \times \frac{c}{\lambda}, \end{aligned} \tag{2.2}$$

where E is the energy of a photon when light interacts with particles; h is Plank's constant (6,623$\times$10^{-34} Js), ν, c and λ were defined in Equation 2.1. Equation 2.2 states that light with shorter wavelength or higher frequency (UV light) has high

Table 2.1: The harmful effects of UV radiation on human beings and their applications.

Band	Wavelength [nm]	Effects	Applications
UV-A	315-400	Premature aging of skin	Pest control
UV-B	280-315	Erythema	Medical applications
UV-C	200-280	Photokeratitis conjunctivitis	Disinfection of air

energy compared to light with longer wavelength or lower frequency (infrared light).

UV radiation covers a small part of the electromagnetic spectrum with wavelengths shorter than visible light, ranging from 100 nm to 400 nm. UV spectral region can be divided into four regions based on the wavelength's biological effects on microorganisms. The CIE divides the UV spectral region into four sub regions: vacuum ultraviolet (VUV) (100 nm – 200 nm), UV-C region (200 nm – 280 nm), UV-B (280 nm – 315 nm) and UV-A (315 nm – 400 nm) [CIE [2003]]. The focus of this study is on the measurement UV-C radiation emitted by lamps studied in this dissertation.

UV-C radiation is important because of its germicidal effectiveness on microorganisms in air and other media. The use of germicidal radiation can help combat the spread of TB in South Africa, mainly at hospitals' waiting areas and treatment rooms where this technology is usually employed. This technology is referred to as the air UVGI [CDC [1994], Harm [1980]], and accurate measurement of UV-C radiation emitted by UVGI lamps is very important for the safety of staff and patients. Over exposure to UV radiation has harmful effects, and the effects are summarized in Table 2.1.

2.1 Behaviour of light

When light encounters a surface, it can either be reflected away from the surface or refracted through the surface to the material beneath [Taylor *et al.* [2000]]. Once in the material, the light can be transmitted, absorbed, or diffused (or some combination) by the material. Each of these properties is discussed in this section.

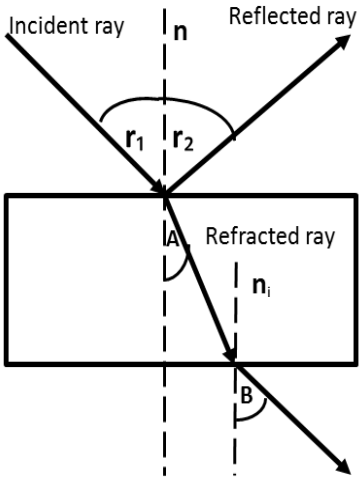

Figure 2.1: Reflection and refraction of light.

2.1.1 Reflection

Light reflection is a change in direction of light when it bounces on a surface or barrier. Light can either be reflected off a mirror (specular) or diffused surface. When light is reflected off a mirror surface, it obeys the law of reflection, which states that: the angle of incidence (r_1) is equal to the angle of reflectance (r_2) resulting in the formation of an image shown in Figure 2.1, where **n** is the surface normal. When light obey the law of refraction it is termed specular reflection. Light is only reflected equally in all directions for a perfect diffuse surface.

2.1.2 Refraction

When light passes through two different media of different materials, the light rays bend and change velocity slightly [Ryer [1997]], an effect referred to as refraction. In the case where light passes from a medium where it travels slower into a medium where it travels faster, a light ray will bend away from the normal and bend in the opposite direction when moving from a medium where it travels faster into a medium where it travels slower. The mathematical description of refraction (which is dependent on the incident angle, and refractive index n of a material) is given by Snell's law:

$$n \sin r_1 = n_i \sin A \tag{2.3}$$

where n and n_i are refractive indexes of two media, r_1 is an incident angle, and *A* is a refracted angle from Figure 2.1.

2.1.3 Diffraction

Diffraction is an effect where light spreads when passing through a slit or by the edge of a narrow aperture approximated by:

$$\theta = \frac{\lambda}{D}, \tag{2.4}$$

where θ is a diffraction angle, λ is a wavelength of light, and *D* is an aperture diameter. This effect is exploited in monochromators using diffraction gratings (explained in detail in Subsection 4.2.2).

2.1.4 Transmission

Transmission of a surface material is its effectiveness to transmit the proportion of the incident light through a material which can be transparent (or semi-transparent). The transmission of a material depends on its thickness, and the type of light (visible, ultraviolet, radio waves etc.) passing through a material.

2.1.5 Absorption

Instead of completely transmitting light, an object can absorb part or all of the incident light, usually by converting it into heat. Many materials absorb some wavelengths while transmitting others, a phenomenon called selective absorption. Lambert's law of absorption states that equal thicknesses of a given homogeneous material absorb the same fraction of light, and is given by the relationship;

$$I = I_o e^{-\alpha a}, \tag{2.5}$$

where I is the intensity of the transmitted light sample, I_o is intensity of light entering the material, α the absorption coefficient in inverse units (cm^{-1}) and a the thickness of the sample measured in the same units for thickness as α.

Chapter 3

Radiometry

3.1 Radiometric background

The science and technology of measuring light across the entire electromagnetic spectrum is known as radiometry [Grum and Becherer [1979]]. In practice the term is limited to measurements in the ultraviolet, the visible and the infrared spectral regions, the region known as optical radiation [Parr [2001]]. In the optical region of the spectrum and with the apertures typically used in optical systems, the diffraction angle is small. For this reason it is frequently possible to use geometrical optics to estimate the path taken by the radiant energy Q and neglect diffraction effects. Measurements of radiant energy are conducted using methods which are suited to the spectral region of interest. The objective of this chapter is to introduce the components and describe the principles, terminology and units used in radiometry [Palmer and Carroll [1999], Duda [1983]].

The components of radiometric measurement system are described in detail in Chapter 4. A basic radiometric measurement system (shown in Figure 3.1) includes a source of radiant energy (lamp), a transmission medium through which radiant energy passes, an optical system (which transmits, reflects, or absorbs radiant flux), a detector (which converts radiant energy into another form of energy), and a signal processing device. A spectroradiometer is the measurement system which consists of an optical system, a detector and a signal processing device [Kostkowski [1997]]. The transmission medium for all the measurements performed in this project was free space and the optical system was the monochromator consisting of an integrating sphere (IS), mirrors, apertures and gratings.

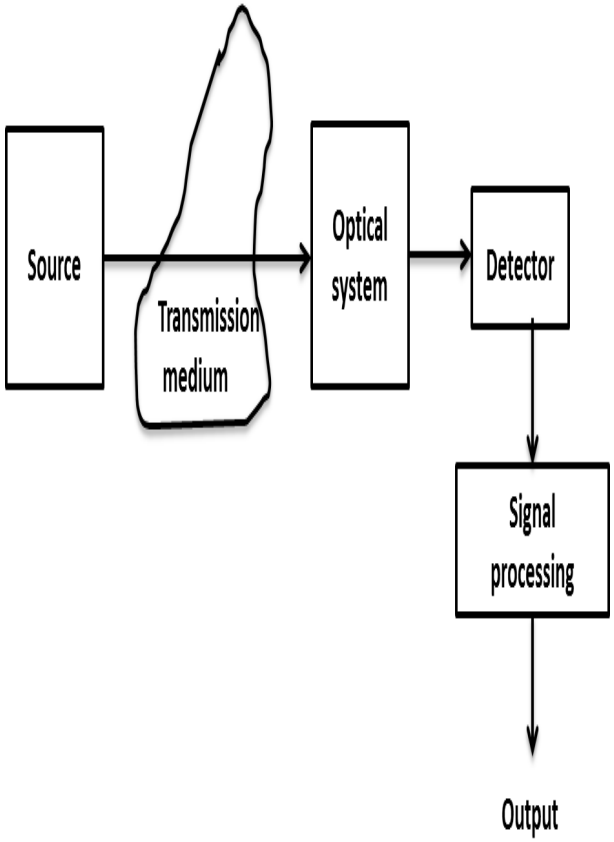

Figure 3.1: A typical configuration of radiometric measurement system [Grum and Becherer [1979]].

3.1.1 Terminology and units

There are different terms and symbols pertaining to optical radiation quantities in radiometry and the results are mostly expressed in units of power (watt), but can also be expressed in units of energy (joule). Radiometric quantities are sometimes measured along the spectrum as a function of wavelength λ or frequency ν, depending on whether the spectrum is taken as a function of wavelength or frequency. These radiometric quantities are referred to as spectral radiometric quantities designated by λ or ν or in brackets.

Radiant energy and power (flux)

Radiant energy is energy that is received, transferred, or emitted in the form of electromagnetic radiation. The measurement unit for radiant energy is joule (J) with the recommended radiometric symbol Q. Spectral radiant energy is energy per unit wavelength λ given by

$$Q_\lambda = \frac{dQ}{d\lambda}, \tag{3.1}$$

where Q_λ is spectral energy measured in joule per nanometer (J/nm), $dQ/d\lambda$ is differential in radiant energy (Q) per unit wavelength (λ).

Radiant power or flux is defined as energy per unit time emitted, transferred, or received in the form of electromagnetic radiation. The symbol for radiant flux is Φ and it is measured in watts (W) and the measurement equation is given by

$$\Phi = \frac{dQ}{dt}, \tag{3.2}$$

where Φ is the flux emitted, transferred, or received, $\frac{dQ}{dt}$ is the time derivative of radiant energy. Spectral radiant flux (Φ_λ) is flux per unit wavelength defined by

$$\begin{aligned} \Phi_\lambda &= \frac{d^2Q}{dtd\lambda} \\ &= \frac{d\Phi}{d\lambda}, \end{aligned} \tag{3.3}$$

d^2Q is the second order differential in energy with respect to differentials in time (dt) and unit wavelegth ($d\lambda$).

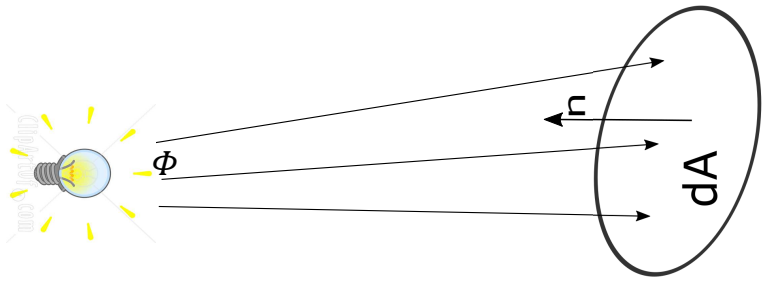

Figure 3.2: A figure illustrating how irradiance on a surface element is measured per unit area dA of that element [Duda [1983]].

It is always possible to convert from one spectral quantity to the other (wavelength to frequency and vice versa). From Equation 3.3, $\Phi_\lambda d\lambda$ is the flux in the wavelength interval λ to $\lambda + d\lambda$, and we can convert from wavelength to frequency as:

$$\begin{aligned}\Phi_\lambda &= \frac{d\Phi}{d\lambda} \times \frac{d\nu}{d\nu} \\ &= \frac{d\Phi}{d\nu} \times \frac{d\nu}{d\lambda} \\ &= \Phi_\nu \times \frac{d\nu}{d\lambda} \\ d\lambda\Phi_\lambda &= d\nu\Phi_\nu\end{aligned} \tag{3.4}$$

Spectral versions of other radiometric quantities are defined similarly as in Equation 3.4.

Irradiance

Irradiance is the quantity that is generally measured in radiometry. Irradiance is the flux emitted by a source incident on an element of a surface area per unit area of that element (Figure 3.2). Irradiance has the symbol E measured in watts per unit area (W.m^{-2}) and given by:

$$E = \frac{d\Phi}{dA}. \tag{3.5}$$

Φ is the incident flux emitted by the source of radiant energy incident on a surface at any direction, dA is the differential unit area of the element surface. Spectral

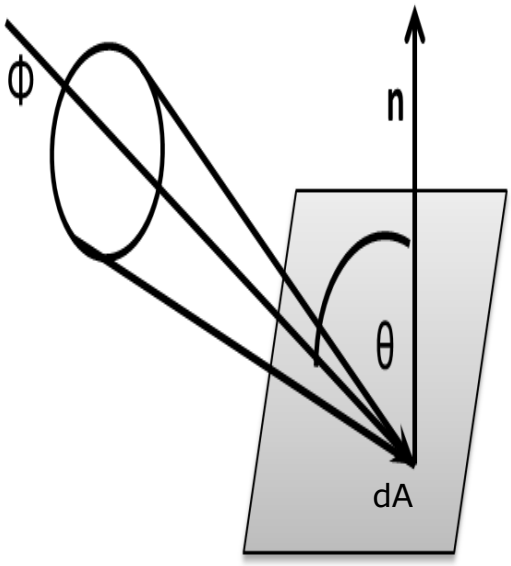

Figure 3.3: The radiance L from the incident flux ϕ measured on an element of surface area dA at an angle θ [Duda [1983]].

irradiance is irradiance measured per unit wavelength defined by

$$E_\lambda = \frac{d^2\Phi}{dAd\lambda}. \tag{3.6}$$

E_λ is the spectral irradiance, $d^2\Phi$ is the second order differential of radiant flux, $d\lambda$ is the width of the wavelength range detected by the monochromator.

Radiance

Radiance is the flux contained in an infinitesimal ray, and it can be leaving or arriving at an element of surface area at an angle θ, to the elements of both the projected area dA and the solid angle $d\Omega$ as shown in Figure 3.3. Radiance is assigned the letter L and measured in watt per steradian per meter squared (W.m^{-2}.Sr^{-1}). The measurement equation for radiance is given by:

$$L = \frac{d^2\Phi}{dAd\Omega} \tag{3.7}$$

where L is radiance. Spectral radiance is the ratio of flux projected at a surface area at an angle normal to the surface, to the elements of the projected area, the

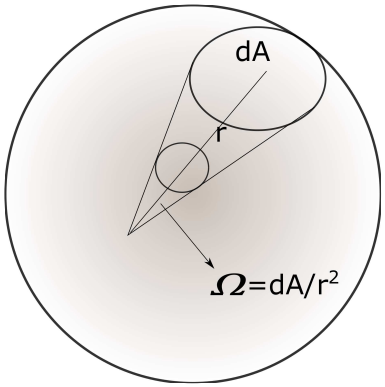

Figure 3.4: The solid angle at the center of the sphere is the surface area enclosed in the base of the cone divided by the square of the sphere radius [Zalewski [1995]].

solid angle and the unit of wavelength .The spectral radiance is given by:

$$L_\lambda = \frac{d^3\Phi}{dAd\Omega d\lambda} \tag{3.8}$$

where L_λ is spectral radiance, $d\lambda$ is the width of the wavelength detected by the monochromator and dA and $d\Omega$ were defined in Equation 3.7.

Solid angle

Solid angle is defined as the part of the area on the sphere divided by the square of the sphere radius as shown in Figure 3.4. The symbol of the solid angle is Ω and measured in steradian (Sr). Solid angle is given by the equation:

$$d\Omega = \frac{dA}{r^2}. \tag{3.9}$$

$d\Omega$ is the solid angle at the center of the sphere, dA is the portion of the area on the sphere, and r is the radius of the sphere.

Radiant intensity

Radiant intensity (or simply intensity) is the ratio of radiant flux emitted by a point source to an element of the solid angle $d\Omega$ in a given direction. The assigned symbol for intensity is I and is measured in watts per steradian (W.Sr^{-1}).

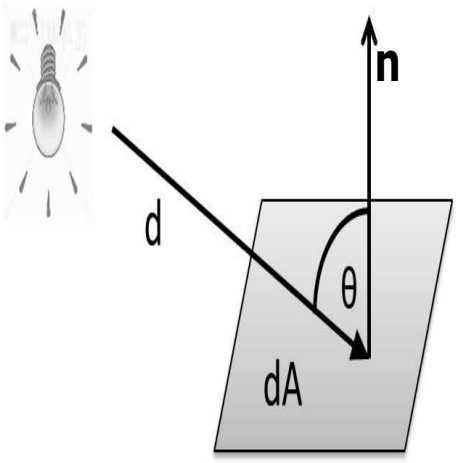

Figure 3.5: The inverse square law of point sources emitting irradiance E at a distance d from the surface of area dA at an angle θ [Ashdown and Eng [2002]].

$$I = \frac{d\Phi}{d\Omega}, \tag{3.10}$$

where $d\Phi$ is the flux emitted by a source, and $d\Omega$ is the differential solid angle propagated in a given direction.

Both irradiance and radiance are defined for an infinitesimal area and solid angles. However, in practice, measurements are performed with finite area detectors and optics with finite field of view. Therefore, when the terms defined above are applied to actual measurements it is assumed that averages are being discussed.

3.2 Basic principles of radiometry

3.2.1 Inverse square law

The inverse square law can be derived from the definition of both the solid angle and irradiance (Equations 3.9 and 3.5) as:

$$\begin{aligned} E &= \frac{d\Phi}{dA} \\ &= \frac{d\Phi}{d^2 d\Omega} \quad (d\Omega = \frac{dA}{d^2}, r = d) \\ &= \frac{I}{d^2}, \end{aligned} \tag{3.11}$$

where dA is the surface area centred on a sphere surface and at a distance d from the light source, and E is the irradiance incident on a surface. Generally, the flux emitted from the source will intercept dA at an angle θ (Figure 3.5) [Ashdown and Eng [2002]]. The inverse square law of point sources is then defined as:

$$E = \frac{I \cos\theta}{d^2} \tag{3.12}$$

3.2.2 Point source approximation

The inverse square law should only be used in cases where the light source approximates a point source. This is achieved by using the "five times rule" for irradiance measurements. The "five times rule" states that: the distance from the detector to a light source must be at least five times greater than the largest dimension of the light source [Ryer [1997]]. Table 3.1 shows the ratios of lamp distance to lamp radius [Ryer [1997]]. A lamp is a point source if the ratio of distance d to the lamp and the largest dimension r of the lamp falls between 10 and 100, with the inverse square law error of less than one percent. When this ratio is below 0,1, the change in distance hardly affects irradiance, and we have an area source. In this case, as the distance from the source decreases, the detector sees less area counteracting the inverse square law, hence no effect generated on irradiance.

Table 3.1: The inverse square law point source approximation

Ratio (d/r)	**Inverse square law approximation**	**Type of lamp**
10 - 100	inverse square law holds	Point source
0,1 - 10	does not hold	Circular source
0,01 - 0,1	does not hold	Area source

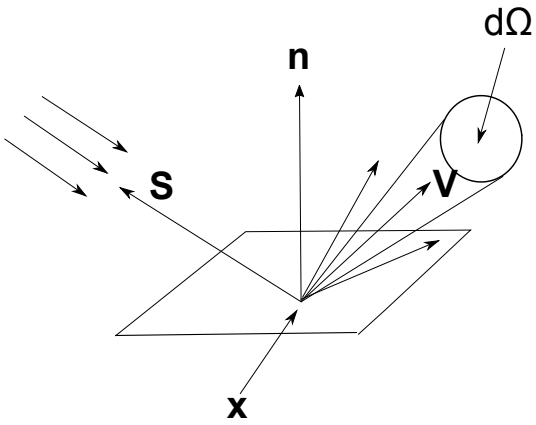

Figure 3.6: A diagram illustrating the diffuse reflectance of a Lambartian surface [Ryer [1997]].

3.2.3 Lambertian surfaces

A surface that exhibits a Lambertian reflectance, reflects light incident on the surface equally in all directions irrespective of the angle of incidence (Figure 3.6). A Lambertian surface is a diffuse or an isotropic surface and its radiance is not dependent on the viewing angle. The reflection on the Lambertian surface is calculated by taking the dot product of the surface normal vector, **n**, and a light direction vector, **S**, pointing from the surface to the light source.

$$\mathbf{S} \cdot \mathbf{n} =\mid S \mid\mid N \mid \cos\alpha, \tag{3.13}$$

where α is the angle between the directions of the two vectors.

The irradiance on the surface with respect to surface normal **n** is given by

$$E(\lambda, \mathbf{x}, \mathbf{n}) = \mathbf{S} \cdot \mathbf{n} E(\lambda, \mathbf{x}, \mathbf{S}), \tag{3.14}$$

where $E(\lambda, \mathbf{x}, \mathbf{n})$ is irradiance on a surface as a function of wavelength λ, with respect to surface position **x** and the surface normal **n**, and $E(\lambda, \mathbf{x}, \mathbf{S})$ is irradiance as a function of light direction **S** pointing from a surface to the light source. The radiance due to a diffuse reflecting surface is

$$L(\lambda, \mathbf{x}, \mathbf{V}) = r(\lambda)\mathbf{n} \cdot \mathbf{S}E(\lambda, \mathbf{x}, \mathbf{S}), \tag{3.15}$$

which is independent of the viewing direction **V**. $r(\lambda)$ is the ratio of radiance to irradiance.

3.2.4 Lambert's cosine law

The irradiance E falling on any surface varies as the cosine of the incident angle, θ, between the observer's line of sight and the surface normal as E_θ. The perceived measurement area perpendicular to the incident flux is reduced at oblique angles, causing light to spread out over a wider area than it would if perpendicular to the measurement plane. The Lambert's cosine law is given as

$$E_\theta = E \cos\theta. \tag{3.16}$$

3.3 Source based radiometry

The quantity to be measured is the spectral irradiance through a source to source calibration. Source-based radiometry relates to the measurement of radiometric quantities traced back to standardized light sources or radiation sources. Calibration of radiation sources is done through a comparison with the respective primary standard using wavelength-dispersive transfer systems as radiation components. This is the case because spectral distributions of sources to be compared are not monochromatic. The realization of spectral irradiance is calibrated traceable through an uninterrupted traceability chain (Chapter 5) to the source primary standard, a high temperature black body radiator. A common secondary standard for this unit in the UV spectral region is the deuterium lamp standard for wavelengths below 270 nm and the quartz tungsten halogen lamp standard lamp for wavelengths above 270 nm.

3.4 Interpolated spectral data

Radiometric calibrations of spectral irradiance are often made for a limited number of wavelengths from the UV to the infrared spectral region. It is both time-consuming and expensive to cover all wavelengths at which reference measurements may be required. NMIs apply interpolation to cover the complete range that may be required to calibrate spectral irradiance lamp transfer standards. Interpolated values are correlated to original data and nearby interpolated points through dependence on the common input set. Interpolation of spectral data to transfer standards and clients' instruments itself adds uncertainties that are random.

3.4.1 Cubic spline interpolation

Cubic spline interpolation is one commonly used interpolation method for interpolating spectral data [Gardner [2003]]. This interpolation method can interpolate data on four different functions: the linear, cubic, Bessel and OneWay splines. Only the first two are discussed. Given the function $y_j = y(x_j)$, where $j = 1, ..., N$, if we focus attention on one interval between x_j and x_{j+1} the linear interpolation in that interval is

$$y = Ay_j + By_{j+1}, \tag{3.17}$$

where $A = \frac{x_{j+1}-x}{x_{j+1}-x_j}$ and $B = 1 - A = \frac{x-x_j}{x_{j+1}-x_j}$. Equation 3.17 has zero second order derivative in the interior of each interval and undefined second derivative at the abscissas x_j. The cubic spline interpolation aims to get an interpolation formula that is smooth in the first derivative and continuous in the second derivative, both within an interval and its boundaries.

If the second derivative is y'' which is a set of numbers y''_j, then the cubic polynomial whose second derivative varies linearly from a value y''_j on the left to a value y''_{j+1} on the right can be added on the right side of Equation 3.17 as

$$y = Ay_j + By_{j+1} + Cy''_j + Dy''_{j+1}. \tag{3.18}$$

$C = \frac{1}{6}(A^3 - A)(x_{j+1} + x_j)^2$ and $D = \frac{1}{6}(B^3 - B)(x_{j+1} - x_j)^2$. Since y_j'' are not known, the relation between them is given by (for $j = 2, ..., N - 1$)

$$\frac{x_j - x_{j-1}}{6} y_{j-1}'' + \frac{x_{j+1} - x_{j-1}}{3} y_j'' + \frac{x_{j+1} - x_j}{6} y_{j+1}'' = \frac{y_{j+1} - y_j}{x_{j+1} - x_j} - \frac{y_j - y_{j-1}}{x_j - x_{j-1}}, \tag{3.19}$$

which is a system of $N - 2$ linear equations in the N unknowns y_j'', $j = 1, ...N$. The natural cubic splines sets $y_j'' = y_N'' = 0$, which has a zero second order derivative on one or both of its boundaries. The program spline is called only once to process an entire tabulated function in arrays x_j and y_j.

Chapter 4

Instrumentation

This chapter describes the three main components of a radiometric measurement system (Figure 3.1): spectral irradiance lamps, a monochromator system and a detector.

4.1 Spectral irradiance lamps

4.1.1 FEL tungsten lamp standards

The modified type FEL 1000 W tungsten lamps is the most commonly used transfer standard (STD) for spectral irradiance in the wavelength region of 250 nm to 2500 nm. This STD is traceable to the HTBB radiator which employs the Plank's radiation law and a temperature measurement based on the international temperature scale [Walker *et al.* [1987]]. They are commonly employed as transfer STD for spectral irradiance due to their good stability and ease of use [CIE [1984]]. To check the form of unknown errors and the worldwide consistency of these standards, the NMIs perform international inter-comparisons of frequently used standards. International inter comparisons allow the NMIs to compare their uncertainties and validate their measurement methods.

The FEL 1000 W tungsten standard lamp commonly referred to as the quartz tungsten halogen (QTH) STD lamp has an overall length of 7,5 cm. The lamp filament is 1,5 cm long with a diameter of 0,375 cm [Kostkowski [1997]. The standard is a commercially available 1000 watt consisting of a clear quartz envelope and a coiled-coil filament structure. The coiled-coil filament structure allows the filament to evaporate at the same rate that a tungsten cylinder would evapor-

ate if the cylinder had the same diameter of the coiled-coil. The QTH STD lamp is filled by a halogen which produces a halogen cycle inside the lamp. In the halogen cycle, halogen gas combines with the tungsten that evaporates from the lamp filament, eventually re-depositing the tungsten on the filament instead of allowing it to accumulate on the bulb wall. This ensures that:

- The lamps have a longer life (2000 - 3500 hours).
- The bulb wall remains cleaner, because the evaporated tungsten is constantly redeposited on the filament by the halogen cycle. This allows the lamp to maintain radiant flux output throughout its life.
- The higher operating temperature of the filament improves luminous efficacy.
- The bulbs are more compact, offering opportunities for better optical control.

Halogen lamps are sometimes called “quartz” lamps because their higher temperature requires quartz envelopes instead of the softer glass. Therefore, the filament can run hotter resulting in a more efficient light source, while reducing evaporation so that the filament will last longer than a straight filament at the same temperature. The lamp filament is fixed to a bi-post base which allowed the lamp to be adjusted to the required height. The QTH STD lamp was operated at a current of roughly 8 amperes direct current (DC), and about 113 volts is required from the DC power supply to realise this current. The uncertainty in current measurements should be less than 0,05 % for it not to greatly affect the uncertainty of the measurements, and this corresponds roughly to 0,25 % in uncertainty of spectral irradiance at 600 nm [Kostkowski [1997]].

The setup for measuring the current in QTH STD lamp is shown in Figure 4.1. The lamp is operated in a vertical position with horizontal beam direction and the base at the bottom. The optical axis of a spectroradiometer is in a horizontal position. To align the lamp, a translational stage motions in three perpendicular directions (optical axis, horizontal axis perpendicular to optical axis, and a vertical axis) and an alignment jig mounted in front of the lamp are used.

The QTH lamp is calibrated at a specified distance from the front surface of the lamp holder to the monochromator entrance aperture. This distance is realised

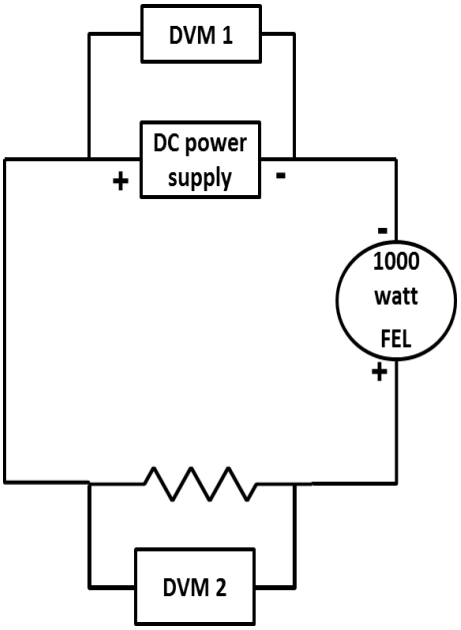

Figure 4.1: The setup for realizing the current of the QTH lamp using the calibrated 0,1 Ω ballast resistor. DVM 1 measured the input electrical lamp voltage and DVM 2 measures the current passing through the standard resistor [Walker *et al.* [1987].

with a calibrated steel rod cut to the required distance. The lamp must be operated in the same conditions as when it was calibrated, since any departure from the alignment and orientation may introduce some uncertainties and normally QTH lamps present a few difficulties in this regard. The tolerance based on the accuracy of mounting the lamp should be provided by stating what percentage uncertainty would be introduced by slightly deviating from the ideal set-up. Radiation reflected from the envelope can contribute some percentage to irradiance produced by a tungsten lamp, therefore, baffles should not hide any part of the envelope, unless the lamp was calibrated under such a condition.

The position of nearby apparatus should be stated, since the performance of some tungsten lamps can be affected by external air convection currents [CIE [1984]]. Standard lamps must be turned on and off by slowly (2 A/min) increasing and decreasing the current using the knobs on the power supply to prevent thermal shock due to brief over-voltage or mechanical shock. Since 0,1 % change in current is bound to cause a change in irradiance, the voltage across the standard resistor should be measured with a digital voltmeter.

4.1.2 Deuterium lamp standards

A deuterium lamp system (DLS) is a discharge lamp that makes use of stable arc discharge of deuterium (D_2) gas [Sperfeld [2008b], Sperfeld *et al.* [2003]]. The D_2 lamp is the most convenient spectral irradiance standard to use for the wavelength range 200 nm to 250 nm [Klose *et al.* [1987], Saunders *et al.* [1978]]. The lamp is used as a source in a wide range of available instruments including spectrometers and chromatographs and has a continuous spectrum from 200 nm to 400 nm.

There are different types of D_2 lamps based on the intended applications. Figure 4.2 shows a D_2 lamp when viewed from the top. Most of these lamps differ in the material and position of the window, size and shape, arc apertures and anode materials. There are two types of windows materials: a UV glass and a quartz glass. UV glass has a lower limit of transmittance at 190 nm wavelength and quartz glass has a lower limit of transmittance at 160 nm wavelength. In applications that require high intensity at lower wavelengths quartz has the best transmission but undergoes solarisation when exposed to UV light which is not a problem with UV glass.

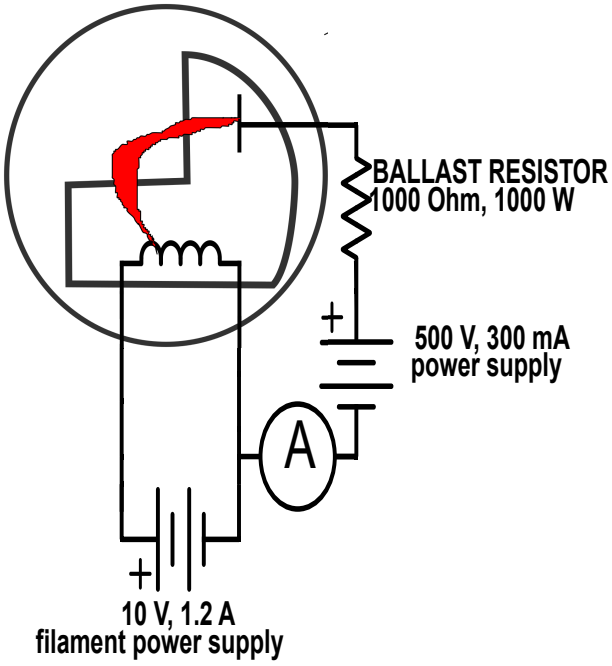

Figure 4.2: The deuterium lamp electrical input power connection [Kostkowski [1997]].

To start the lamp, the cathode is first heated for 5 seconds by a DC filament power supply (10 V at 0,8 A) to provide some free electrons which makes it easy to initiate the discharge. The voltage of approximately 400 V is applied to the lamp, an arc discharge forms between the anode and cathode. Most of the UV light is generated at the narrowing aperture located in front of the anode. A DC power supply of 500 V, 300 mA with 0,1 % of current regulation is required to operate the lamp. A 1 kΩ, 1000 W ballast resistor is used in the anode circuit because most power supplies cannot react fast enough to maintain constant arc. After the arc is started, the voltage drops to 100 V, at this point the heater current is switched off, and the lamp output stabilizes in 20 minutes or less. After the lamp is switched off it should be allowed to cool down to room temperature before restarted.

D_2 lamps are calibrated at a current of 300 mA. There is usually a 100 V drop across the lamp so that the lamp's electrical power dissipation is 30 W, which is lower than 1000 W required for the QTH STD lamp. The maximum spectral power of a D_2 lamp is at 200 nm with a favourable ratio of UV to visible radiant power. The disadvantages of a D_2 lamp is that it is limited to wavelengths above 165 nm due to the presence of many line molecular band system below 165 nm.

Another disadvantage is the wavelength dependent ageing of the lamp with an interdependence to spectral irradiance reduction of 0,1 % per hour of operation time. D_2 lamp also has a poor reproducibility between different arc ignitions.

4.1.3 Argon mini-arcs

Argon mini-arc is one spectral irradiance standard that covers the wavelengths below 165 nm. The argon mini-arc has a known spectral irradiance calibrated in the wavelength region of 140 nm to 335 nm [Klose *et al.* [1987], Bridges and Ott [1977]]. The expanded uncertainty of the argon-mini arc based on National Institute of Standards and Technology (NIST) measurements is 10 % for wavelengths below 200 nm and 5 % above 200 nm. The lamp has an arc reproducibility of 1 % and a drift rate comparable to D_2 lamp (0,1 % per hour at 250 nm), especially when the window is not used. [Klose *et al.* [1987]] has observed drift rate ten times greater than this, hence it is recommended to experimentally check the drift rate of the standard to be used.

The argon mini-arc is derived from the black body and hydrogen-arc in a way similar to D_2 STD lamp. Argon mini-arc should be used below 250 nm only when it is inconvenient to compare the D_2 lamp to a QTH lamp above 250 nm at each lighting. The argon mini-arc has a shorter wavelength limit of 140 nm than 165 nm of the D_2 lamp. The lamp consists of a group of water cooled copper discs separated by silicon rubber insulating gaskets. The electrodes are made of thoriated tungsten, and there is a magnesium fluoride (MgF_2) removable window.

The argon mini-arc can be operated without a window since window transmittance can change one to two percent in few hours of use due to UV radiation damage or tungsten deposits. The argon mini-arc has a number of disadvantages: it is not a shelf item, it is complex to use, it requires water cooling and 99,998 % pure argon, it requires 1200 watts power supply, and frequent shaping of the cathode electrode. Signal instability indicates the need for reshaping. NMISA does not have the argon-mini arc spectral irradiance lamp standard for reasons mentioned above, hence it won't be used for measurements and will not be discussed any further.

4.1.4 Low pressure mercury lamps

UV lamps produce different spectral bands of germicidal UV, due to different sizes and shapes. There are different types of UV lamps currently in use for air disinfection applications. They include, LP UV lamps that produce narrow band of UV-C wavelengths, medium pressure (MP) UV lamps which produce broad-band UV-B/UV-C wavelengths and light-emitting diodes (LEDs) [Kowalski [2010]]. Nearly all UV lamps generate radiation by means of a gas discharge. The lamps are produced with lengths varying between a few centimetres and four meters. They have irradiance levels between 0,1 W/cm and 400 W/cm, spectral emission from the deep vacuum UV (VUV) up to the long wave UV-A and radiant efficiencies between a few percent up to 60 %. Radiant efficiency is the ratio of radiant output power to electrical input power. UV discharge lamps have lifetimes of about few hundred hours up to many thousands hours, depending on the lamp used.

LP Hg vapour lamps have the highest UV radiant efficiency in air. They contain Hg gas at pressure of about 10 torr or less and emit UV light in a narrow band of wavelengths centered around 253,7 nm when this gas is stimulated by electrical charge. LP Hg lamps radiate 95 % of their energy around this wavelength which is close to the peak of germicidal effectiveness around 260 nm to 265 nm. They are generally used in disinfection of microorganisms in air and surfaces and are similar in operation to fluorescent lamps which are also LP Hg discharge lamps. LP UV lamps consist of an envelope made of quartz glass or other UV- transmitting glass, a pair of electrodes and a Hg amalgam. Ballasts provide the required starting voltage and the proper lamp current.

The electric current that passes between the electrodes heats up the Hg vapour which stimulates electronic transitions and causes emission of UV and visible light. In fluorescent lamps, the glass is coated on the inside with phosphors which absorb UV and re-emit the energy as visible light. With UV lamps, there are no phosphors and the glass is transparent to UV wavelengths. In LP lamps about 60 % of the electrical input power is converted to light of which about 85 % occurs near the 253,7 nm Hg line. They also emit lower levels of radiation at wavelengths of about 185 nm, 312 nm, 365 nm and at higher wavelengths.

4.1.5 Wavelength standard source

All spectroradiometers are calibrated for wavelength. The calibration must be performed the same day the spectral irradiance measurements are performed. Atomic emission spectral lines are used as wavelength standards for calibrating a spectroradiometer [Schwarzmaier *et al.* [2013], Meggers *et al.* [1961]], from the VUV to about 400 nm. There are five factors to consider when selecting the emission line wavelength standards: a spectral line, width of the line, irradiance of the line, wavelength separation between lines and number and distribution of lines in the wavelength range being calibrated. In spectroradiometry, the uncertainty of a spectral line is sometimes smaller than required. Uncertainty of 0,1 nm is enough and it is rare though possible that wavelengths disagree by more than 0,01 nm [Zaidel' *et al.* [1970]]. Therefore, the accuracy of wavelength standard is not a problem in spectroradiometry.

The wavelength of the spectral line is dependent on the pressure, electron density and temperature within the source. However, it is possible to control the dependency to less than 0,001 nm when these parameters are controlled [Giacchetti *et al.* [1970]] and therefore the recommended lamps for optimum spectroradiometric wavelength standard should operate at low pressure (0,5 mmHg), low electric current (12 mA) and at controlled temperature inside the lamp. The width of the spectral line should be much narrower than the width of the spectral slit. The observed line is then the slit scattering function z and with monochromator in good optical alignment, z will be a symmetric function. Narrow spectral lines are obtained from the low pressure, low electron density sources recommended for low wavelength uncertainties. The width of the lines are less than 0,01 nm [Kostkowski [1997]] to a few nanometers for spectral slit width used in spectroradiometry.

The irradiance of the spectral line should be large enough to get the wavelength calibration precision required. When the spectral line is hardly visible above the signal noise, the wavelength calibration will have an imprecision of about the spectral slit width $\Delta\lambda_e$.

$$\Delta\lambda_e = \int_{CR} \frac{R(\lambda_0\lambda).d\lambda}{R(\lambda_0\lambda_0)}. \tag{4.1}$$

Equation 4.1 assumes that a $\Delta\lambda_e$ of a spectroradiometer is valid for a sufficiently narrow central wavelength region (CR) of flux responsivity $R(\lambda_0\lambda)$. $R(\lambda_0\lambda)$ is a function of two wavelengths; λ_0 is the wavelength setting of the spectrora-

diometer and λ is wavelength of an element of incident flux. $R(\lambda_0\lambda)$ reflects the fact that flux responsivity may have a different spectral shape and height $R(\lambda_0\lambda_0)$ for every λ_0.

In spectroradiometry, $\Delta\lambda_e$ is usually as large as 1 nm, but a wavelength imprecision still needs to be limited to 0,1 nm and sometimes to 0,01 nm or less. The SNR at the peak of the measured spectral line is addressed to understand the importance of spectral line irradiance in spectroradiometry wavelength calibrations. The wavelength of the peak of the line is used to determine the wavelength of an observed spectral line. Closer to the peak the observed line is almost flat, so a very small noise is required to determine the peak wavelength precisely. [Kostkowski [1997]] shows that

$$(N/S)_{linepeak} \cong 0,6\frac{\sigma(\lambda_{peak})}{\Delta\lambda_e}, \tag{4.2}$$

where $(N/S)_{linepeak}$ is the noise-to-signal ratio at the observed line peak, $\sigma(\lambda_{peak})$ is the standard deviation of the measured wavelength peak and $\Delta\lambda_e$ is the spectral slit width.

Wavelength separation from other lines is the fourth factor to consider when selecting an emission line as a wavelength standard. When one line is too close to the standard, depending on the relative irradiances of the lines, the two lines will blend into a single peak (or center wavelength) somewhere between the wavelength of the two lines. When the two lines have an equal irradiance, they are barely visible when their separation is $\Delta\lambda_e$. To identify a possible blending effect, [Kostkowski [1997]] recommends the wavelength calibration be performed with two or more spectral slit widths differing by a factor of two. For the wavelength calibration in Section 6.3.2, to avoid the blending effect, we avoided double and higher split Hg lines.

Pencil discharge lamp

The commonly used wavelength standard in spectroradiometry is a pencil sized, low pressure, cold cathode discharge lamp popular known as the pencil discharge lamp. The pencil discharge lamp is inexpensive, easy-to-use and available with filling of four different gases, three metals which provide good wavelength coverage in the UV and visible region. The lamp is made of double bore fused silica which makes it possible for both the electrodes and the lead

wires to be at one end of the lamp. The lamp is cool when lit with lamp temperatures rarely exceeding 100 °C. The lamp has a power of few watts and its moderate temperature and small size enables the lamp to be mounted close to an averaging sphere at entrance slit of monochromator.

Pencil discharge lamps are available with fillings of argon (Ar), krypton (Kr), neon (Ne), xenon (Xe), mercury (Hg), cadmium (Cd) and zinc (Zn) and, with some mixtures of these elements. A Hg pencil discharge lamp is the most frequently used wavelength standard between 250 nm and 440 nm. The strong emission line at 253,7 nm makes the Hg lamp useful and this line can be used to determine the slit scattering function at this wavelength.

The Hg pencil discharge lamp used for wavelength calibration (Section 6.3.2) has a filling of Hg and argon (Ar) and produces 90 % of its output in the line 253,7 nm with 18 mA power supply. The lamp is made of double-bore quartz tubing which allows both electrodes to be at one end, and is a low-pressure, and a cold cathode Hg UV lamp. The miniature size and light weight makes these lamps ideal for a wide variety of applications which includes monochromatic sources for optical systems, spectroscopic wavelength calibration, ozone production and many others. The peak emission at 253,7 nm has a lighted length of 54 mm which allows over-filling of monochromator slit or IS aperture and the lamp quartz diameter is 6,5 mm. The Hg pencil discharge lamp has a rated life 5000 hours.

UV radiation can burn skin and injure eyes, therefore it is important to wear protective clothing and shield when working with a Hg lamp.

4.2 Monochromator system

4.2.1 Input optics

In the measurement of irradiance, direct irradiation of the monochromator and the photo cathode of the detector (exit slit) by lamp's light output is avoided due to resultant variation in the irradiance distribution in the monochromator [CIE [1984]]. An integrating sphere (IS) or averaging sphere is used in the measurements of spectral irradiance placed before the entrance slit of the monochromator and is a spherical shell with an entrance and exit ports and coated internally with a reflective material of which the reflectance is spatially uniform and uniformly diffuse [Kostkowski [1997]] with the aim to combine radiant flux.

The entrance port of the IS is located on the sphere wall perpendicular to the monochromator axis. One advantage of an IS is that, the entrance port can be made the same area and shape as when the standard lamp was calibrated. To prevent light entering an IS to directly illuminate the area of the sphere wall that the monochromator views, baffles are mounted inside it. It should be noted that baffles will result in inaccuracies since the sphere is no longer a perfect sphere.

The IS is internally coated with a thick layer of polytetrafluorethylene (PTFE) powder. A high purity $BaSO_4$ coating can also be used but it has less reflectance than PTFE at certain wavelengths [Weidner and Hsia [1981]]. $BaSO_4$ has lower reflectance values than PTFE below 275 nm and above 1100 nm [Grum and Luckey [1968]]. Weak fluorescence was observed from PTFE coatings, while fluorescent excitation is below wavelengths of 290 nm, and fluorescent emission is between 310 nm and 350 nm [Weidner and Hsia [1981], Saunders and Ott [1976]].

One major disadvantage of an IS is high attenuation. Attenuation of the integrating sphere is proportional to its diameter and inversely proportional to the reflectance of the inner diffuse surface. To keep attenuation small, small IS with high reflectance for the inside coating are used.

4.2.2 Double grating monochromator

A monochromator is an optical element which consists of an entrance slit, a dispersive element, and an exit slit. A monochromator transmits a narrow band of light selected from a range of wavelengths available at the input. Monochromator can either be a single monochromator (have a single dispersive element, light diffracted once) or double monochromator (have two dispersive elements, light diffracted twice). Double monochromators are used for the purpose of achieving low stray light radiation compared to single monochromators. A dispersive element of the monochromator can either be a prism or a diffraction grating.

In a prism monochromator, the bandwidth is directly proportional to its wavelength, longer wavelengths results in wider bandwidths for a fixed slit setting. In a grating monochromator, to remove second or higher orders radiation filters may be employed however, this is not a problem with a prism monochromator [CIE [1984]]. Prism monochromators are rarely produced due to high cost

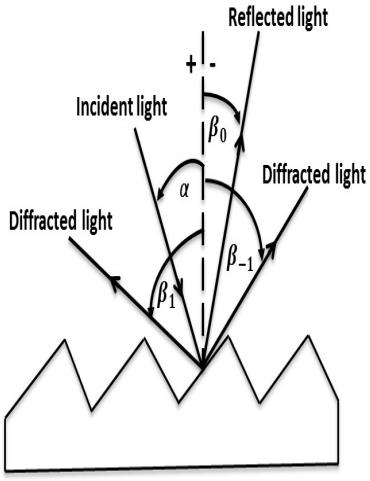

Figure 4.3: Diffraction by a plane grating. The sign convention for the angles α and β is shown by the + and – signs on either side of the grating normal [Palmer and Loewen [2005]].

and small angular dispersion [Kostkowski [1997]]. In this study, a double grating monochromator was used.

Diffraction Gratings

A diffraction grating is an optical element which splits and diffracts light into several beams travelling in different directions. The directions of these beams depends on the spacing of the grating and wavelength of the light so the grating can act as a dispersive element. Gratings usually have ridges on their surface rather than black lines, and such gratings can either be transmissive or reflective. A transmission grating has a grating superimposed on a transparent surface, while a reflection grating has a grating superimposed on a reflective surface. The fundamental principle of operating a grating is illustrated in Figure 4.3, which shows a reflective grating [Palmer and Loewen [2005]].

There are two types of diffraction that occurs: Fraunhofer and Fresnel diffraction. Fraunhofer diffraction is a form of diffraction that occurs when the diffraction pattern is viewed at a long distance from the aperture. Field waves passed through an aperture or slit causes only the size of an observed aperture image to change due to the far-field location of observation. Fresnel diffraction is a process of diffraction that occurs when a wave passes through an aperture and diffracts in the near field, causing any diffraction pattern observed to differ in size and

shape, depending on the distance between the aperture and the projection. It occurs due to the short distance in which the diffracted waves propagate, which results in a Fresnel number (slit size/focal length) greater than 1 (F > 1). Because of the large distace in Fraunhofer diffraction, the Fresnel number is less than 1. In this study, Fraunhofer diffraction is applicable: the slit size used was 8 mm and the focal length is equal to 100 mm, the Fresnel number was less than one.

A collimated beam of light ray of wavelength λ incident on a reflective grating surface at an angle α and is diffracted along angles β_m. The angles β_m of the diffracted beam from the grating are determined by the condition that components from different grooves add up in phase with each other. This happens when the optical path difference between the diffracted beams from adjacent grooves is an integral multiple of the wavelength, that is when

$$P_1 - P_2 = m\lambda, \tag{4.3}$$

where P_1 is given by $d\sin\alpha$, and P_2 is given by $\pm d\sin\beta_m$, and equation 4.3 becomes:

$$d(\sin\alpha \pm \sin\beta_m) = m\lambda, \tag{4.4}$$

where d is the groove spacing, λ is wavelength and m is the diffraction order (or spectral order) which is an integer. Where $m = 0$ the grating acts as a mirror and all wavelengths are superimposed at the same angle. However, when $m \neq 0$, the incident light at an angle α will be diffracted to an angle β_m which depends on wavelength. Equation 4.4 is known as the grating equation.

The sign convention for the diffraction angles depends on whether the light is diffracted on the same side as the incident light (positive sign) or on the opposite side as the incident light (minus sign). Angles $\alpha > 0$ and $\beta_1 > 0$ since they are measured counter clockwise from the grating normal and $\beta_0 < 0$ and $\beta_{-1} < 0$ since are measured clockwise from the grating normal. The most common way of writing the grating equation is

$$Gm\lambda = \sin\alpha \pm \sin\beta_m. \tag{4.5}$$

Where $G = \frac{1}{d}$, is groove density or frequency and it's validity is limited to cases in which the incident and diffracted rays are perpendicular to the grooves - this kind of setup is called classical diffraction. When the incident light is not perpendicular to the grooves, the grating equation becomes

$$Gm\lambda = \cos\epsilon(\sin\alpha \pm \sin\beta_m). \tag{4.6}$$

Here ϵ is the angle between the incident light path and the plane perpendicular to the grooves at the grating center. If the incident light lies in this plane, $\epsilon = 0$ and Equation 4.6 reduces to equation 4.5. In geometries in which $\epsilon \neq 0$, the diffracted spectra lie on a cone rather than in a plane, in such cases it's termed conical diffraction. In special cases in which the incident light is diffracted back in the direction to which it came from $(\alpha = \beta_1)$ it is called the Littrow configuration, and the grating equation becomes

$$m\lambda = 2d \sin \alpha \tag{4.7}$$

Dispersion

Dispersion is the phenomenon in which light is separated according to its wavelengths when it strikes a grating. There are two types of light dispersion: angular dispersion (which expresses the spectral range per unit angle) and the linear dispersion (which expresses spectral range per unit length). Angular dispersion $\frac{\partial \beta_m}{\partial \lambda}$ is described by the angular separation of wavelengths and is derived by differentiating Equation 4.4 keeping the incident angle fixed. Then

$$\frac{\partial \beta_m}{\partial \lambda} = \frac{m}{dcos\beta_m}, \tag{4.8}$$

where an increase in groove density G increases the angular separation of wavelengths for a given order m. Since m and d are not independent quantities, substituting Equation 4.8 into 4.4 yields

$$\frac{\partial \beta_m}{\partial \lambda} = \frac{sin\alpha \pm sin\beta_m}{\lambda cos\beta_m}. \tag{4.9}$$

Equation 4.9 shows that angular dispersion is a function of angles of incidence and diffraction for a light of wavelength λ. This is clear if we consider the Littrow configuration

$$\frac{\partial \beta_m}{\partial \lambda} = \frac{2}{\lambda} tan\beta_m. \tag{4.10}$$

Linear dispersion P is the product of angular dispersion with the effective focal length f as

$$\begin{aligned} P &= \frac{\partial \beta_m}{\partial \lambda} f \\ &= \frac{mf}{dcos\beta_m}, \end{aligned} \tag{4.11}$$

and the focal length may depend on the diffracted angles.

Resolving power

The resolving power R of a grating is a measure of its ability to separate adjacent spectral lines of average wavelength λ and is expressed as a dimensionless quantity [Morrison [2013]]

$$R = \frac{\lambda}{\Delta\lambda} \tag{4.12}$$

$\Delta\lambda$ is the difference in wavelength between two lines of the same intensity that can be distinguished. The resolving power depends on the spectral order m and the total number of illuminated grooves on the surface of the grating, and is given by

$$R = mN \tag{4.13}$$

Where N is the total number of grooves illuminated on a surface of a grating. The grating equation can be used to replace m to achieve a more meaningful equation with the incident and diffracted angles for $m \geq 0$,

$$R = \frac{Nd(\sin\alpha + \sin\beta_1)}{\lambda} \tag{4.14}$$

For a Littrow configuration i.e. $(\alpha = \beta_1)$, Equation 4.14 becomes

$$R = \frac{2W\sin\alpha}{\lambda} \tag{4.15}$$

where $W = Nd$. For a planar grating W is the width of the grating. The possible maximum resolving power of a grating monochromator occurs when $\sin\alpha = 1$,

$$R = \frac{2W}{\lambda}. \tag{4.16}$$

From Equation 4.16 (for a planar diffraction grating) it can be seen that the resolving power of a grating is independent of the groove spacing d and the number of grooves N.

Spectral resolution

Spectral resolution is the measurement ability to resolve nearby wavelengths taking into account the entrance and exit slits (dimensions and locations), and the images (aberrations and magnifications) [Keppy and Allen [2008]]. The minimum wavelength difference $\Delta\lambda$ between two wavelengths that can be resolved clearly

is the limit of resolution, or simply resolution and can be determined by convoluting the image of the entrance aperture with the exit aperture. Spectral resolution is arguably more important than is resolving power since it takes into account the image effects of the system. Spectral resolution unlike resolving power have spectral units, usually in nanometers.

Bandpass (or spectral bandwidth)

The bandpass $\Delta\lambda_e$ is the width of the wavelength interval that passes through the exit slits of the monochromator, defined by the difference in wavelengths between the points of full width at half maximum (FWHM) on the either side of an intensity maximum that passes through the exit slits. When a monochromator is set to a certain wavelength, light with Gaussian intensity distribution pass through the exit slit. Bandpass is given by

$$\Delta\lambda_e = W \times P. \tag{4.17}$$

Where W is the width of the slits (depending on which is larger) and P is the linear dispersion. Bandpass is directly related to the width of the slits where a small slit width results in a smaller bandpass and hence can resolve wavelengths that are closer together than with larger bandpass. Bandpass is also called a spectral bandwidth.

Scattered and stray light

Any light reaching the image plane not originating from the grating, is referred to as stray light, and unwanted light coming from the grating itself is called scattered light.

4.3 Detectors

A detector is a device used to detect or receive radiation at its surface. There are different types of detectors used in optical radiation measurements varying with the intended purpose of measurements. For this measurements, a PMT detector was used.

4.3.1 Photomultiplier tubes

A PMT detector is a vacuum tube that converts light into electrical signal and consists of an input window, a photo cathode material, focusing electrodes, an electron multiplier and an anode. When light reaches the photo cathode, electrons are excited so that photoelectrons are emitted into the vacuum. The valence band of the PMT detector is supplied with electrons from the incident light and the electrons need to have enough energy to overcome the energy gap and the electron affinity of the conduction band to be emitted into the vacuum as photo electrons.

Antimony-Cesium (Sb-Cs) photo cathode material was selected for the PMT detector used for the measurements in this research project because this material has a spectral response from UV to visible (VIS) (185 nm - 650 nm) and is chiefly employed in reflection-mode photo cathodes. The photoelectron emission process of photocathodes is classified into a reflection and transmission mode. In a reflection mode, photo electrons are emitted in the opposite direction of the incident light, and for transmission mode, photoelectrons are emitted in the same direction of the incident light.

The PMT detector input windows are made of different materials which limits the spectral sensitivity in the short wavelength spectral region. The window material used is a UV-transparent glass which has a lower wavelength cut-off of 190 nm. The focusing electrodes focuses the photo electrons onto the first dynode area. For the input system to work, two requirements must be met: (a) collection efficiency - focus the maximum number of electrons into the first dynode regardless of the initial velocity and where on the photo cathode the electrons originate, and (b) the transit time of electrons between the first dynode and cathode must be independent of their initial velocity and point of origin.

The electron multiplier of the PMT is used to multiply photo electrons from the first dynode to the last by means of secondary emission and is repeated at each successive dynodes. The dynode stages of the electron multiplier are arranged so that the electric field between them causes the electrons emitted by each dynode to strike the next with energy of a few hundred electron-volts. As a result of secondary emission, the number of electrons increases from dynode to dynode giving the required multiplication. The anode collects secondary electrons multiplied in the multi-stage dynodes and outputs the electron current to an external circuit.

Stability

Stability of a spectroradiometer is the extent to which the responsivity or output signal changes with time. The limiting factor in the stability of spectroradiometer is detector instability. The change in an output of a PMT with operating time is called drift. Fatigue is the results of the performance deterioration due to hysteresis and ambient conditions. Instability over a short time is referred to as time stability or drift, while instabilities over times longer than 10^3 to 10^4 hours is called life characteristics. Drift and life characteristics depend on changes in the secondary emission characteristics of the dynodes due to constant bombardments with electrons, the less the bombardment, the smaller the drift. Low drift is as a result of good stability of cathode sensitivity of a PMT tube even after long periods of operation. The PMT manufacturer recommend limiting the anode current to a few microamperes; $(10^{-8}A)$ to limit the drift to $0,1\%$ per hour.

Aging is a process by which a new PMT is operated continuously for several hours to several tens of hours, without exceeding the maximum rating of the anode output current, in order to allow its responsivity to stabilize. By following this procedure before taking measurements, drift can be effectively stabilized. Before the PMT detector is used, it must be warmed up to further stabilize drift. At NMISA the PMT detector is warmed up for 120 minutes to stabilize drift. At the initial phase of operation of the PMT, warm up time is longer, and is expected to decrease with operation time. The warm up period can be shortened at a higher anode current, and be longer at lower anode current.

Hysteresis

Hysteresis is the effect that, when the supply voltage or incident flux is changed in a step function, the PMT may not produce an output signal commensurate with the step function. Hysteresis happens in two ways: the output overshoots (it first increases before it settles) or undershoots (the output current first decreases before it settles). For example, in the case where the shutter is momentarily closed the output current undershoots its previous recent level, and in another case when the shutter is momentarily opened, the output current signal overshoots its previous level. Hysteresis is further divided into light hysteresis and voltage hysteresis depending on the factor that was changed.

With light hysteresis the PMT is operated at a constant supply voltage while changing the incident light in a step function. The PMT may show a change in the

anode current after the incident light is changed. The PMT must be allowed to warm up for a specified time at an anode current of 1 microampere. The incident light is blocked (shut off) for a specified time and then unblocked again, and this method must be repeated to check repeatability. Light hysteresis can be expressed as a percentage:

$$H_L = \frac{(I_{MAX} - I_{MIN})}{I_i} \times 100\% \tag{4.18}$$

where H_L is light hysteresis, I_{MAX} is the maximum output current, I_{MIN} is the minimum output current, and I_i is the initial output current.

Unlike in light hysteresis, voltage hysteresis is observed when the photomultiplier operate at neither a constant supply voltage nor at a constant incident light level. Voltage hysteresis occurs with the incident light being operated in a cycle (shutter off and on) at specified constant time intervals, while the supply voltage is also changed at a constant voltage range. When the incident light is shutt off say for a minute while the supply voltage is increased by a constant step of say 200 volts, then after the incident light and the supply voltage are returned to their original conditions the variations in anode output are measured. This procedure is repeated to confirm reproducibility of the PMT. In general, if the supply voltage change is high, the voltage hysteresis will also be high, the voltage hysteresis can be expressed in percentage as shown;

$$H_V = \frac{(I_{MAX} - I_{MIN})}{I_i} \times 100\% \tag{4.19}$$

where I_{MAX} is the maximum output current, I_{MIN} is the minimum observed output current, and I_i is the initial output current.

Hysteresis can be reduced by limiting the time during which the incident light is shuttered-off to reduce light hysteresis. Select and apply the supply voltage you intend to use and let the PMT warm up for an hour. Another method which can be employed to minimize hysteresis is to irradiate the tube with the flux you plan to measure an hour before commencement of measurements. This may not be ideal since standard lamps have sensitive operational hours and other lamps have limited operating hours with their output known to decrease with operating hours.

Chapter 5

Traceability of UV-C spectral irradiance measurements

5.1 Introduction

This chapter addresses the traceability of spectral irradiance measurements in the UV-C region of the electromagnetic radiation spectrum. Traceability is defined as the property of the measurement results through which the results can be compared to a reference through an unbroken chain of calibrations [BIPM and OIML [2008]]. With traceability, uncertainties increase down the traceability chain. It is a method that demonstrates the measurement's accurate representation of the measured value according to relevant national and or international standards traceable to the SI. Traceability doesn't only require calibration against a reference standard but also the validation and the competency of the personnel to carry out the task. With traceability the measured results are more likely to be reliable and accurate if the procedure is correctly implemented. In this chapter we show the traceability of the UV-C spectral irradiance measurements to international standards and bodies.

NMISA is responsible for disseminating the unit of spectral irradiance in South Africa. NMISA national primary standards for spectral irradiance are the QTH and the deuterium lamps which are calibrated at PTB or the National Research Council (NRC). They can either calibrate our standards against their national primary standards (HTBB) or their secondary working standards lamps (which were calibrated against their HTBB). The application of spectral irradiance unit to measurement requires an unbroken traceability chain to basic SI units. The unit of spectral irradiance is derived from a HTBB based on the Planck's radiation law

[Planck [1901]]. If the temperature inside the cavity is exactly known, the spectral irradiance can be obtained as

$$E_\lambda(\lambda, T) = \varepsilon(\lambda) \cdot \frac{A_{BB}}{d_{BB}^2} \cdot \frac{2hc^2}{n^2\lambda^5} \cdot \frac{1}{e^{\left(\frac{hc}{n\lambda kT}\right)} - 1}, \tag{5.1}$$

where c, k and h are the fundamental constants of light velocity, Boltzmann constant and Planck's constant respectively. $\varepsilon(\lambda)$ is the effective emissivity taken into account as well as the refractive index n of air. A_{BB} the radiant area of the black body radiator and the distance d_{BB} to the irradiated area, are used as geometric parameters for the irradiance. For a determined radiator temperature T, the spectral irradiance $E(\lambda, T)$ can be calculated for any wavelength λ.

The temperature of the black body radiator is accurately determined with filter radiometers [Sperfeld *et al.* [2013]]. Filter radiometers are used to measure the radiance of the HTBB source in one particular wavelength band, and through Planck's law, determines the black body temperature and spectral output at all wavelengths [Metzdorf *et al.* [1987]]. Filter radiometers are traceable to the cryogenic radiometer, which comprises of an optical detector, a wavelength selection device and a method to define the geometry in which light is detected. The cryogenic radiometer is the primary standard for optical power measurements. This instrument is an electrical substitution device (that can operate near the temperature of liquid helium) used to link optical power measurements to the watt [Gentile *et al.* [1996]]. This is accomplished by comparison of the temperature rise induced in an absorbing mass by incident optical radiation and temperature induced by electrical heating.

Using the substitution method, the spectral irradiance realised by the primary standards is transferred to the secondary standards using a spectroradiometer. At PTB, the incident radiation from the primary standard is spectrally dispersed with a double monochromator and measured with a photo detector as a photo current $i(\lambda)$. Through a direct comparison of the photo currents of the HTBB and the secondary standards using a spectroradiometer, the spectral irradiance of the secondary standard $E_s(\lambda)$ is obtained using

$$E_s(\lambda) = E_{BB}(\lambda, T) \cdot \frac{i_s(\lambda)}{i_{BB}(\lambda)} \cdot \prod_{k=1}^{m} a_k(\lambda), \tag{5.2}$$

$i_s(\lambda)$ and $i_{BB}(\lambda)$ are the photo currents of the secondary and primary HTBB and standards lamps, respectively, and $a_k(\lambda)$ are the respective adjustment factors

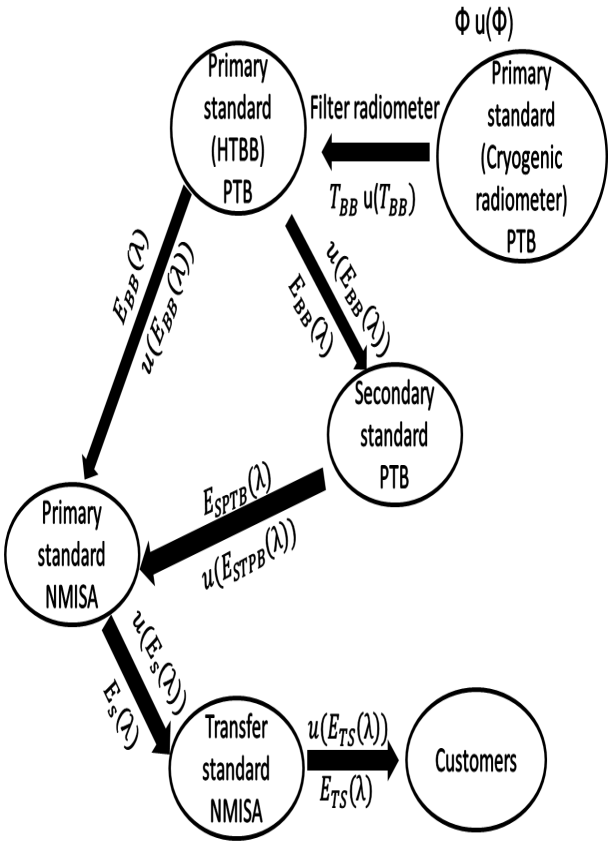

Figure 5.1: The traceability chain at NMISA of the spectral irradiance unit traceable to the HTBB at PTB.

for the comparison of different radiators.

5.2 Traceability chain

Figure 5.1 shows the traceability of the unit of spectral irradiance at NMISA. The black body radiator temperature (T_{BB}) determined with the filter radiometer has an associated uncertainty in temperature of $u(T_{BB})$. The filter radiometer is traceable to the cryogenic radiometer, the primary standard for optical power Φ with a determined uncertainty $u(\Phi)$. The HTBB is traceable to the SI unit of Kelvin from the filter radiometer and the derived unit of the watt from the cryogenic radiometer.

The realised spectral irradiance from the HTBB $E_{BB}(\lambda)$ is transferred with a calculated uncertainty $u(E_{BB}(\lambda))$ through a calibration using a substitution method to the 30 W deuterium and 1000 W QTH lamps, which are used as spectral irradiance transfer standards. They are calibrated at discrete wavelengths, 200 nm to 400 nm (in 5 nm steps) for the deuterium lamp and 250 nm to 2500 nm (in 10 nm steps) for the QTH lamp. At PTB and NRC these standards are secondary standards for spectral irradiance whereas at NMISA they are the national standards for spectral irradiance.

The calibrated NMISA primary standards (with spectral irradiance $E_S(\lambda)$ and associated uncertainties $u(E_S(\lambda))$ are used to calibrate NMISA transfer standards (using a substitution method) which are then used to calibrate customers lamps and detectors. NMISA transfer standards are calibrated directly against NMISA primary standards using spectroradiometer and has a calibrated spectral irradiance $E_{ST}(\lambda)$ and a calculated uncertainty $u(E_{ST}(\lambda))$.

5.3 Key comparisons

In 1999, the MRA was signed with the objective to establish the degree of equivalence of national measurement standards at NMIs. The MRA also provides the mutual recognition of calibration and measurement certificates issued by NMIs. The degree of equivalence at NMIs is determined by the set of key comparisons chosen and signed by consultative committees of the BIPM, working together with the regional metrology organisation (RMO). The CCPR is one committee of the BIPM, which is responsible for organizing key comparisons in the metrology area of Photometry and Radiometry. The CCPR identified a number of key comparisons at its meeting in March 1997. Two of these comparisons were the CCPR k1-a and CCPR k1-b for spectral irradiance quantity.

5.3.1 CCPR k1-a

The key comparison for spectral irradiance for wavelength range 250 nm to 2500 nm is the CCPR k1-a which was carried out (between the years 2000 and 2005 and final report published in June 2006) by 13 participating NMIs. The used artifacts were tungsten halogen lamps and the comparison was arranged in a star comparison due to fragile nature of these lamps. The order of the comparison was participant - pilot -participant. NPL acted as the pilot laboratory for this comparison [Woolliams *et al.* [2006]].

Table 5.1: The mean uncertainties for NPL in the CCPR k1-a key comparison for measured irradiance when compared to CENAM [Woolliams *et al.* [2006]]. E_{NPL} was the spectral irradiance measured by NPL.

Wavelength [nm]	$\bar{E}_{NPL}$ **[W.m^{-2}.nm^{-1}]**	$u(\bar{E}_{NPL})$ **[%]**
250	1,46$\times 10^{-4}$	2.53
260	2.54$\times 10^{-4}$	2.34
270	1.10$\times 10^{-4}$	2.22
280	6.64$\times 10^{-4}$	1.69

The participating NMIs excluding the pilot were: National bureau of Metrology - National Metrology Institute BNM-INM (France), CENAM (Mexico), CSIRO (Australia), HUT (Finland), IFA-CSIC (Spain), MSL-IRL (New Zealand), NIM (China), NIST (USA), PTB (Germany), NMIJ (Japan), NRC (Canada) and VNIIOFI (Russian Federation). As the pilot laboratory, NPL was responsible for organising the comparison, writing the technical protocol (in discussion with the working group consisting of the NPL, NIST, and PTB), purchasing and distributing the technical artefacts. NPL was also responsible for organising the measurement reports from participants, analysing and preparing the draft report. Each participant was allowed to measure three to four lamps on two occasions and the pilot also measured the lamps on two occasions.

The weighted mean of the effective spectral irradiance of all the NMIs known as the key comparison reference value (KCRV) was determined for all participants. The calculated uncertainties of the CCPR k1-a are summarized in Table 5.1.

5.3.2 CCPR k1-b

The key comparison in the spectral region 200 nm to 350 nm, is one comparison identified by CCPR to determine the degree of equivalence at NMIs of spectral irradiance in the UV region of electromagnetic spectrum. PTB was nominated as the pilot laboratory for this key comparison which happened in 2003 and 2004 and final report approved by CCPR and published in September 2008. Five NMIs including the pilot laboratory participated in this key comparison: PTB, BNM-INM, NRC, NIST and NPL. As the pilot laboratory PTB was responsible for organising the key comparison, purchasing and distributing artefacts to all participating NMIs, analysing the results and drafting the report.

Table 5.2: The averaged KCRV uncertainties $u(E_{KCRV})$ for the CCPR k1-b comparison piloted by the PTB NMI are given below [Sperfeld [2008a]].

Wavelength [nm]	$\bar{E}_{KCRV}$ **mW.m^{-2}.nm^{-1}**	$u_{rel}(\bar{E}_{KCRV})$ **[%]**
200	1,0029	2,1
250	0,6611	0,9
260	0,5652	0,8
280	0,4089	1,2

The comparison artefacts used for the inter comparison were DLS developed, assembled, aligned and pre-aged at PTB. The participating NMIs were allowed to use three to four artefacts for the inter comparison. The measurements for the inter comparison were done in the pilot-NMI-pilot-NMI sequence. The results were averaged to reduce uncertainties due to multiple measurements with a group of three to four lamps per NMI. The measurements were divided into two parts to produce comparability and equivalence with other participants, using two independent sets of deuterium lamp systems. In one set of measurements, the lamps were calibrated as transfer standards similar to the measurements done by the participating laboratories. In the other set, the lamps were used by the pilot PTB as comparison reference standards to compare the calibration of all the participants including the pilot PTB. The relative uncertainties $u(E_{KCRV})$ of the KCRV spectral irradiance E_{KCRV} (measured in mW.m^{-2}.nm^{-1}) values are summarized in Table 5.2.

The CCPR k1-a and k1-b shows the international equivalence of the measurement capabilities of the NMIs such as PTB and NPL of QTH and D_2 used in this study and provides the mutual recognition of calibration certificates attached in appendix B. Since the uncertainty at 250 nm wavelength is higher for the QTH lamp than the D_2 lamp, the D_2 lamp was ultimately used to calibrate LP Hg lamp. The uncertainty for the D_2 lamp we used at 250 nm wavelength is higher than PTB's values in Table 5.2, because our D_2 lamp is calibrated against a secondary standard (Figure 5.1).

Chapter 6

Spectral irradiance calibration

6.1 Introduction

The measurement of the UV-C spectral irradiance distribution emitted by lamps is of great importance in a wide range of applications including but not limited to UVGI air disinfection. NMISA is mandated by government through the Department of Trade and Industry (DTI) to disseminate the unit of spectral irradiance in South Africa and the African continent at large. As a result, research plays a vital role in improving the measurements with the aim to lower uncertainties and provide accurate results. The spectral irradiance unit [W.m^{-2}.nm^{-1}] in the UV-C spectral region is disseminated from 250 nm to 280 nm.

6.2 Measurement setup

Spectral irradiance measurements are performed on a dedicated work bench where optical instruments can be aligned. Spectroradiometry measurements also require the laboratory walls to be painted black to restrict light reflections from the walls during measurements. Highly reflecting instruments must be removed or covered if placed close to the optical bench during measurements. The laboratory ambient conditions must be controlled to within specified limits to avoid excessive fluctuations during calibrations.

The schematic of the spectral irradiance measurement setup is shown in Figure 6.1. The components in the setup are as follows: QTH and D_2 are the quartz tungsten halogen and deuterium STD lamps. The lamps' electrical connections

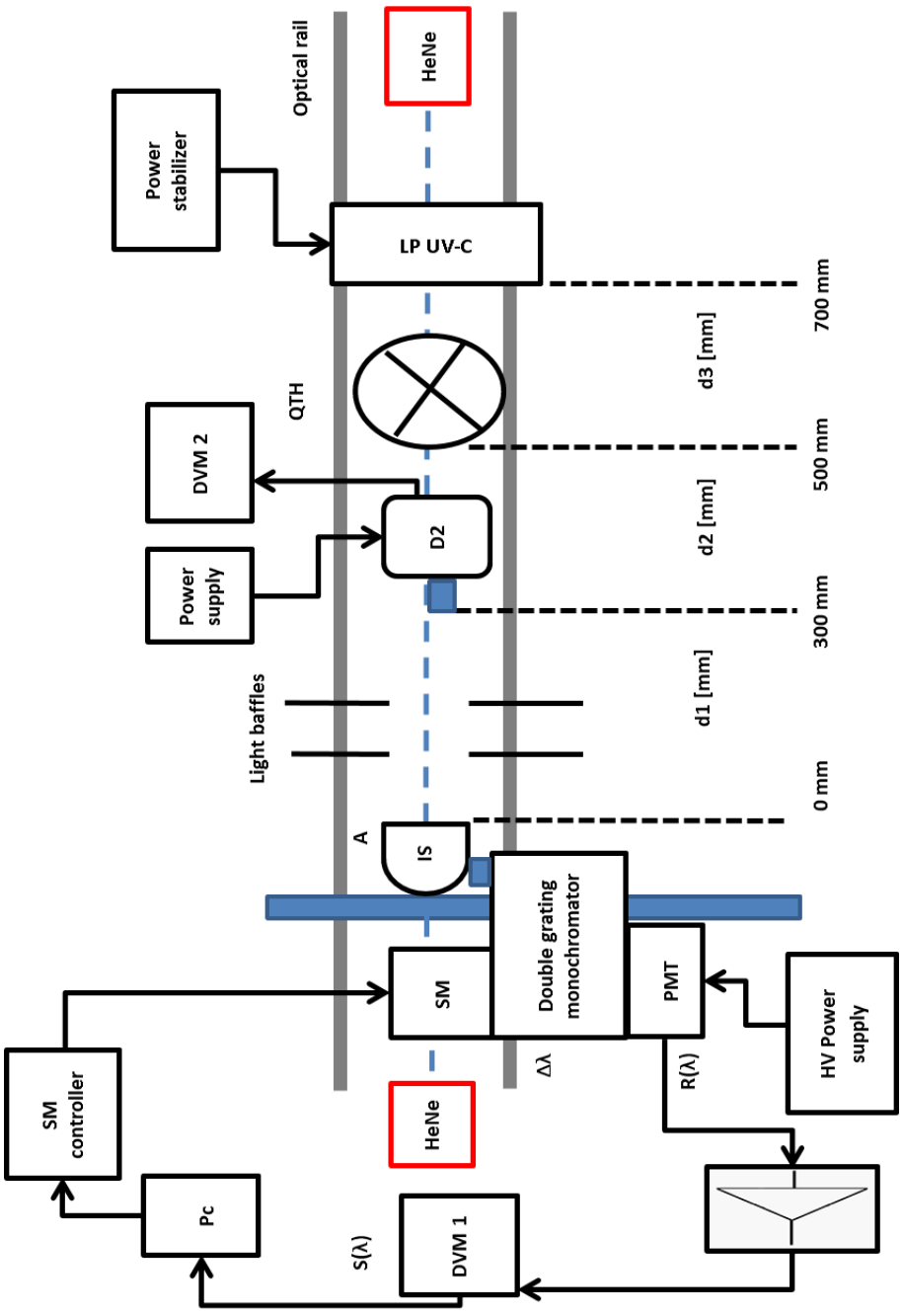

Figure 6.1: The measurement setup for disseminating the spectral irradiance unit in a source based radiometry at NMISA.

were explained in Chapter 4 Subsections 4.1.1 and 4.1.2. LP UV-C is the LP Hg UV-C lamp measured as the unit being calibrated (UUT). HeNe is the helium neon laser shined horizontally on the optical bench, and is used to align optical instruments. DVM 1 was the digital voltmeter used to measure the spectral output voltage $S(\lambda)$ from the system. DVM 2 was the digital voltmeter used to measure the input current and voltage across the D_2 lamp. IS is an integrating sphere with opening area A mounted at the entrance slit of the monochromator with bandwidth $\Delta\lambda$. PMT is the photomultiplier tube detector at the exit slit of the monochromator powered by the high voltage (HV) power supply. The PMT has a spectral response $R^{PMT}(\lambda)$. The trans-impedance amplifier (TIA) with a gain G was used to convert photo currents from the PMT into a voltage signal measured by DVM 1 which was read via computer (PC). SM was the stepper motor controller for the monochromator, which rotates the gratings.

The electrical connections must be verified after setting up the instruments. The following connections are required:

- A BNC cable from the detector output to the TIA input.
- A BNC to banana plug cable from the TIA output to the DVM 1 input.
- RS-232 to USB cable from the DVM 1 output to the PC.
- A connection cable from the stepper motor drive to the stepper motor.
- An USB to RS-232 cable from the stepper motor drive to the PC.

In spectroradiometry, a spectroradiometer is an instrument used to measure spectral flux emitted by lamps and which is incident on the IS. A spectroradiometer consists of: a monochromator with an IS at the entrance slit and a detector at the exit slit [Kostkowski [1997]]. The spectroradiometer converts the flux emitted by lamps into a PMT photo current, which is then converted to an output voltage signal by the TIA. The spectral responsivity $R(\lambda)$ of the spectroradiometer system is the quotient of the spectroradiometer spectral output $S(\lambda)$ and the spectroradiometer input. When measuring spectral irradiance $E(\lambda)$, the responsivity is given by

$$R(\lambda) = \frac{S(\lambda)}{E(\lambda)}, \tag{6.1}$$

where $E(\lambda)$ is the spectral irradiance of the lamp.

The components contributing to the spectral responsivity of the spectroradiometer system are: the IS (with an aperture area A and throughput $\rho(\lambda)$), the monochromator (with diffraction efficiency $M(\lambda)$, spectral bandwidth $\Delta\lambda$ set by the slit width) and PMT (with spectral response $R^{PMT}(\lambda)$ and the TIA gain G). $R(\lambda)$ is then given by

$$R(\lambda) = \rho(\lambda) \cdot M(\lambda) \cdot R^{PMT}(\lambda) \cdot G. \tag{6.2}$$

With the spectroradiometer used in this study, the measured quantity was the spectral output voltage $S(\lambda)$. By substitution into Equation 6.1 it follows that

$$S(\lambda) = \rho(\lambda) \cdot M(\lambda) \cdot R^{PMT}(\lambda) \cdot G \cdot E(\lambda). \tag{6.3}$$

Equation 6.3 is known as the measurement equation for spectral irradiance.

The measurement setup in Figure 6.1 makes use of the substitution measurement method, which is a direct comparison with the value of a reference standard having similar properties to the unit being measured. During an actual calibration, the spectral irradiance of a UUT is determined by a direct comparison with a calibrated spectral irradiance standard lamp with known spectral irradiance.

For the measurement equation to be valid, $R(\lambda)$ when measuring the STD must be the same as that when measuring the UUT. Therefore both lamps are measured using the same spectroradiometer settings. When measuring the standard lamp, Equation 6.3 becomes

$$S^{STD}(\lambda) = R(\lambda) \cdot E^{STD}(\lambda), \tag{6.4}$$

where $S^{STD}(\lambda)$ is the measured spectral output voltage of the standard lamp and $E^{STD}(\lambda)$ is the spectral irradiance emitted by the standard lamp. Similarly, the spectral output voltage of the UUT is modelled by:

$$S^{UUT}(\lambda) = R(\lambda) \cdot E^{UUT}(\lambda). \tag{6.5}$$

$S^{UUT}(\lambda)$ is the measured spectral output voltage of the UUT and $E^{UUT}(\lambda)$ is the spectral irradiance of the UUT. Since $R(\lambda)$ must be the same for both lamps for the calibration to be valid, from Equations 6.4 and 6.5 we get:

$$E^{UUT}(\lambda) = \frac{S^{UUT}(\lambda)}{S^{STD}(\lambda)} \cdot E^{STD}(\lambda). \tag{6.6}$$

Equation 6.6 is the spectral irradiance lamp calibration equation.

The measurement setup was characterized before the spectral irradiance lamp calibration to quantify sources of uncertainties of the measurement setup. UV radiometry has higher uncertainties mainly due to low SNR, hence characterizing the setup is important to provide an overview of the uncertainties. Common uncertainties from spectroradiometric measurements arise from incorrect positioning or alignment of instruments (lamps, monochromator etc.), scattered light entering the monochromator, the responsivity change due to position change of the detector and uncertainties in the operation of the standard lamp.

6.3 Characterisation

The spectroradiometer was characterized for the following aspects: the system's noise, monochromator wavelength, alignment of lamps and the system's temperature.

6.3.1 Noise characterisation

The noise of a spectroradiometer is defined as an unwanted disturbance of a useful signal and it degrades accuracy and precision of a measurement. The ratio of the output signal without an IS shutter in place to the output signal with an IS shutter in place is the SNR. It compares the level of a desired signal to the level of the unwanted noise signal. At NMISA, the spectroradiometer noise was measured and found to be equivalent (at the same spectroradiometer settings) to the spectroradiometer background signal measured with the lamp radiant flux blocked by closing the baffle closest to the lamp with a black cloth. Instead of a SNR, a SBR was characterised as it is used at NMISA to correct the measured signal for scattered light entering the monochromator.

The SBR is calculated as a ratio of the measured light signal level $S^{light}(\lambda)$ to the measured background signal $S^{bg}(\lambda)$ expressed in unit of decibel (dB) as

$$SBR = \frac{S^{light}(\lambda)}{S^{bg}(\lambda)}, \tag{6.7}$$

and converting to dB

$$SBR_{dB} = 10 \times \log_{10}(SBR). \tag{6.8}$$

The unwanted flux enters the monochromator after being reflected or scattered by the baffles or other surfaces or may originate from sources not positioned on the optical axis. The background is always corrected for by subtracting it from the measured signal. In this study we characterised the background signal for dependence on the monochromator bandwidth and the PMT detector supply voltage. The light signal was also characterised - this was to determine spectroradiometer settings (PMT high voltage and monochromator bandwidth) that ensured good SBR.

In the UV-C region the photo cathode of the PMT detector used has a spectral response increasing from 2,5 mA/W at 200 nm to approximately 50 mA/W at 280 nm [Hamamatsu [1998a]]. PMT detectors have a high gain which is strongly dependent on the supply voltage. Consequently, the PMT was not operated at extremely high supply voltage. The PMT supply voltages tested were 800 V, 1000 V and 1200 V with monochromator bandwidths of 2 nm, 4 nm and 8 nm determined by slit sizes of 0,5 mm, 1 mm and 2 mm respectively. For each PMT supply voltage, spectroradiometer light and background signals were measured for all monochromator bandwidths. The lamp used was a 1000 W QTH lamp.

The measured background signals showed that the PMT at a supply voltage of 1000 V had a lower measured background signal for all monochromator bandwidths (Figure 6.2) compared to 800 V and 1200 V supply voltages. At a supply voltage of 1000 V, the background signal's dependence on monochromator bandwidths was observed in an increasing order 8 nm < 2 nm < 4 nm. This was the same at a supply voltage of 1200 V. It was not clear why this order was observed, but it is speculated that it might have been due to diffraction effects and the temperature effect on the PMT noise (Subsection 6.3.6).

The light signal was tested at 1000 V supply voltage because of the lower background signal (Figure 6.3). As expected, at a monochromator bandwidth of 8 nm, the measured light signal was higher compared to measured signal with a 2 nm and 4 nm monochromator bandwidths. The light signal test helped us perform measurements below the maximum allowed spectroradiometer measured $S(\lambda)$ value of 120 mV set by the PMT detector current. The combination of 1000 V supply voltage and 8 nm monochromator bandwidth ensured a sufficiently high

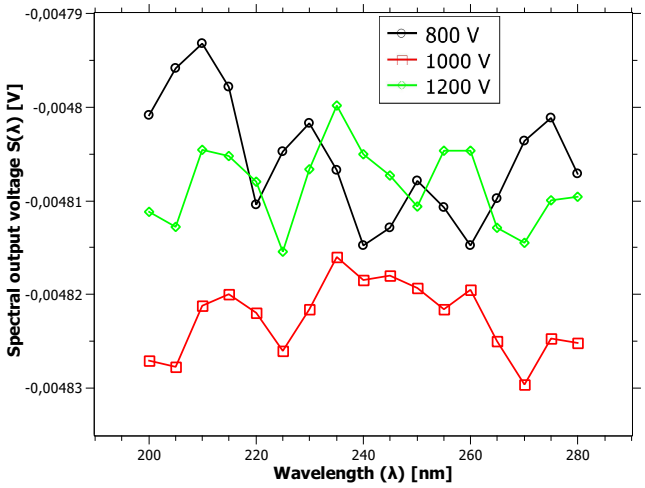

Figure 6.2: The background signal levels measured at 800 V, 1000 V and 1200 V PMT supply voltages with the monochromator set to 8 nm bandwidth. The signal was measured as voltage from the PMT detector. The QTH standard lamp was used to illuminate the monochromator, with the baffle closest to the lamp covered.

SBR. The SBR and SNR calculated values at 1000 V PMT supply voltage and 8 nm monochromator bandwidth are given in Table 6.1.

6.3.2 Wavelength calibration

The standard procedure for wavelength calibration of a monochromator in the UV and VIS region uses Hg pencil discharge lamps with known spectral emission lines as primary wavelength standard. The Hg pencil lamp was mounted in a vertical orientation in front of the IS. Ideally, the monochromator bandwidth and PMT supply voltage used must be the same as those used in the spectral irradiance calibration. Instead of 8 nm monochromator bandwidth, a 2 nm monochromator bandwidth was used, because with the 8 nm monochromator bandwidth, the Hg line peaks were too broad.

The light emitted by a Hg pencil-type lamps has 19 spectral lines in the region 253 nm to 579 nm [Sansonetti *et al.* [1996]]. They are used as standard lines during the wavelength calibration of a monochromator. The exact wavelengths of these spectral lines have been listed in research papers and different laboratories' databases. The NIST Atomic Spectral Database (ASD) has listed spectral lines data for standard air (20 °C temperature, 50 %RH and 760 mmHg baromet-

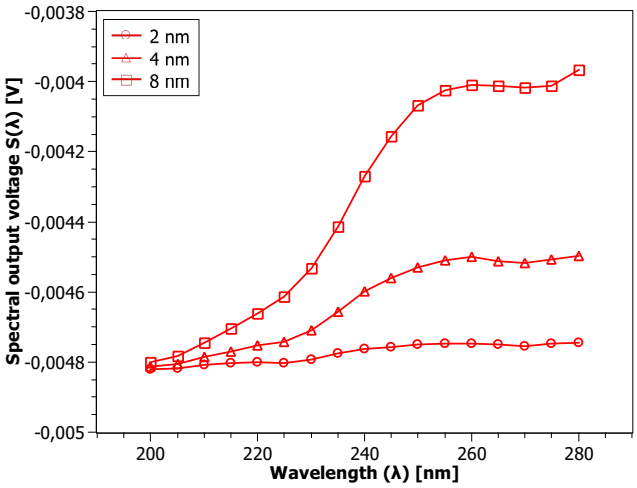

Figure 6.3: The light signal levels measured at 1000 V PMT supply voltage with 2 nm, 4 nm and 8 nm monochromator bandwidth. The monochromator was illuminated with the QTH standard lamp.

Table 6.1: The QTH lamp calculated SBR and SNR values at a PMT supply voltage of 1000 V and a monochromator bandwidth of 8 nm.

Wavelength [nm]	SBR [dB]	SNR [dB]
250	-0,2	-0,3
280	-1,9	-2,0
300	-7,2	-7,4
350	10,9	10,7
400	19,2	19,1

ric pressure) or for vacuum [Kramida *et al.* [2018]]. The NMISA typical conditions in the Photometry and Radiometry (P&R) laboratories (24 °C, 50 %RH, and 657 mmHg barometric pressure) were used in the NIST Engineering Metrology Toolbox (EMT) which uses either the Edlén or Ciddor equations to calculate the index of refraction of air to calculate the wavelengths in air from vacuum wavelengths.

The two methods [Ciddor [1996]] and [Edlén [1966]] for calculating the refractive indexes n have minor differences; one can use one method or the other. The NIST EMT page accepts input values for vacuum wavelengths in the range of validity proposed by Ciddor, ranging from 300 nm to 1700 nm. The differences in the Ciddor and Edlén equations in the range of validity are largest at very low temperature (-40 °C) and high pressure (120 kPa). The difference in n ranges from 1,4$\times 10^{-7}$ at a wavelength of 1700 nm to 1,6$\times 10^{-7}$ at 300 nm wavelength. For dry air at temperatures between 5 °C and 40 °C, pressures between 60 kPa and 110 kPa and wavelengths between 300 nm and 1700 nm, the maximum differences do not exceed 1×10^{-8}. The performed wavelength calibration used the Edlén equation to calculate the refractive indexes of air [Birch and Downs [1993]], [Birch and Downs [1994]].

The wavelength positions of the Hg lines were identified with wavelength scans, which also identifies changes in the bandwidth of the monochromator. The stepper position of the monochromator grating is usually set by a first order polynomial $y = +a\lambda + b$, where λ is wavelength and y is the stepper motor position. A reference position is selected by looking at the monochromator display. With the monochromator used in this study, it was found that the reference position was not reproducible, and therefore this position needs to be checked before performing a calibration. The measurements were corrected for background light reflections.

Results

Segments were chosen where Hg spectral lines were expected, and no overlap with higher order lines occurred. Four mercury lines were chosen as standards for calibrating the monochromator in the UV and VIS. The selected vacuum wavelengths with their relative intensities are tabulated in Table 6.2. Three sets of wavelength scans were performed around the expected Hg line peaks (253,6 nm, 435,9 nm, 546,1 nm, and 576,9 nm) to determine repeatability uncertainties (see Section 7.2).

Table 6.2: The mercury lines for wavelength calibration.

Element	λ_{vac} [nm]	Refractive index n_{air} [1]	λ_{air} [nm]	Relative intensity
Hg I	253,73	1,0002438	253,67	900000
Hg I	435,96	1,0002351	435,85	12000
Hg I	546,23	1,0002324	546,10	6000
Hg I	577,12	1,0002319	576,99	1000

Table 6.3: The monochromator's wavelength calibration results. The acronyms and symbols used are as follows: λ_{air} is the wavelength in ambient air calculated using Equation 6.9, $y1$, $y2$ and $y3$, are the stepper positions corresponding to the wavelength peaks measured from set 1, 2 and 3 respectively, $\bar{y}$ is the average of the stepper positions $y1$, $y2$ and $y3$. ESD is the standard deviation of the three sets, and ESDM is the experimental standard deviation of the mean calculated by dividing the ESD with the square root number of sets measured (n=3). $\bar{y}-\bar{y_0}$ is the shifted stepper motor positions calculated by subtracting the initial stepper motor value at the 253,6665 nm Hg line from $\bar{y}$.

λ_{air} [nm]	$y1$	$y2$	$y3$	$\bar{y}$	ESD	ESDM	$\bar{y}-\bar{y_0}$
253,67	260	260	260	260	0	0	0
435,85	109312	109312	109312	109312	0	0	109052
546,10	175308	175308	175308	175308	0	0	175048
576,99	194344	194284	194224	194284	60	34,641	194024

In Table 6.2, λ_{vac} is the vacuum wavelength of the reference Hg line, and was used to calculate the refractive index (n_{air}) of air using NMISA atmospheric conditions (NMISA P&R laboratories) in the NIST EMT. λ_{air} is the wavelength in ambient air calculated from the λ_{vac} and n_{air} relationship [Stone Jr and Zimmerman [2001]]

$$\lambda_{vac} = n_{air}\lambda_{air}. \tag{6.9}$$

The Hg line around 254 nm was used as a reference in the UV-C spectral region, but falls outside the range of validity of the equation for the refractive index proposed by Ciddor. Approximation to calculate this line was made using the Hg vacuum line at 300 nm. This was because the refractive index of air does not vary significantly from 250 nm to 300 nm [Meggers and Peters [1919]].

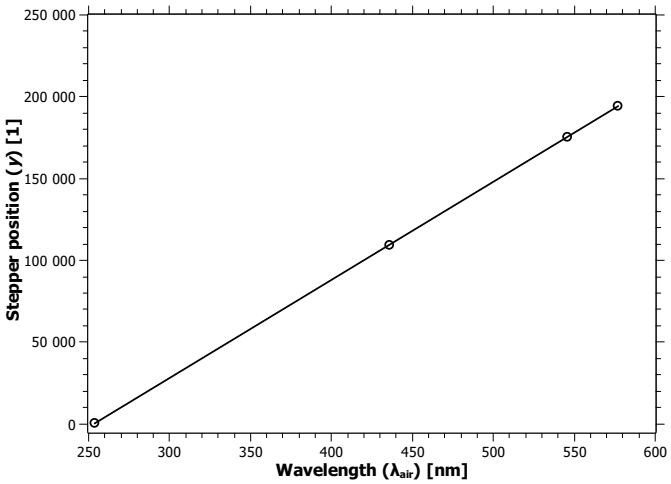

Figure 6.4: The wavelength stepper positions $\bar{y}$ plotted as a function of wavelength in air λ_{air} (Table 6.3). The linear fit equation was $y = 599,5\lambda_{air} - 151888,6$ with the coefficient of determination $R^2 = 0,99$. The markers were the λ_{air} stepper positions. This linear equation was used as the monochromator reference equation.

The measured wavelength line peaks with their corresponding monochromator stepper motor positions are tabulated in Table 6.3. $\bar{y}$ was adjusted so that the Hg line at 253,67 nm was at $y = 0$. To get the monochromator reference equation, we plotted $\bar{y}$ versus λ_{air} (Figure 6.4). The fit was a straight line in a format $y = m\lambda_{air} - c$. To calculate λ_{air} as a function of stepper position, the linear function could be re-written as

$$\begin{aligned} \lambda_{air} &= \frac{y}{m} + \frac{c}{m} \\ &= (0,00166795y + 253,78)\text{nm}. \end{aligned} \tag{6.10}$$

The light output of the Hg pencil lamp was simultaneously monitored with a temperature stabilized UV enhanced silicon detector throughout the calibration. The results are shown in Figure 6.5. The stability calculated as relative uncertainty in percentage was 5,02 %. The worst case occurs between 1300 s and 1600 s in Figure 6.5.

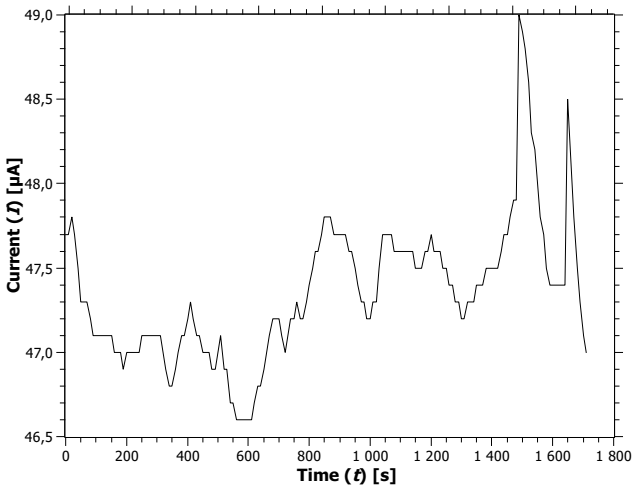

Figure 6.5: The output of the Hg pencil discharge lamp monitored with a UV enhanced silicon detector.

Wavelength calibration verification

The wavelength calibration measurement was verified using the same lamp, monochromator with the same bandwidth and the same PMT detector with the same supply voltage. The verification measured results in Table 6.4 showed that the 253,67 nm line peak was measured at 254,13 nm giving a difference of 0,5 nm. Whenever the wavelength test is performed before measurements, the calibration is taken to be still valid, if the difference is within the wavelength uncertainty.

6.3.3 Alignment of spectral irradiance lamps

The spectral irradiance measurements are sensitive to alignment and positioning of the lamps. This section investigates the effect of lamps' alignment on the measured $S(\lambda)$. With regard to alignment and positioning, there are two steps in uncertainty estimation. First is to determine the smallest increments in translation and orientation that may be detected on the optical bench. These were 1 mm in translation and 2 degrees in orientation about a vertical axis. Secondly, determining the fractional changes in $S(\lambda)$ due to these increments.

All lamps used were mounted in a vertical orientation. This ensured that light emitted by the lamps propagated in a horizontal plane. Translational increments

Table 6.4: The verification of the wavelength calibration measured results. The headings of the measured and calculated data are: λ_{air} is the ambient air wavelength calculated using NMISA ambient conditions (Table 6.2), λ_{set1}, λ_{set2}, and λ_{set3} are wavelengths of mercury lines measured in set 1, set 2 and set 3. $\bar{\lambda}_{ver}$ was the average of three sets, and the difference was calculated by subtracting $\bar{\lambda}_{ver}$ from λ_{air}.

λ_{air} [nm]	λ_{set1} [nm]	λ_{set2} [nm]	λ_{set3} [nm]	$\bar{\lambda}_{ver}$ [nm]	ESD [nm]	ESDM [nm]	Difference [nm]
253,67	254,0	254,2	254,2	254,1	1,15	0,67	0,5
435,85	436,1	436,1	436,1	436,1	0	0	0,3
546,10	546,2	546,2	546,2	546,2	0	0	0,1
576,99	577,7	577,8	577,8	577,8	0,58	0,33	0,8

Table 6.5: The $\Delta S(\lambda)/\Delta d$ calculated as a percentage change for all lamps. The wavelengths are indicated on the table headings.

Distance	QTH lamp	D_2 lamp		LP Hg lamp
[mm]	450,5 nm	255 nm	350 nm	255 nm
+1	0,1 %/mm	0,2 %/mm	0,2 %/mm	0,02 %/mm
-1	0,03 %/mm	0,2 %/mm	0,2 %/mm	0,03 %/mm

perpendicular to the optical axis are equivalent to angular increments, where 1 mm in translation was calculated to be equivalent to 0,1 degrees for an object 500 mm away. Therefore translational increments perpendicular to the optical axis were not investigated.

Measurement results for translation

In translation the lamps were displaced closer and further away from the reference positions to calculate the change in $S(\lambda)$ as a function of Δd. Because of the high demand for accuracy of measurements at NMIs, alignment of instruments plays a critical role in evaluating uncertainties in spectroradiometry. The uncertainties introduced by translation were included in the spectral irradiance lamp calibration uncertainty budget whenever the lamps were used for calibration.

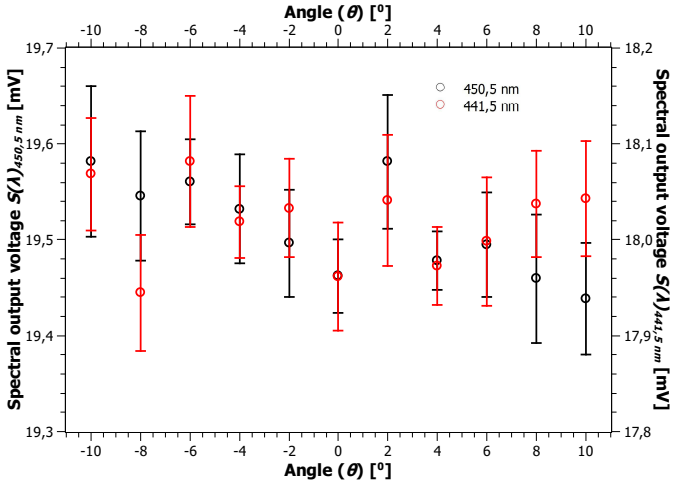

Figure 6.6: The measured $S(\lambda)$ of the spectroradiometer when illuminated with the QTH STD lamp due to a change in angular position of the lamp around vertical axis. The measurements were performed at wavelengths of 450,5 nm and 441,5 nm.

The measured changes in measured $S(\lambda)$ are tabulated in Table 6.5. In Table 6.5, -1 mm was when the lamps were moved closer to the spectroradiometer and +1 mm was when the lamps were moved further away from the spectroradiometer.

Orientation

Another uncertainty in positioning was due to the orientation (or rotation about the vertical axis) of the lamps. The effect was investigated at the calibrated positions of the lamps. The filament of the QTH STD lamp closely approximates a cylindrically symmetric emitter and, therefore, theoretically the orientation of the QTH STD lamp should not have a significant effect on measured $S(\lambda)$ signal. However the same did not hold for the D_2 and the LP Hg lamps. These lamps emitted radiation preferentially in one direction.

The effect of orientation on measured $S(\lambda)$ for all lamps is shown in Figures 6.6 (QTH lamp), 6.7 (LP Hg lamp) and 6.8 (D_2 lamp). As expected, the QTH lamp had a smaller angular dependence with an average lower uncertainty compared to both the LP Hg and the D_2 STD lamps. The LP Hg lamp showed an asymmetric distribution, probably due to misaligned lamp tubes or lower output from one of the tubes. On the negative angles, the lamp output dropped faster than on the

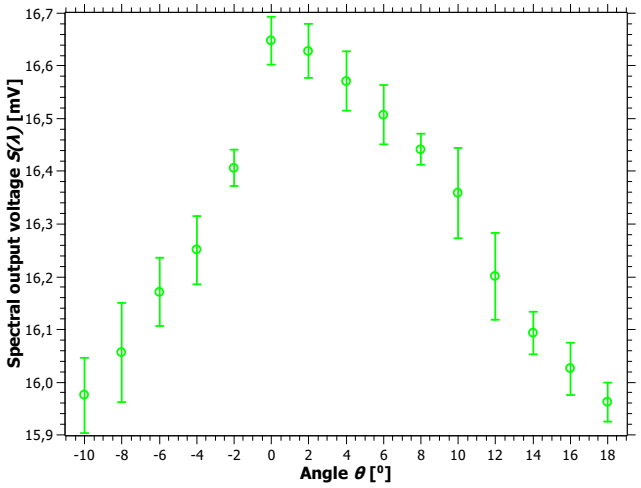

Figure 6.7: The measured spectral output voltage of the spectroradiometer when illuminated with the LP Hg lamp at 255 nm wavelength from different lamp orientations around its vertical axis.

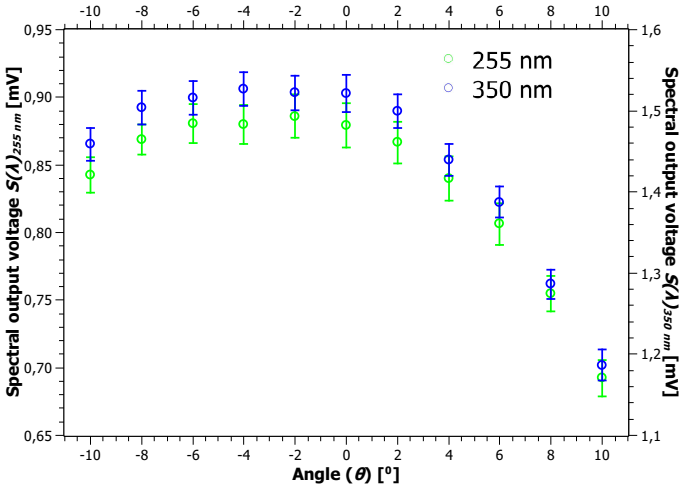

Figure 6.8: The measured spectral output voltage of the spectroradiometer when illuminated with the D_2 STD lamp due to a change in orientation around its vertical axis. The measurements were performed at 255 nm and 350 nm wavelengths.

Table 6.6: The change in measured $S(\lambda)$ calculated as a percentage due to changing the orientation of the lamps.

Angle	QTH lamp		Deuterium lamp		LP Hg lamp
[°]	450,5 nm	441,5 nm	255 nm	350 nm	255 nm
-2	+0,1 %	+0,1 %	+0,3 %	+0,2 %	-0,1 %
+2	+0,1 %	+0,1 %	-0,3 %	-0,2 %	-1 %

positive angles with a percentage difference of 1,5 % (at negative angles) to 0,1 % (at positive angles).

Due to a small limiting aperture size of the D_2 lamp, it was expected to have a higher angular dependence. The D_2 STD lamp measured $S(\lambda)$ dropped faster on the positive angles than on the negative angles (see Figure 6.8), and this phenomenon was repeatable. This showed that the lamp must be positioned for maximum light output. The LP Hg lamp had a higher calculated uncertainty of 0,5 % on average compared to 0,1 % and 0,3 % for the QTH and D_2 STD lamps, respectively (Table 6.6).

6.3.4 Inverse square law approximation

This subsection investigates the accuracy of inverse square law approximation of the QTH, D_2 and LP Hg lamps. Since $E(\lambda)$ and $S(\lambda)$ have a 1:1 correspondence (Equation 6.3), we investigated $\Delta S(\lambda)$ as a function of Δd. The change in $S(\lambda)$ can be calculated as a fractional change $\frac{\Delta S(\lambda)}{S(\lambda)}$ of measured $S(\lambda)$ at two distance positions derived from Equation 3.12 as

$$\begin{aligned} S(\lambda) &= k\frac{I(\lambda)}{d^2} \\ \frac{\Delta S(\lambda)}{\Delta d} &\approx \frac{\partial S(\lambda)}{\partial d} \rightarrow \frac{\partial S(\lambda)}{\partial d} = -2k\frac{I(\lambda)}{d^3} \\ \frac{\Delta S(\lambda)}{S(\lambda)} &\approx -2\frac{\Delta d}{d}, \end{aligned} \tag{6.11}$$

where $S(\lambda)$ is the measured spectral output voltage, d is the distance from the lamp to the IS and $I(\lambda)$ is the intensity of the incident light from the lamps.

It is expected that the distance of the lamp from the spectroradiometer along the optical axis changes $S(\lambda)$ by roughly the inverse square law, where, for a lamp measured at 500 mm, 1 mm increment correspond to 0,2 % change in distance which change the output signal by 0,4 %. The inverse square law (Equation 3.12) was used to model theoretical values. To account for an offset in distance d, a parameter b was added in the inverse square law

$$y = \frac{a}{(d+b)^2}, \tag{6.12}$$

where y is the theoretical $S(\lambda)$, a is a constant, d is the displacement position and b is an offset in d. In Equation 3.12 θ was equal to zero for all translation measurements because the orientation was fixed at zero degrees. Since the QTH STD lamp has a low SNR below 300 nm wavelength (Table 6.1), the lamp was measured at wavelengths 441,5 nm and 450,5 nm. The wavelengths was selected to match the bandpass filters used with the monitor detector. The measurements with the 441,5 nm wavelength show that the results are repeatable.

As expected the lamp closely approximated a point source (Figure 6.9) with a value b=31 mm. This was because the reference position for measuring the position of the lamp from the IS was the reference position in front of the lamp and not the lamp filament. The actual horizontal distance from the lamp filament to the lamp reference position was measured to be 22 mm. The source of the discrepancy is not clear, but it might be ascribed to the QTH lamp having a finite area, and not being an ideal point source.

Because of the large dimensions of the LP Hg lamp, it deviated from a point source approximation as shown in Figure 6.10. The ratio of the lamp's distance d to the lamp's largest dimension r was 2,5 at 800 mm distance position. As a result, the LP Hg lamp approximated a finite surface source. The lamp was therefore not expected to fit the inverse square law. Due to the deviation from inverse square law, the value of b in this case had no direct physical significance.

The point source approximation of the D_2 lamp was measured at 300 mm distance position, the calibrated reference position of the lamp. The ratio of the D_2 lamp's distance to the lamp's aperture (which was the lamp's largest dimension) was 20, and according to [Ryer [1997]], the D_2 lamp was expected to approximate a point source using an inverse square law. Indeed as shown in Figure 6.11, the lamp approximated a point source. The theoretical b value was measured from the lamp's filament to the front aperture. The lamp aperture is used as a reference

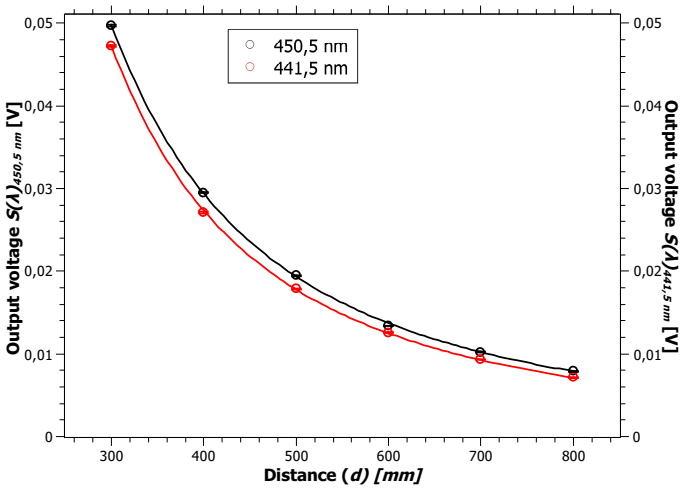

Figure 6.9: Investigating the applicability of the point source approximation of the QTH standard lamp using the measured spectral output voltages at different distances. The measurements were performed at 450,5 nm and 441,5 nm wavelengths. The markers are measured results and the line is the model.

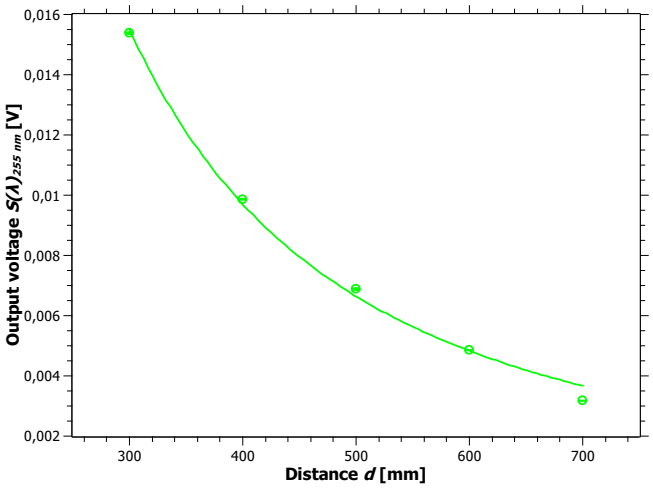

Figure 6.10: The spectral output voltage signal measured at different distances to approximation a point source of the LP Hg lamp. The measurements were performed at 255 nm wavelength.

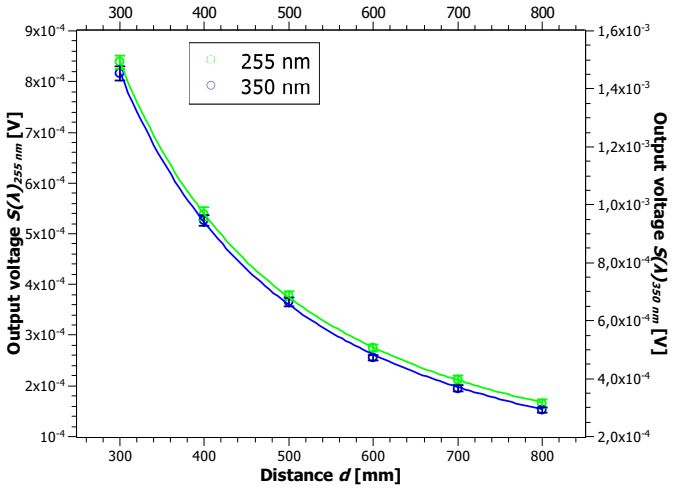

Figure 6.11: The point source approximation of the D_2 spectral irradiance STD lamp was performed at 255 nm and 350 nm wavelengths.

position for measuring the lamp's distance to the IS. The b value obtained via curve fitting was 103 mm $\pm$ 2 mm at 255 nm wavelength and 107 mm $\pm$ 5 mm at 350 nm wavelength. The measured b value was 82 mm.

6.3.5 Short term drift

A spectroradiometer short term drift is a change in the measured $S(\lambda)$ over a short period, where a maximum change is documented. This change may be caused by changes in temperature in various systems, PMT time dependence and the lamp's stability. Long term drift measurement is not a problem for comparator measurements because such drift would be constant from calibration to measurement.

When irradiated with the QTH lamp, the spectroradiometer had a measured drift of 8 % below 300 nm wavelength compared to 4 % above 300 nm (Figure 6.12). When irradiated with the D_2 lamp the spectroradiometer had a least measured drift of 1 % over 40 minutes (Figure 6.13). The drift was lower compared to 5 % when irradiated with the LP Hg lamp measured over 20 minutes (Figure 6.14). This showed that the LP Hg lamp drifted by 5 % over 20 minutes.

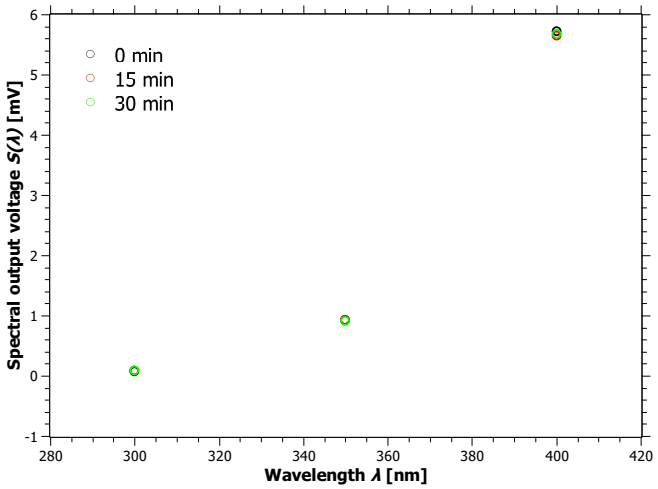

Figure 6.12: The spectroradiometer measured $S(\lambda)$ short term drift when irradiated with a QTH lamp measured over 30 minutes.

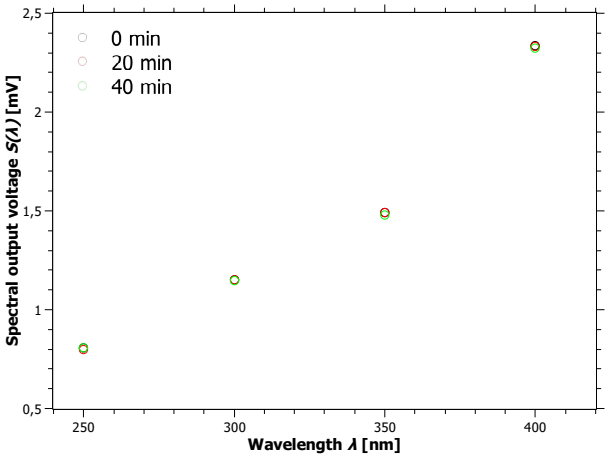

Figure 6.13: The spectroradiometer measured $S(\lambda)$ short term drift when irradiated with a D_2 lamp measured over 40 minutes.

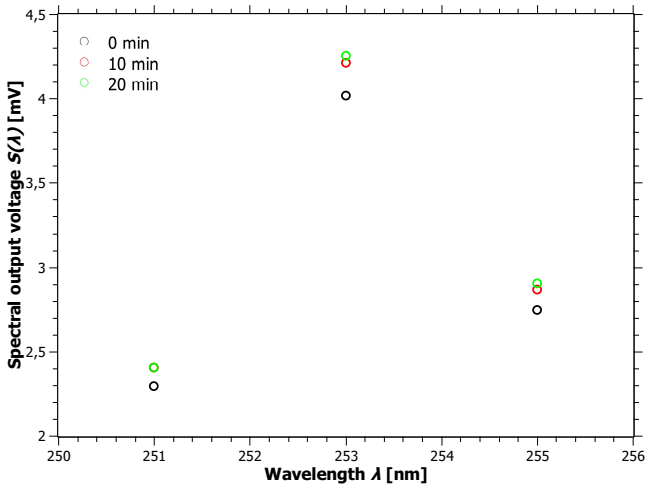

Figure 6.14: The meassured spectroradiometer $S(\lambda)$ short term drift when irradiated with a LP Hg lamp measured over a period of 20 minutes.

6.3.6 Spectroradiometer temperature dependence

Temperature changes in a laboratory during measurements of spectral irradiance may influence the measured spectral output voltage $S(\lambda)$. Components of the spectroradiometer such as detectors and current amplifiers are susceptible to changes in ambient conditions. Any deviation from the nominal value of ambient temperature can to a first order be corrected by a linear correction function with a relative temperature coefficient [Hamamatsu [1998b]]. A temperature coefficient $\alpha_{S(\lambda)}$ expresses a relation between a change in a measured output $\Delta S(\lambda)$ and a change in ambient temperature ΔT. The temperature coefficient is calculated from

$$\alpha_{S(\lambda)} = \frac{\Delta S(\lambda)}{\Delta T} \times 100\% \tag{6.13}$$

where

$$\Delta S(\lambda) = \frac{2 \times [S(\lambda)_2 - S(\lambda)_1]}{[S(\lambda)_1 + S(\lambda)_2]}, \tag{6.14}$$

is the relative change in spectral output voltage between temperature T_1 and T_2. The associated MU of the temperature coefficient depends on the linearity and resolution of the meter especially for small temperature differences. The MU of

$\alpha_{S(\lambda)}$ is given by

$$u^2_{rel}(\alpha_{S(\lambda),rel}) = \left(\frac{2S(\lambda)_1 S(\lambda)_2}{S(\lambda)^2_1 - S(\lambda)^2_2}\right)^2 (u^2_{rel}(S(\lambda)_1) + u^2_{rel}(S(\lambda)_2)) + \frac{u^2(T_1) + u^2(T_2)}{(T_1 - T_2)^2} \tag{6.15}$$

For a linear temperature dependence, the linear model holds:

$$S(\lambda)' = S(\lambda)(1 + \alpha_{S(\lambda)}\Delta T) \tag{6.16}$$

$S(\lambda)$ was investigated for dependence on temperature using the measurement setup in Figure 6.15. Since the laboratory ambient conditions are controlled, it is rare that the temperature changes by more than $\pm$ 5 °C during measurements. The temperature dependence was investigated over a range (23 $\pm$ 4) °C in 2 °C steps. The settings of the PMT detector supply voltage, monochromator bandwidth and amplifier gain were the same used during the spectral irradiance lamp calibration (Section 6.2).

Instead of a usual 1000 W QTH and 30 W deuterium standard lamps, a 250 W QTH lamp operated within a lamp housing was used. The reason for using this lamp was that its light output was controlled by a feedback mechanism to remain constant during measurements. The 250 W QTH was powered by a highly regulated commercial power supply and light intensity controller combination. The light intensity controller makes use of a temperature controlled silicon (Si) photodiode [Instruments [2015]] providing continuous feedback of the light output to the light intensity controller that in turn adjusts the power supply to keep the QTH lamp's intensity constant.

The 250 W QTH lamp was measured at two signal levels: signal level 1 was equivalent to the 1000 W QTH lamp signal and signal level 2 to the 30 W deuterium lamp signal. These signals were produced by adjusting the power supply voltage. Unlike the 250 W QTH lamp, the light output of the LP Hg lamp could not be controlled by a feedback mechanism. It was however, monitored with a temperature-stabilized UV-enhanced Si (UV-E-Si) detector [Housego [2018]]. Since the UV-E-Si detector is temperature stabilized, any temperature changes in the laboratory should have negligible effect on the detector.

The temperature of the laboratory was controlled by an air conditioner, and was allowed to stabilise overnight at each room temperature setting before measurements were performed. Two sets of measurements were performed at each

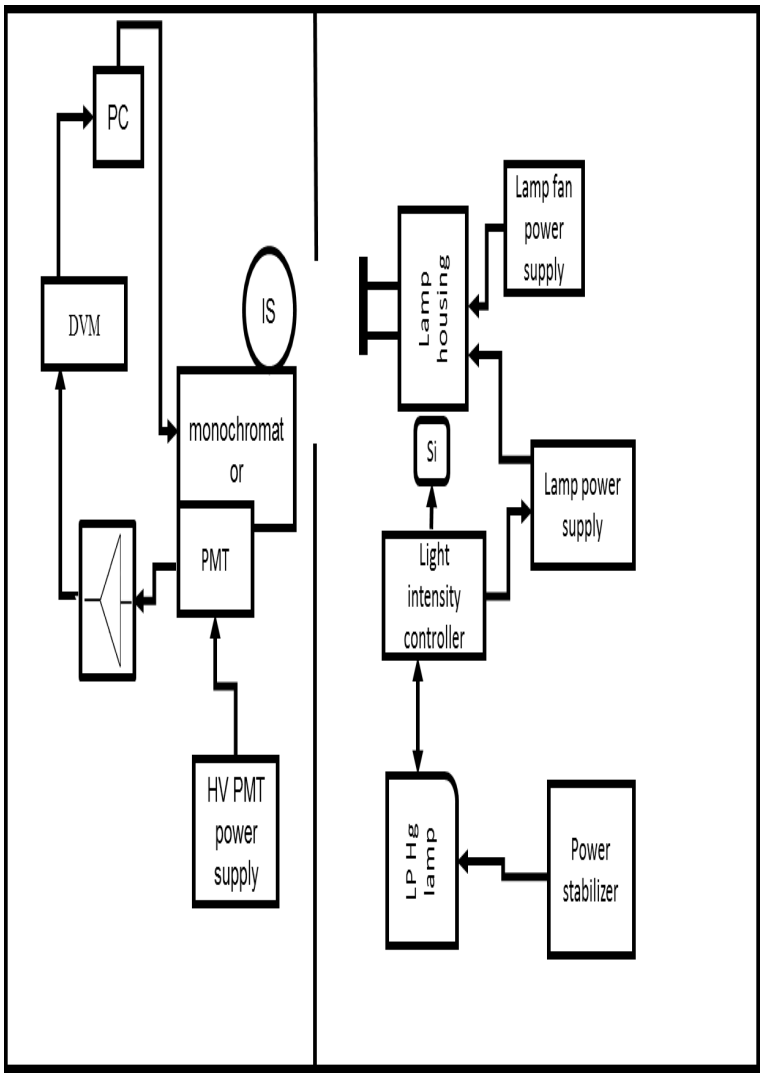

Figure 6.15: The apparent spectral irradiance $E(\lambda)$ measurement system. The setup makes use of a lamp substitution method and was used to investigate the measurement system's and the lamp's dependence on temperature. All the equipment was isolated from the air flow of the room air-conditioner.

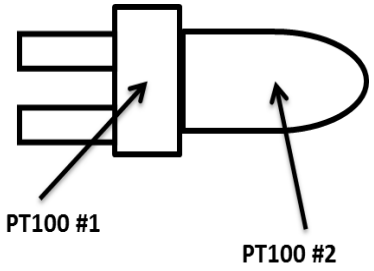

Figure 6.16: The PT100 probes mounted on the surface of the PMT detector to measure its temperature.

air-conditioner temperature setting, approximately two hours apart to account for the short term drift. The QTH lamp was switched off and on between the two sets while the LP Hg lamp was left switched-on between the sets because the lamp takes long to warm-up.

The ambient temperature was monitored with a calibrated platinum resistance thermometer (PT100) probe (PT100 #3) mounted next to the monochromator to isolate it from direct air flow of the air-conditioner. The surface temperature of the PMT detector was measured with two calibrated PT100 probes as shown in Figure 6.16. PT100 #1 measured the temperature at the base and PT100 #2 measured the temperature of its aluminium housing.

The measurements were performed at wavelengths where $S(\lambda)$ is at its maximum for both lamps: 254 nm for a LP Hg lamp and 280 nm for a 250 W QTH lamp. The PMT is more susceptible to temperature than the other electronic components shown in Figure 6.15. Therefore, the PMT must be left for an hour or longer until the photomultiplier tube reaches its operating temperature and its characteristics become stable.

The temperature characteristics of a PMT's cathode sensitivity are dependent on wavelength. The temperature coefficients of the cathode sensitivity vary significantly from a negative value to a positive value near the wavelength cut-off [Hamamatsu [2006]]. For the photocathode material, antimony-caesium (Sb-Cs), the temperature coefficient varies significantly from -0,56 %/°C at 200 nm to +0,6 %/°C at 650 nm.

Table 6.7: The temperature readings measured at different settings of the room air-conditioner, with the PT100#1 and #2 probes positioned as shown in Figure 6.16 and PT100#3 probe placed next to the monochromator.

Room temp [℃]	**PT100 #1 [℃]**	**PT100 #2 [℃]**	**PT100 #3 [℃]**
19	22,9	21,8	21,3
21	23,8	22,7	22,1
23	24,7	23,6	23,6
25	26,4	25,7	25,6
27	27,0	26,1	25,6

A small current, the anode dark current, flows in a PMT detector even when it is operated in a completely dark state. The dark current greatly depends on the supply voltage. It is due to thermionic emissions of electrons even at room temperature because of the very low work functions of the photocathode materials. Cooling the PMT photo cathode material is more effective in reducing thermionic emissions.

Results

Table 6.7 gives the measured temperature readings compared to the air-conditioner setting. The PT100 #1 probe measured higher PMT detector surface temperatures than PT100 #2 probe. This was because PT100 #1 probe was mounted on the warmer side (socket) of the PMT. The socket generated more electrical heat than the PMT inside the aluminium housing.

Figure 6.17 shows the dependence of the measured dark spectrum $S(\lambda)_{dark}$ on temperature. The dark current of the PMT depends on the photo cathode type and ambient temperature. According to [Hamamatsu [2006]], PMT detector dark counts have a positive linear dependence on temperature. In Figure 6.17 it is shown that $S(\lambda)_{dark}$ was indeed higher when operated at higher temperatures. It is also shown that the dark current is wavelength dependent.

The measurement system when illuminated with a LP Hg lamp seemed to have a negative linear temperature dependence as shown in Figure 6.18. The lamp light output was simultaneously monitored with the UV-E-Si detector; the results are shown in Figure 6.19. The results suggested that the lamp itself had a negative temperature dependence. Because the order of measurements were

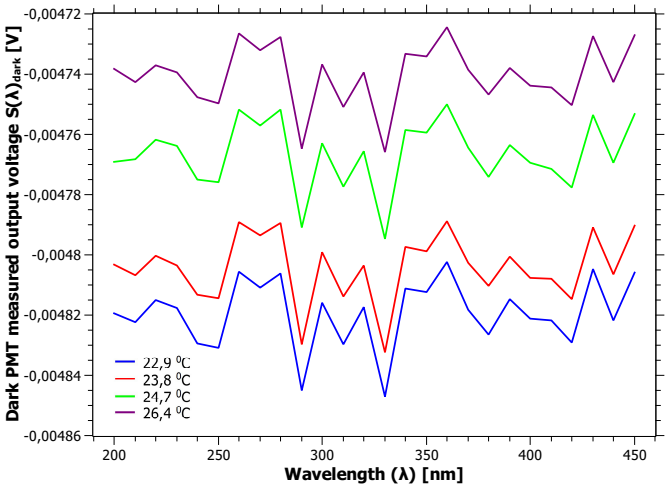

Figure 6.17: The measurement system dark spectral output voltage $S(\lambda)$ dependence on temperature measured at 1000 V PMT supply voltage and 8 nm monochromator bandwidth. The measurements were performed from low to high temperatures.

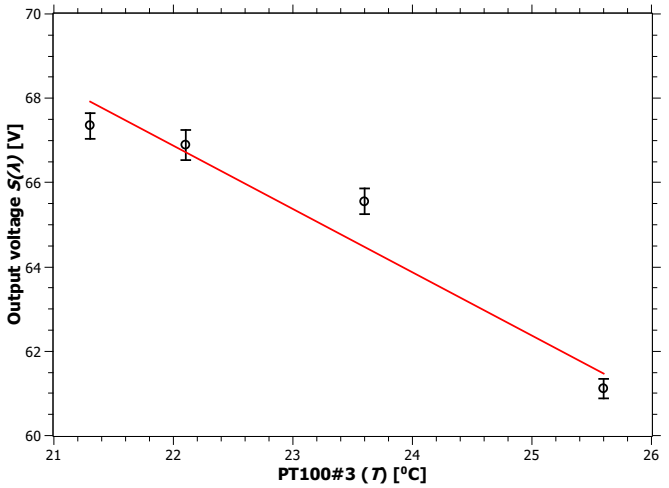

Figure 6.18: Dependence of the measured $S(\lambda)$ from the LP Hg UV-C lamp on the temperature T. The observed decreasing linear dependence of $S(\lambda)$ on T had the straight line function $S(\lambda) = -1{,}5$ mV/°C·$T+$ 99,9 mV, where T is measured in °C.

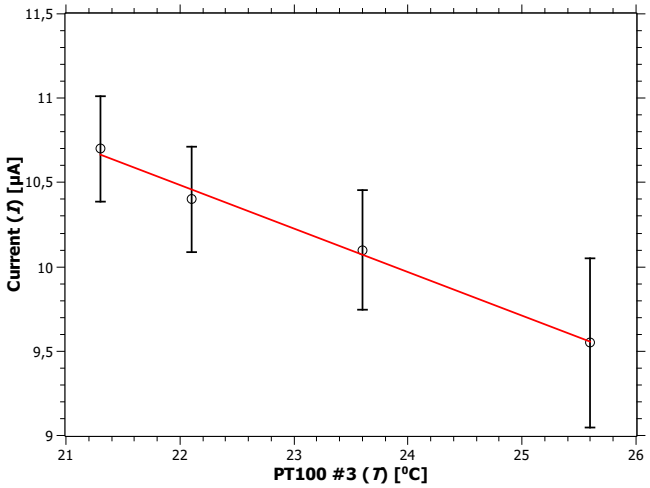

Figure 6.19: The light output of the LP Hg lamp measured as current dependence on ambient temperature. The light output was measured with a UV-E Si detector after the lamp had warmed-up for 120 minutes. The linear model was I=-0,259 (μA/°C)$\times T$+16 μA with $R^2 = 0,99$. T was measured in °C.

from low to high temperatures, the lamp output dependence on temperature was suspected to be caused by either one of two reasons: either the lamp output was lower at higher temperatures or was rapidly decreasing with usage time.

Further measurements at the same room temperature using UV-E Si detector (Figure 6.20) showed that the output of the LP Hg lamp did not decrease rapidly with usage time. This showed that the LP Hg lamp itself is sensitive to temperature changes; therefore the assumed sensitivity of the spectroradiometer is in part a lamp temperature dependence. The variation in the output during the day is explained as follows: when the lamp is started, the ballast provides high initial voltage to create the starting arc to provide proper lamp current [Kowalski [2010]]. This causes the lamp light output to first increase before it gradually drops and stabilises.

Figure 6.21 shows the measurement system dependence on temperature when corrected for the temperature dependence of the lamp. $S(\lambda)$ was calculated from Equation 6.16; $S(\lambda)$ was the measured output voltages (Figure 6.18) with $\alpha_{S(\lambda)}$ of the LP Hg lamp. The measurement system with effects of the lamp excluded, was not sensitive to temperature. The difference in $S(\lambda)$ (maximum and minimum) for the measurement system only was roughly 3 % (Figure 6.18)

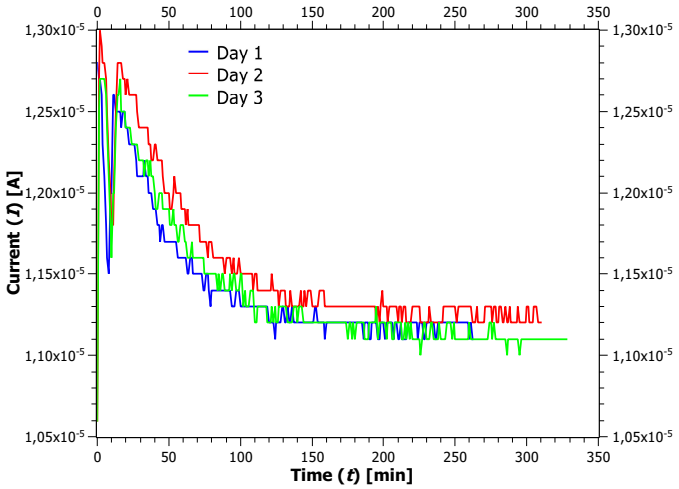

Figure 6.20: The stability of the LP Hg UV-C lamp measured at 23 °C room temperature for three consecutive days, five hours per day with the UV-E Si detector.

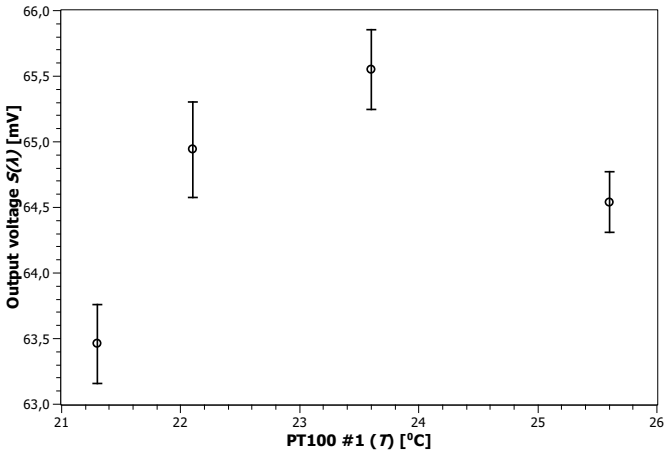

Figure 6.21: The temperature dependence of the measurement system when corrected for the temperature dependence of the LP Hg lamp.

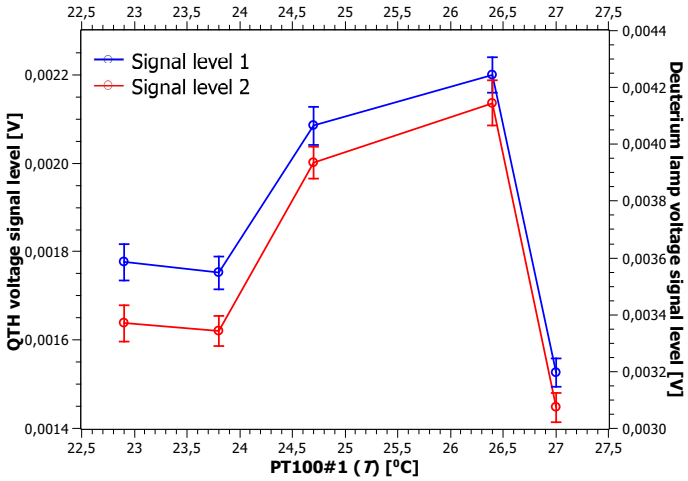

Figure 6.22: The spectroradiometer measured $S(\lambda)$ dependence on temperature when illuminated with a QTH lamp. The monochromator wavelength was set at 280 nm to achieve maximum $S(\lambda)$.

compared to 10 % (Figure 6.18) and 12 % (Figure 6.19) of the measurement system with the lamp and lamp only.

The temperature dependence of the measurement system when illuminated with a 250 W QTH lamp is shown in Figure 6.22. The measured results seem to suggest a triangular temperature dependence with $S(\lambda)$ maximum at 26,4 °C. Since below 300 nm wavelength, a QTH lamp has a low spectral distribution and a PMT detector used has a lower spectral response; the measured $S(\lambda)$ had a lower SNR. As shown in Figure 6.23, signal level 1 had a measured SNR of -2 dB at 22,9 °C increasing to -1,7 dB at 27 °C and -5,2 dB at 22,9 ° increasing to -4,6 dB at 27 °C for signal level 2. Therefore, the temperature dependence must be measured with a much better SNR.

Taken as an average, the calculated temperature coefficients in Table 6.8 were compared to literature values given in Table 6.9. The larger differences between the experimental and literature values could be due to the fact that literature values were determined for larger temperature differences using different techniques; from +20 °C to +40 °C [Singh and Wright [1987]] and from -10 °C to +40 °C as an average of 23 standard PMTs [Ogio *et al.* [2009]]. Therefore, the literature temperature coefficients were those of the PMTs not the measurement system. The standard temperature coefficient of the PMT detector used for this

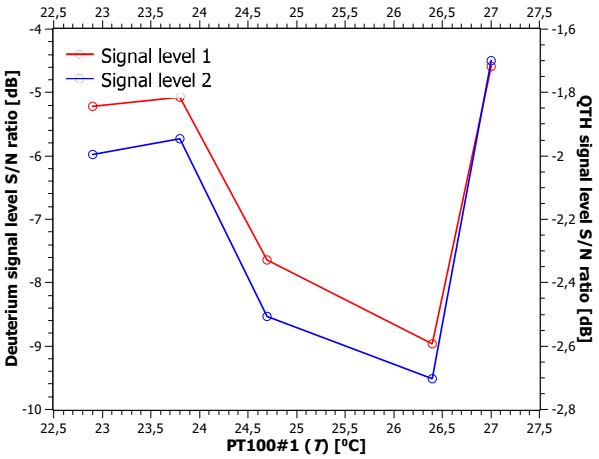

Figure 6.23: The calculated SNR of the QTH lamp at both signal levels.

Table 6.8: The temperature coefficients of the measurement system (MS) plus LP Hg lamp and measurement system only determined for ambient temperatures. The associated MU of the temperature coefficients were 1,2 % calculated using Equation 6.15.

PT100 #3 [°C]	$\alpha_{S(\lambda)}$ **of MS plus lamp [%/°C]**	$\alpha_{S(\lambda)}$ **of Lamp [%/°C]**
21,3	-1,2 $\pm$ 0,2	-2,5 $\pm$ 0,01
22,1	-1.4 $\pm$ 0,2	-2,0 $\pm$ 0,01
25,6	-3,5 $\pm$ 0,2	-2,8 $\pm$ 0,01
Average	-2,03	-2,4

Table 6.9: The literature PMT temperature coefficients.

Wavelength [nm]	**Literature** $\alpha_{m,rel}$ **[%/°C]**
200 - 300	-0,6 [Hamamatsu [2006]]
320 - 400	-0,7 [Ogio *et al.* [2009]]
400 - 800	-0,2 [Singh and Wright [1987]]

experiment is approximately -0,6 %/°C in the UV-C region [Hamamatsu [2006]].

6.4 Calibration

6.4.1 Pre-calibration procedure

Before the start of the spectral irradiance lamp calibration, the following tasks were performed (Figure 6.1):

- All electrical connections were confirmed.
- All equipment not used on the optical bench was removed to avoid light reflections into the monochromator system.
- The PMT detector power supply, the DVMs and the LP Hg lamp power stabilizer were switched on 180 minutes before the start of the measurements to allow sufficient time to warm-up.
- The maximum signal at the PMT detector was checked for all lamps. This is performed before measurements to avoid saturation of the PMT signal which could lead to non-linearity of the PMT detector. This resulted in the LP Hg lamp being calibrated at 700 mm displacement position.

6.4.2 Calibration procedure and measurements

The monochromator wavelength test was performed using the wavelength standard lamp to check if the wavelength shift of the 253,67 nm mercury line was within $\pm$ 0,2 nm as determined in Section 7.2.

Primary standards verification

The spectral irradiance calibration of the LP Hg lamp involves the use of spectral irradiance standard lamps with known spectral irradiance values. Deciding on a suitable spectral irradiance standard is one of the first steps in a lamp calibration. The D_2 STD lamp is the preferred primary standard lamp for calibrating the LP Hg lamp because of its higher signal compared to the QTH lamp in the UV-C region. For verification, the QTH STD lamp was used as the verification standard and the D_2 lamp as the UUT.

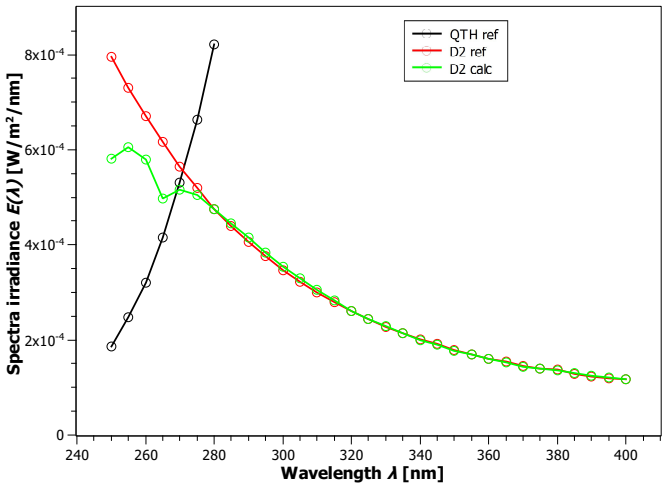

Figure 6.24: The D_2 STD lamp spectral irradiance values were verified against the values of the QTH standard lamp. QTH ref indicates the reference spectral irradiance values of the QTH lamp. D2 ref and D2 clac indicates the reference and calculated spectral irradiance values of the D_2 lamp.

The new spectral irradiance values of the D_2 lamp (indicated as D2 calc in Figure 6.24) were calculated using Equation 6.6. $\frac{E^{STD}(\lambda)}{S^{STD}(\lambda)}$ was the spectral irradiance responsivity obtained from the calibration of the measurement system with the QTH standard lamp positioned 500 mm from the IS. $S^{UUT}(\lambda)$ was the measured spectral output voltage of the D_2 lamp. In Figure 6.24, when D2 ref and D2 calc were compared, the error was 27 % for wavelengths below 280 nm. This was suspected to be caused by the low spectral distribution of the QTH standard lamp in this region. Above 280 nm where QTH lamp signal was higher, the error was 1,2 %. It is clear that the higher differences in spectral irradiance values below 280 nm was not due to the D_2 STD lamp but due to the low spectral distribution of the QTH STD lamp in this wavelength region. Therefore, the D_2 STD lamp was verified for use as a standard for calibrating the LP Hg lamp.

Spectral irradiance calibration of the LP Hg lamp

For the calibration the D_2 lamp was measured as the STD lamp and the LP Hg lamp as the UUT. The STD lamp was measured before (Set 1) and after (Set 2) the UUT. This was to check for repeatability of the STD lamp under the same measurements conditions. The STD lamp input electrical current and voltage were measured with DVM 2 throughout the calibration. This was to calculate the uncertainty of the lamp's input electrical current voltage in terms of stability and

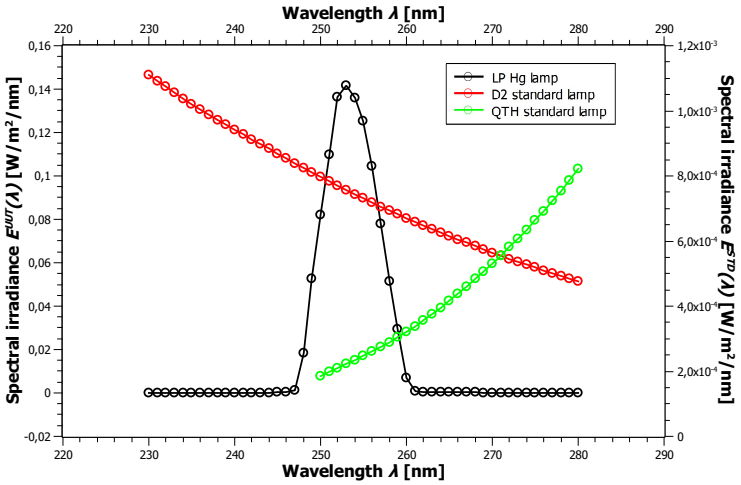

Figure 6.25: The calculated spectral irradiances of the LP Hg lamp calibrated against the responsivity determined with the D_2 STD lamp. The reference spectral irradiances of the QTH and deuterium standard lamps are also plotted.

drift. The STD lamp's light output monitoring technique was used when the lamp was switched on and again when was switched off for both sets to measure the short term drift of the lamp's output. This was used to calculate the uncertainty in the light output of the STD lamp.

The measurement system was calibrated with the D_2 STD lamp to obtain the spectral irradiance responsivity $E^{STD}(\lambda)/S^{STD}$. The measured spectral output voltage from the UUT was $S^{UUT}(\lambda)$. Spectral irradiance of the UUT was calculated from Equation 6.6 using the spectral irradiance responsivity of the measurement system and the measured $S^{UUT}(\lambda)$. The STD lamp has reference $E^{STD}(\lambda)$ values in 5 nm wavelength steps from 200 nm to 400 nm; but the UUT spectral irradiance values were desired in 1 nm wavelengths step. The cubic splines interpolation method (explained in Section 3.4) was used to interpolate the calculated spectral irradiance values in 1 nm wavelength steps. The spectral irradiance of the STD and UUT are plotted in Figure 6.25.

The literature UV-C irradiance of the UUT at 254 nm (measured at 500 mm displacement position) is 0,00275 W/m^2 [Kowalski [2010]] for 8 hours. The calculated total UV irradiance of the UUT was 1,12 W/m^2 (700 mm displacement position) from 230 nm to 375 nm wavelength region. The total UV-C irradiance was 1,08 W/m^2 from 230 nm to 280 nm wavelength region; which accounted 96

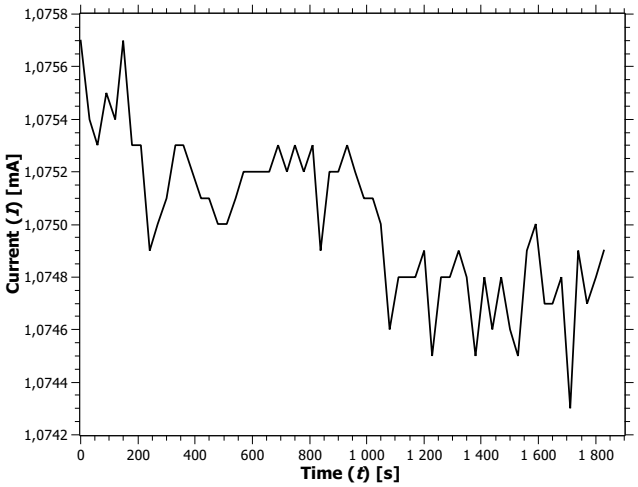

Figure 6.26: The stability of the QTH STD lamp measured with the UV-E Si detector during the period t of the standard verification. The relative uncertainty was 0,13 %.

Table 6.10: The relative uncertainties of the pencil, D_2, QTH and LP Hg lamps in terms of stability when monitored with the UV-E Si detector.

Lamps	QTH	D_2	LP Hg
Relative stability [%]	0,13	0,11	1,6

% of the total UV irradiance, and 93 % was emitted in the 248 nm to 259 nm wavelengths region because of the 253,7 nm Hg line.

Stability of spectral irradiance lamps

The stability of the spectral irradiance lamp refers to the degree to which the lamp output remains stable over time. When the lamps were measured during the calibration, their light outputs were simultaneously monitored with a UV-E Si detector for a period t. Figures 6.26, 6.27 and 6.28 shows the stability of the monitored light current output of the lamps over time t. The lamp's light output stability relative uncertainties were calculated using the ratio of ESDM and the averaged values are given in Table 6.10.

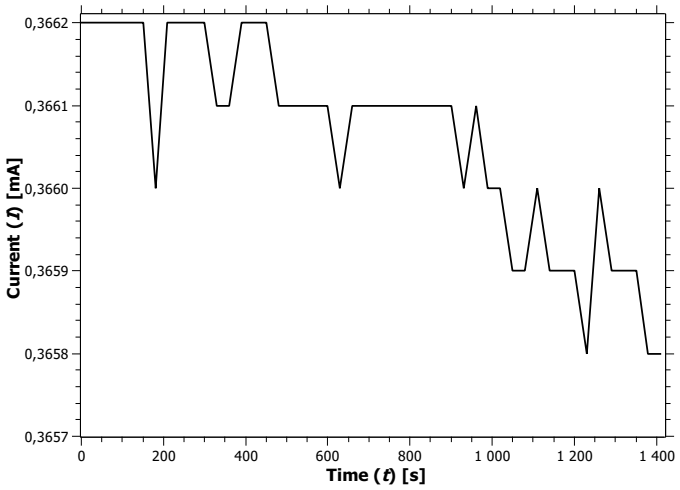

Figure 6.27: The light output of the D_2 STD lamp measured with the UV-E Si detector during the period t of the calibration. The calculated relative uncertainty was 0,11 %.

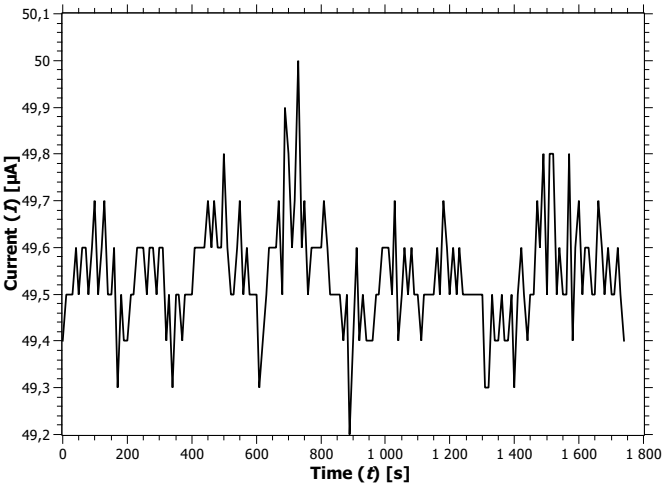

Figure 6.28: The light output of the LP Hg lamp monitored with the UV-E Si for 30 minutes. The calculated relative uncertainty was 1,6 %.

Table 6.11: The signal, current, and voltage short term stability of the deuterium spectral irradiance standard lamp. The headings in this table are defined as follows: Set 1 and 2 are the two measurements of the D_2 lamp, $\bar{x}$ was the average of Set 1 and 2, ESDM was the experimental standard deviation of the mean calculated by dividing the square root of the sum of squares of the standard deviations of light and dark measurements (before and after for the lamp signal) by the total number of measurements n (current n=9868, voltage n=9869, and signal n=539) and percentage uncertainties were calculated as a fraction of the ESDM to $\bar{x}$.

	Set 1	**Set 2**	$\bar{x}$	**ESDM**	**Uncertainty [%]**
Current [A]	0,299437	0,299439	0,29944	$2{,}4\times10^{-10}$	$8{,}1\times10^{-8}$
Voltage [V]	80,67	80,59	80,63	$2{,}1\times10^{-6}$	$2{,}6\times10^{-6}$
Signal [V]	0,02257	0,02250	0,02254	$3{,}4\times10^{-4}$	1,5

Table 6.12: The percentage difference between the experimental and theoretical electrical current and voltage input to the D_2 spectral irradiance STD lamp.

	Theoretical	**Experimental**	**Difference**
Current [A]	0,29945	0,29944	$7{,}3\times10^{-6}$
Voltage [V]	80,42	80,63	0,2
Signal [V]		0,022	

Table 6.13: The change in measured ambient temperature and humidity recorded throughout the calibration. $\bar{x}$ was the average of a total number of measurements (n=114), σ was the standard deviation for n=114, ESDM and uncertainties were defined in Table 6.11.

	$\bar{x}$	σ	**ESDM**	**Uncertainty [%]**
Temperature [°C]	22,14	0,14	0,013	0,057
Humidity [%RH]	44,16	0,34	0,032	0,072

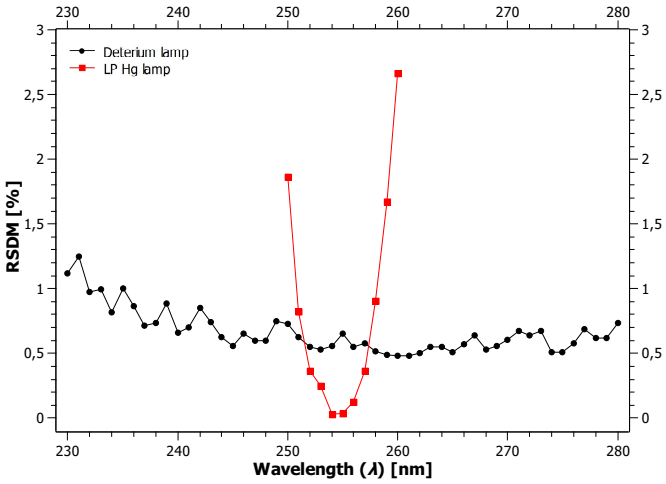

Figure 6.29: The repeatability of the D_2 STD lamp and LP Hg lamp. The repeatability was expressed as a percentage of the relative standard deviation of the mean (RSDM) as a function of wavelength.

The stability of the D_2 spectral irradiance standard lamp in terms of the input electrical current and voltage throughout Set 1 and Set 2 of the spectral irradiance lamp calibration was measured, and the results are summarized in Table 6.11. The experimental input electrical current was measured in volts and Ohm's law ($I = \frac{V}{R}$) was used to calculate the current in Amperes. I was the lamp current calculated from the lamp voltage V measured via the DVM and R was the built-in current measurement resistor of the D_2 lamp (R =1 Ω). The comparison of the theoretical (calibration certificate values) and experimental values of the input electrical current and voltage are shown in Table 6.12. Throughout the calibration ambient temperature and humidity were recorded and the uncertainties are given in Table 6.13.

The repeatability of spectral irradiance lamps

Repeatability of a measurement is the closeness of the agreement between the results of successive measurements repeated over a short period of time [BIPM and OIML [2008]]. Figure 6.29 shows the repeatability of the D_2 STD lamp from Set 1 and 2 and the repeatability of the LP Hg lamp calculated from results measured before calibration. The D_2 STD lamp had a calculated repeatability (at 254 nm wavelength) of 0,56 % compared to 0,027 % of the LP Hg lamp.

Chapter 7

Uncertainty budget

7.1 Introduction

An uncertainty budget (UB) is the table of components that contribute to the uncertainty in the measurement results. The UB is an important tool used by metrologists to perform uncertainty analysis with the goal to calculate measurement uncertainty using a well-structured approach. It provides evidence that uncertainty analysis was performed and with the aim to improve the quality of results by identifying the biggest contributors to uncertainty and identifies where improvements can be made. The UB also help increase confidence in decision-making, preventing occurrence of errors in uncertainty analysis and reduce measurement risks. The UB is made up of a number of components for each measurement uncertainty, and they are briefly described in this chapter.

More information about the uncertainty components can be found in [BIPM *et al.* [2008]], and all the uncertainties described in this section were referenced from the same document.

7.1.1 Description of uncertainties

7.1.2 Types of uncertainties and distributions

There are two types of evaluating standard uncertainties, namely: Type A and Type B.

- A Type A is a method of evaluating standard uncertainties by the statistical

analysis of a series of observations, which includes an arithemic mean, ESD, ESDM etc.

- A Type B evaluation of standard uncertainty is by using scientific judgement based on all the available information, previous measurement data, manufacturer's specifications and calibration certificates.

Probability distributions are commonly used for estimating the measurement uncertainties. The probability distributions are bounded by upper and lower limits with measurements lying in the range $x-a$ to $x+a$ where x is the true value. The standard deviation of the distribution may be written as a/K, where the divisor K depends on the type of the distribution. For instance, for a uniform distribution the value of K is 1. More information on the different types of distributions can be found in [BIPM *et al.* [2008]].

7.1.3 Standard uncertainty

The starting point when calculating the standard uncertainty $u(x_i)$ is the uncertainty estimate, which has the same units as the standard uncertainty. $u(x_i)$ is given by the quotient of the uncertainty estimate and the distribution divisor, K. The uncertainty estimate can be the semi-range (a) for values obtained in calibration certificates or manufactures' specifications.

7.1.4 Sensitivity coefficients

When evaluating uncertainties in a measurement, sensitivity coefficients (c_i) are used to convert the units of $u(x_i)$ into the units of the measurand. c_i is taken as the partial derivative of the function f in terms of a parameter contributing to uncertainty (x_i).

$$c_i = \frac{\partial f}{\partial x_i} \tag{7.1}$$

7.1.5 Uncertainty contribution

The uncertainty in the measurand, in the units of the measurand, is known as the uncertainty contribution $u(y_i)$ and is given by

$$u(y_i) = u(x_i)c_i. \tag{7.2}$$

The units of $u(y_i)$ of different uncertainty contributors must be in the units of the measurand.

7.1.6 Combined standard uncertainty

The combined standard uncertainty $u_c(y)$ takes into account all the contributors in uncertainty in the measurement system. In a case where all the input quantities are independent, $u_c(y)$ is given by the square root of the sum of squares of the uncertainty contributors

$$u_c(y) = \left(\sum_{i=1}^{n} u(y_i)^2 \right)^{\frac{1}{2}} \tag{7.3}$$

When there is a correlation the appropriate expression of the combined uncertainty must include an extra term. This is outside the scope of this study.

7.1.7 Expanded uncertainty

The expanded uncertainty U is the measure of uncertainty that defines an interval about the measurement result within which the value of the measurand lies with a certain level of confidence. U is obtained through the product of $u_c(y)$ and the coverage factor k.

$$U = kU_c(y). \tag{7.4}$$

The coverage factor is a value larger than one determined by the required level of confidence for the expanded uncertainty.

7.2 Wavelength calibration UB

The double grating monochromator was calibrated for wavelength using the Hg pencil discharge lamp lines as the standard. In this section the uncertainties are reported as absolute values.

7.2.1 Measurement model

There were two measurement equations used for calibrating the monochromator and are given below

- The first equation was used to correct the vacuum Hg lines to ambient air in the NIST EMT. The equation was (Equation 6.9)

$$\lambda_{vac} = n_{air}\lambda_{air} \tag{7.5}$$

- The second equation used relates the ambient air wavelength λ_{air} to the monochromator stepper positions y (Equation 6.10) as

$$\lambda_{air} = \frac{y}{m} + \frac{c}{m} \tag{7.6}$$

7.2.2 Uncertainty estimates

The uncertainty contributors for wavelength calibration were determined from empirical tests and literature. The contributors to uncertainty considered were:

- The uncertainty of the Hg reference line from atomic spectral database (ASD). The uncertainty was 0,0001 nm [Kramida *et al.* [2018]] at λ_{vac} of 435,96 nm, 546,23 nm and 577,12 nm. Since the Hg line at 253,73 nm falls outside the proposed range of validity, the stated uncertainty was used. It was assumed the uncertainty included the stability of the Hg line.
- The ambient conditions are the common contributors of uncertainty in the wavelength calibration. The uncertainty estimates were: 2 °C for ambient temperature, 15 %RH for relative humidity and 11,5 mmHg for pressure.

7.2.3 Sensitivity coefficients

The definition of the sensitivity coefficients and the formula was explained in subsection 7.1.4 and the formula is given by Equation 7.1. The refractive index, ambient temperature, ambient pressure and the ambient relative humidity are parameters that affect the results of wavelength calibration. To approximate the sensitivity coefficients, we changed the NMISA Photometry and Radiometry (P&R) laboratory ambient conditions in the NIST EMT with its stated limits to measured the change in ambient wavelength. A change in environmental conditions changes the refractive index of air which then changes λ_{air} according to Equation 6.9.

The uncertainties in the ambient conditions used were (24±2) °C for temperature, and (50±15) %RH for relative humidity. At the time of the measurements

Table 7.1: The change in refractive indexes of air after changing ambient parameters (temperature, pressure, and humidity) with the uncertainties of the P&R laboratory. n_{air} was the refractive index of air calculated using the nominal P&R ambient conditions, Δn_T, Δn_p and $\Delta n_{\%RH}$ were the changes in refractive index of air caused by a change in temperature, pressure and relative humidity. The ambient temperature was changed by $\pm$2 °C, pressure $\pm$ 11,5 mmHg (1,75 %) and relative humidity was changed by $\pm$15 %RH.

λ_{air} [nm]	n_{air} [1]	$\Delta n_T \pm 2°C$ [1]	$\Delta n_P \pm$11,5 mmHg [1]	$\Delta n_{\%RH} \pm$15 %RH [1]
253,67	1,00024365	$\pm$1,70$\times10^{-6}$	$\pm$4,27$\times10^{-6}$	$\pm$2,6$\times10^{-7}$
435,85	1,00023507	$\pm$1,65$\times10^{-6}$	$\pm$4,13$\times10^{-6}$	$\pm$1,6$\times10^{-7}$
546,10	1,00023241	$\pm$1,63$\times10^{-6}$	$\pm$4,08$\times10^{-6}$	$\pm$1,6$\times10^{-7}$
576,99	1,00023193	$\pm$1,63$\times10^{-6}$	$\pm$4,07$\times10^{-6}$	$\pm$1,6$\times10^{-7}$

Table 7.2: The calculated ambient air wavelengths using Equation 6.9 and the refractive index in Table 7.1.

λ_{air} [nm]	$\Delta\lambda_T$ [nm]	$\Delta\lambda_P$ [nm]	$\Delta\lambda_{\%RH}$ [nm]
253,666431	$\pm$4,32$\times10^{-4}$	$\pm$1,084$\times10^{-3}$	$\pm$6,7$\times10^{-5}$
435,853543	$\pm$7,18$\times10^{-4}$	$\pm$1,797$\times10^{-3}$	$\pm$6,8$\times10^{-5}$
546,099883	$\pm$8,91$\times10^{-4}$	$\pm$2,227$\times10^{-3}$	$\pm$8,7$\times10^{-5}$
576,987179	$\pm$9,40$\times10^{-4}$	$\pm$2,348$\times10^{-3}$	$\pm$9,2$\times10^{-5}$

NMISA P&R laboratory had no stated uncertainties for ambient pressure, however, the pressure does not change by more than 1,75 % ($\pm$11,5 mmHg) from the 657 mmHg. The changes in the refractive index are given in Table 7.1.

From Equation 6.9 we calculated the new ambient air wavelengths λ_i given in Table 7.2, where i was T (temperature), P (pressure) and %RH (relative humidity). Using Microsoft Excel Index and Linest function, these wavelengths were then used to derive the following equations:

$$\lambda_T = (0,0016679545y + 253,345835)\text{nm}, \tag{7.7}$$

$$\lambda_P = (0,001668279y + 253,33196973)\text{nm}, \tag{7.8}$$

$$\lambda_{\%RH} = (0,0016679544y + 253,345847)\text{nm}, \tag{7.9}$$

where Equations 7.7, 7.8 and 7.9 are wavelength reference equations relating to the changes in ambient temperature, pressure and percentage relative humidity. The changes in ambient conditions showed that humidity had the least influence on the wavelength in air, followed by temperature and pressure with the highest recorded change in wavelength. The λ_{air} and λ_i in Table 7.2 differed by at most 0,00043 % which showed that changes in ambient conditions within the uncertainties of the P&R laboratories do not introduce significant changes on the monochromator ambient wavelengths positions in the UV and VIS spectrum.

The approximate sensitivity coefficient equations were derived from Equation 6.9 as

$$\begin{aligned} &\partial\lambda_{equation} \longleftarrow \partial\lambda_{air} \longleftarrow \partial n_{air} \longleftarrow \partial i \\ &\approx \Delta\lambda_{equation} \longleftarrow \Delta\lambda_{air} \longleftarrow \Delta n_{air} \longleftarrow \Delta i, \end{aligned} \tag{7.10}$$

$\Delta\lambda_{equation}$ is the wavelength reference equation after changing the parameters i, $\Delta\lambda_{air}$ is the change in ambient air wavelength as a result of changing n_{air} caused by Δi. The derived approximate sensitivity coefficients were:

$$\begin{aligned} c_n &= \frac{\partial\lambda_{equation}}{\partial\lambda_{air}} \cdot \frac{\partial\lambda_{air}}{\partial n_{air}}, \\ &\approx \frac{\Delta\lambda_{equation}}{\Delta\lambda_{air}} \cdot \frac{\Delta\lambda_{air}}{\Delta n_{air}} \end{aligned} \tag{7.11}$$

The sensitivity coefficient equation for ambient temperature was

$$\begin{aligned} c_T &= \frac{\partial\lambda_{equation}}{\partial\lambda_{air}} \cdot \frac{\partial\lambda_{air}}{\partial n_{air}} \cdot \frac{\partial n_{air}}{\partial T} \\ &\approx \frac{\Delta\lambda_{equation}}{\Delta\lambda_{air}} \cdot \frac{\Delta\lambda_{air}}{\Delta n_{air}} \cdot \frac{\Delta n_{air}}{\Delta T}, \end{aligned} \tag{7.12}$$

for ambient pressure

$$\begin{aligned} c_p &= \frac{\partial\lambda_{equation}}{\partial\lambda_{air}} \cdot \frac{\partial\lambda_{air}}{\partial n_{air}} \cdot \frac{\partial n_{air}}{\partial P} \\ &\approx \frac{\Delta\lambda_{equation}}{\Delta\lambda_{air}} \cdot \frac{\Delta\lambda_{air}}{\Delta n_{air}} \cdot \frac{\Delta_{n_{air}}}{\Delta P} \end{aligned} \tag{7.13}$$

Table 7.3: The values of the sensitivity coefficients calculated from Equations 7.12, 7.13 and 7.14.

Parameters	$\frac{\Delta\lambda_{equation}}{\Delta\lambda_{air}}$ **[1]**	$\frac{\Delta\lambda_{air}}{\Delta n_{air}}$ **[nm]**	$\frac{\Delta n_{air}}{\Delta i}$	c_i
T	2,24	450,81	$8{,}26\times10^{-7}$ °C^{-1}	$8{,}34\times10^{-4}$ nm/°C
P	0,90	450,58	$3{,}60\times10^{-7}$ mmHg^{-1}	$1{,}45\times10^{-4}$ nm/mmHg
% RH	21,30	425,07	$1{,}23\times10^{-8}$ % RH^{-1}	$1{,}11\times10^{-4}$ nm/%RH

and for relative humidity

$$\begin{aligned} c_{\%RH} &= \frac{\partial\lambda_{equation}}{\partial\lambda_{air}} \cdot \frac{\partial\lambda_{air}}{\partial n_{air}} \cdot \frac{\partial n_{air}}{\partial \%RH} \\ &\approx \frac{\Delta\lambda_{equation}}{\Delta\lambda_{air}} \cdot \frac{\Delta\lambda_{air}}{\Delta n_{air}} \cdot \frac{\Delta n_{air}}{\Delta \%RH}. \end{aligned} \tag{7.14}$$

The values for the sensitivity coefficients are given in Table 7.3. The sensitivity coefficient of the Hg reference uncertainty was assigned the value 1.

7.2.4 Uncertainty contributor, combined and expanded uncertainties

The table of the uncertainty analysis is shown in Figure 7.4. $u(x_i)$ was calculated using Equation 7.2, $u_c(y)$ using Equation 7.3 and U using Equation 7.4. The reliability of the uncertainty contributors was 100 % for a Type B uncertainty evaluation which gives infinite degrees of freedom. The expanded uncertainty was calculated using a coverage factor of k=2, which for infinite degrees of freedom (100 % measurement reliability) corresponds to a level of confidence of 95,45 %. The monochromator UV-C reference wavelength position had a calibrated uncertainty of 253,67 nm $\pm$ 0,20 nm.

Table 7.4: The monochromator wavelength calibration uncertainty contributors.

	Description	Type	Uncertainty estimate	Distribution	Divisor	$u(x_i)$	Units	c_i	$u(y_i)$	Scaled units	Reliability	Degrees of freedom
Pencil lamp	Reference line (253,73 nm)	B	1,00E-04	k=2	2,00E+00	5,00E-05	nm	1,00E+00	5,00E-05	nm	100	infinite
Ambient conditions	Temperature	B	2,00E+00	Triangular	2,45E+00	8,16E-01	℃	8,34E-04 nm/℃	6,81E-04	nm	100	infinite
	Relative humidity	B	1,50E+01	Triangular	2,45E+00	6,12E+0	%RH	1,110E-04 nm/%RH	6,80E-04	nm	100	infinite
	Pressure	B	1,15E+01	Rectangular	1,73E+00	1,33E+01	mmHg	1,45E-04 nm/mmHg	9,63E-04	nm	100	infinite
								Combined Uncertainty	7,03E-02			
								Coverage factor	k=2			
								Expanded uncertainty	0,20			

7.3 Uncertainty analysis for spectral irradiance

7.3.1 Measurement model

The first step in the analysis of uncertainty is to develop a measurement model that relates the measurand (spectral irradiance) to the input quantities from the measurement setup. The model for determining spectral irradiance was derived in Equation 6.6 as

$$E^{LPHg}(\lambda) = \frac{S^{LPHg}(\lambda)}{S^{D_2}(\lambda)} \cdot E^{D_2}(\lambda) \tag{7.15}$$

- $E^{LPHg}(\lambda)$ is the calculated spectral irradiance of the lamp being calibrated, the LP Hg lamp.
- $S^{LPHg}(\lambda)$ is the spectral output voltage measured with the LP Hg lamp.
- $S^{D_2}(\lambda)$ is the measured spectral output voltage of the deuterium standard lamp.
- $E^{D_2}(\lambda)$ is the reference spectral irradiance of the deuterium standard lamp.

Since the model is multiplicative it is simpler to use relative uncertainties.

7.3.2 Sources of uncertainties

The spectroradiometer measurement setup was characterised for uncertainties in some parameters from the setup. Other sources of uncertainties were calculated from the measured results, imported from the calibration certificates and manufactures' specifications. The sources of uncertainties considered for the uncertainty analysis were:

- The STD lamp spectral irradiance reference uncertainty at 255 nm wavelength. The uncertainty estimate was 2 %, the calibration certificate is attached in Appendix B.
- The STD lamp measured input electrical voltage and current calculated uncertainties. The estimates of uncertainties were summarized in Tables 6.11 and 6.12.
- The measured $S^{STD}(\lambda)$ and $S^{UUT}(\lambda)$ short term drift. The values for estimating uncertainties were calculated from Figures 6.13 and 6.14 and are 1 % for the STD lamp and 5 % for the LP Hg lamp.

- Instability of the lamp's light output monitored with a UV enhanced Si detector. The uncertainty estimates are imported from Tables 6.10 and 6.11 as relative uncertainties and are 0,11 % for the D_2 lamp and 1,6 % for the LP Hg lamp.

- The repeatability of the LP Hg lamp and D_2 STD lamp. The repeatability was calculated as ESDM at 254 nm. The uncertainty estimates were: 0,56 % for the D_2 STD lamp and 0,027 % for the LP Hg lamp. The reproducibility of the LP Hg lamp was 0,21 % calculated from Figure 6.20.

- Misalignment of spectral irradiance lamps during calibration can introduce uncertainties of about a percent or more. The uncertainty contributors considered in alignment were discussed in Subsection 6.3.3. The uncertainty estimates are $\pm$ 1 mm in translation and $\pm$ 2 degrees in orientation.

- Information from instruments calibration certificates: includes temperature and humidity data loggers, DVMs and length rod.

7.3.3 Calculating sensitivity coefficients

The approximate sensitivity coefficients are calculated from the measurement equation for sources of uncertainties associated with the measurement model. For sources of uncertainties not associated with the measurement equation, the sensitivity coefficients were determined through a series of measurements. Alternatively the sensitivity coefficients can be calculated from the equation relating a source of uncertainty to the measurand (spectral irradiance). The sensitivity coefficients for the stated sources of uncertainties were derived as follows:

- The sensitivity coefficients of the lamp's stability, repeatability and reproducibility measurement conditions have a 1:1 influence on the measured $S^{STD}(\lambda)$ and $S^{UUT}(\lambda)$. The sensitivity coefficient was 1.

- The sensitivity coefficient used to scale the uncertainty of the length rod (used to measure the distance from the lamps to the integrating sphere opening) was derived in Equation 6.11. The equation relates the measured $S(\lambda)$ to distance d. The sensitivity coefficient was -2.

- The sensitivity coefficients of translation d and orientation θ were determined through measurements and were summarized in Table 7.5.

- The sensitivity coefficient for current related standard uncertainties is 6 [Schanda [2007]].

Table 7.5: The sensitivity coefficients for translation and orientation relative uncertainties (Table 6.5 and 6.6).

	Deuterium lamp 255 nm	**LP Hg lamp 255 nm**
Translation [%/mm]	0,24	-0,028
Orientation [%/°]	-0,13	0,50

7.3.4 Combined and expanded uncertainty

The uncertainty analysis is shown in Tables 7.6 and 7.7. $u(x_i)$ was calculated using Equation 7.2, $u_c(y)$ using Equation 7.3 and U using Equation 7.4. The reliability of the uncertainty contributors was 100 % for a Type B uncertainty evaluation which gives infinite degrees of freedom. For a Type A uncertainty evaluation, the degrees of freedom is given by $n-1$, where n is the number of measurements. The expanded uncertainty was calculated using a coverage factor of k=2, which for infinite degrees of freedom (100 % measurement reliability) corresponds to a level of confidence of 95,45 %. The largest uncertainty contributors calculated as a percentage of the total combined uncertainty are shown in Tables 7.6 and 7.7. The largest uncertainty contributors are:

- For the D_2 STD lamp, the largest contributors were: the spectral irradiance reference uncertainty, the lamp input electrical voltage drift, the measured $S^{UUT}(\lambda)$ short term drift and the lamp signal stability.
- For the LP Hg lamp, the largest contributors were: the measured $S^{STD}(\lambda)$ short term drift and the orientantion of the lamp.
- For the equipment, the largest contributors were the humidity and temperature uncertainties of the data logger.

Table 7.6: The uncertainty contributors from the deuterium STD and the LP Hg lamps.

	Description	Type	Uncertainty estimate	Distribution	Divisor	Standard uncertainty	Units	Sensitivity coefficient	Uncertainty contributor	Scaled units	Reliability	Degrees of freedom	Percentage contribution
STD lamp	Reference uncertainty	B	2,00E+00	k=2	2,00E+00	1,00E+00	%	1,00E+00	1,00E+00	%	100	infinite	25
	Lamp stability	A	1,10E-01	k=1	1,00E+00	1,10E-01	%	1,00E+00	1,10E-01	%	100	47	2,8
	Current	A	8,08E-08	Rectangular	1,73E+00	4,66E-08	%	6,00E+00	2,80E-07	%	100	9867	7,06E-06
	Voltage	A	2,64E-06	Rectangular	1,73E+00	1,52E-06	%	6,00E+00	9,15E-06	%	100	9868	2,31E-04
	Lamp signal	A	1,53E+00	Rectangular	1,73E+00	8,83E-01	%	1,00E+00	8,83E-01	%	100	538	22,3
	Current drift	A	2,45E-03	Rectangular	1,73E+00	1,41E-03	%	6,00E+00	8,47E-03	%	100	9867	0,21
	Voltage drift	A	2,61E-01	Rectangular	1,73E+00	1,51E-01	%	6,00E+00	9,05E-01	%	100	9868	22,8
	Translation	B	1,00E+00	Rectangular	1,73E+00	5,77E-01	mm	0,24 %/mm	1,39E-01	%		19	3,5
	Orientation	B	2,00E+00	Rectangular	1,73E+00	1,15E+00	degree	-0,13 %/degree	-1,50E-01	%		19	3,8
	Short term drift	B	1,00E+00	Rectangular	1,73E+00	5,77E-01	%	1,00E+00	5,77E-01	%		19	14,6
	Repeatability	A	5,60E-01	Rectangular	1,73E+00	3,23E-01	%	1,00E+00	3,23E-01	%		51	8,2
								Combined uncertainty	1,76				
UUT	Lamp stability	A	1,60E+00	k=1	1,00E+00	1,60+00	%	1,00E+00	1,60+00	%			40,4
	Translation	B	1,00E+00	Rectangular	1,73E+00	5,77E-01	mm	-0,028 %/mm	-1,62E-02	%	100	infinite	0,41
	Orientation	B	2,00E+00	Rectangular	1,73E+00	1,15E+00	degree	0,5 %/degree	5,77E-01	%	100	100	14,6
	Short term drift	B	5,00E+00	Rectangular	1,73E+00	2,89E+00	%	1,00E+00	2,89E+00	%	100	infinite	72,3
	Repeatability	B	2,72E-02	Rectangular	1,73E+00	1,57E-02	%	1,00E+00	1,57E-02	%		9	3,21
	Reproducibility	B	2,10E-01	Rectangular	1,73E+00	1,21E-01	%	1,00E+00	1,21E-01	%		329	3,06
								Combined uncertainty	3,96				

Table 7.7: Uncertainty contributors of the equipment used during calibration.

	Description	Type	Uncertainty estimate	Distribution	Divisor	Standard uncertainty	Units	Sensitivity coefficient	Uncertainty contributor	Scaled units	Reliability	Degrees of freedom	Percentage contribution
Environmental conditions	Temperature	A	5,71E-02	Triangular	2,45E+00	2,33E-02	%	1,00E+00	2,33E-02	%			0,6
	Humidity	A	7,17E-02	Triangular	2,45E+00	2,93E-02	%	1,00E+00	2,93E-02	%	infinite		0,74
DVM	Resolution	B	6,20E-05	Rectangular	1,73E+00	3,58E-05	%	6,00E+00	2,15E-04	%	100	infinite	0,01
	Uncertainty	B	6,00E-04	k=2	2,00E+00	3,00E-04	%	6,00E+00	1,80E-03	%	100	infinite	0,05
	Offset	B	1,00E-04	Rectangular	1,73E+00	5,77E-05	%	6,00E+00	3,46E-04	%	100	infinite	0,01
	Resolution	B	1,67E-04	Rectangular	1,73E+00	9,64E-05	%	6,00E+00	5,78E-04	%	100	infinite	0,02
	Uncertainty	B	3,10E-04	k=2	2,00E+00	1,55E-04	%	6,00E+00	9,29E-04	%	100	infinite	0,03
	Offset	B	0,00E+00	Rectangular	1,73E+00	0,00E+00	%	6,00E+00	0,00E+00	%	100	infinite	0,00E+00
	Resolution	B	5,00E-05	Rectangular	1,73E+00	2,89E-05	%	6,00E+00	1,73E-04	%	100	infinite	4,37E-03
	Uncertainty	B	1,99E-06	k=2	2,00E+00	9,94E-07	%	6,00E+00	5,96E-06	%	100	infinite	1,51E-04
	Offset	B	4,00E-04	Rectangular	1,73E+00	2,31E-04	%	6,00E+00	1,39E-03	%	100	infinite	0,03
	Resolution	B	5,00E-05	Rectangular	1,73E+00	2,89E-05	%	6,00E+00	1,73E-04	%	100	infinite	4,37E-03
	Uncertainty	B	2,40E-04	k=2	2,00E+00	1,20E-04	%	,00E+00	7,21E-04	%	100	infinite	0,02
	Offset	B	1,00E-04	Rectangular	1,73E+00	5,77E-05	%	6,00E+00	3,46E-04	%	100	infinite	0,01
Length rod	Uncertainty	B	3,11E-04	k=2	2,00E+00	1,56E-04	%	-2,00E+00	-3,11E-04	%	100	infinite	0,01
	offset	B	2,11E-01	Rectangular	1,73E+00	1,22E-01	%	2,00E+00	2,43E-01	%	100	infinite	6,14
Temp & Hum data logger	Resolution	B	2,26E-01	k=2	2,00E+00	1,13E-01	%	1,00E+00	1,13E-01	%	100	infinite	2,9
	Uncertainty	B	1,35E+00	k=2	2,00E+00	6,77E-01	%	1,00E+00	6,77E-01	%	100	infinite	17,1
	Resolution	B	1,13E-01	k=2	2,00E+00	5,65E-02	%	1,00E+00	5,65E-02	%	100	infinite	1,4
	Uncertainty	B	1,81E+00	k=2	2,00E+00	9,04E-01	%	1,00E+00	9,04E-01	%	100	infinite	22,8
Wavelength calibration	Uncertainty	B	5,54E-02	k=2	2,00E+00	2,77E-02	%	1,00E+00	2,77E-02	%	100	infinite	0,7
								Combined uncertainty	1,16				

Table 7.8: The spectral irradiance total uncertainty calculated for a level of confidence of 95,45 %.

Combined uncertainty [%]	**Coverage factor [1]**	**Expanded uncertainty [%]**
$u_c(y)$ = 3,96	k = 2	U = 8,0

The spectral irradiance had a calibrated uncertainty of 8 % for a coverage factor of k=2 (Table 7.8), which was the total contribution (combined uncertainty) of the STD, UUT and equipment used. The P&R has a calibration measurement capability (CMC) uncertainty of 11 % for UV-C lamps calibration [Sanas [2016]].

Chapter 8

Conclusion

This research developed and investigated the measurements for calibrating a LP Hg lamp. This lamp is used as a source standard at NMISA for disseminating the unit of spectral irradiance to industry, research facilities and health sector. The resolutions to the investigated practical aspects were:

- Noise of the measurement system: From the measurements it was found that to ensure sufficiently high SNR, the monochromator bandwidth must be set to 8 nm when working with a PMT supply voltage of 1000 V.
- Monochromator wavelength calibration: The monochromator is calibrated for wavelength at least once a year using a pencil lamp as the standard. The wavelength calibration performed had a calibrated expanded uncertainty of 0,2 nm. It was found that a wavelength test had to be performed before measurements to ensure that the wavelength shift of the monochromator remains within $\pm$ 0,2 nm of the 253,67 nm Hg line.
- Alignment of lamps: Alignment of lamps has an influence on the measured spectroradiometer spectral output voltage $S(\lambda)$. Uncertainties introduced by $\pm$1 mm displacement position were $\pm$ 0,005 % for a LP Hg lamp and $\pm$ 0,2 % for a D_2 STD lamp. Orientation around a vertical axis ($\pm$ 2 degrees) had uncertainties of $\pm$ 0,6 % and $\pm$ 0,3 % for a LP Hg lamp and D_2 STD lamp, respectively. The uncertainties showed that alignment of lamps have a significant influence on the measured $S(\lambda)$. Consideration must be given to alignment of lamps as this aspect greatly influence the measured spectroradiometer spectral output voltage $S(\lambda)$.
- Short term drift: The spectral output voltage $S(\lambda)$ was measured to determine drift over a short period. The drift was 1 % when the spectroradiometer

was irradiated with a D_2 lamp and 5 % when irradiated with a LP Hg lamp. Given the 1 % drift when the D_2 lamp was used compared to 5 % when the LP Hg was used, it can be deduced that the light output of the LP Hg lamp changed by roughly 5 %.

- Temperature dependence: The dependence of measurement system on ambient temperature in the region 23$\pm$4 °C was investigated. The measured results showed that the measurement system was less sensitive to ambient temperature than the LP Hg lamp. The LP Hg lamp had a measured decreasing linear dependence on ambient temperature with a calculated average temperature coefficient of -2,4 %/°C.

Even though the spectroradiometer system had a measured higher drift when irradiated with the LP Hg lamp, it was however calibrated with an expanded uncertainty of 8 %. The expanded uncertainty was lower than the 11 % for which NMISA is accredited for. The lamp had a calibrated total UV-C irradiance of 1,08 W/m^2 from wavelengths from 230 nm to 280 nm. The study recommends LP Hg lamps for use as a source standard, due to their good light output stability of 1,6 %. Note should, however, be taken of a significant temperature dependence of their output as well as sensitivity toward orientation about the horizontal axis.

Appendices

Appendix A

List of acronyms

ASD atomic spectral database

BIPM International Bureau of Weights and Measures

CCPR Consultative Committee of Photometry and Radiometry

CGPM General Conference on Weights and Measures

CIPM International Committee for Weights and Measures

CIE International Commission on Illumination

D_2 deuterium

DC direct current

DLS deuterium lamp system

CMC calibration measurement capability

DNA deoxyribonucleic acids

DTI Department of Trade and Industry

DVM Digital voltmeter

EMT Engineering Metrology Toolbox

EMR electromagnetic radiation

ESD experimental standard deviation

ESDM experimental standard deviation of the mean

Hg mercury

HTBB high temperature blackbody

IS integrating sphere

KCRV key comparison reference value

LP low pressure

MRA mutual recognition agreement

MU measurement uncertainty

NMI national metrology institute

NMIs national metrology institutes

NMISA National Metrology Institute of South Africa

NIST National Institute of Standards and Technology

NPL National Physical Laboratory

NRC National Research Council

PMT photo multiplier tube

PTB Physikalisch-Technische Bundesanstalt

PTFE polytetrafluorethylene

QTH quartz tungsten halogen

RMO regional metrology organisation

RSDM relative standard deviation of the mean

SI International System of Units

SBR signal-to-background ratio

SNR signal-to-noise ratio

STD standard

TB tuberculosis

UB uncertainty budget

UUT unit being calibrated

UV ultraviolet

UVGI ultraviolet germicidal irradiation

VUV vacuum ultraviolet

VIS visible

WHO world health organisation

Appendix B

Calibration certificates of standards lamps

Physikalisch-Technische Bundesanstalt

Braunschweig und Berlin

Kalibrierschein
Calibration Certificate

Gegenstand: *Object:*	Eine Deuteriumlampe im Lampengehäuse
Hersteller: *Manufacturer:*	Schreder
Typ: *Type:*	Deuterium-Lampen-System J1016 (DLS-J1016) bestehend aus Deuteriumlampe im Lampengehäuse (S/N L1171),Netzgerät (S/N 09-0883200038), Justierhilfe (JIG) und Monitordetektor (MON)
Kennnummer: *Serial number:*	1171
Auftraggeber: *Applicant:*	NMISA CSIR Campus Meiring Naude Road Pretoria Brummeria South Africa
Anzahl der Seiten: *Number of pages:*	6
Geschäftszeichen: *Reference No.:*	PTB-4.11-4062392
Kalibrierzeichen: *Calibration mark:*	40007-13-PTB
Datum der Kalibrierung: *Date of calibration:*	14.03.2013

Es wird hiermit beglaubigt, dass die Fotokopie mit der Urschrift übereinstimmt.
Braunschweig, 25.10.13
i.A. Hildy

Im Auftrag
On behalf of PTB
Dr. Peter Sperfeld

Braunschweig, 2013-04-15
Siegel
Seal

Im Auftrag
On behalf of PTB
Sven Pape

391 00b h

Kalibrierscheine ohne Unterschrift und Siegel haben keine Gültigkeit. Dieser Kalibrierschein darf nur unverändert weiterverbreitet werden. Auszüge bedürfen der Genehmigung der Physikalisch-Technischen Bundesanstalt.
Calibration certificates without signature and seal are not valid. This calibration certificate may not be reproduced other than in full. Extracts may be taken only with the permission of the Physikalisch-Technische Bundesanstalt.

Physikalisch-Technische Bundesanstalt

Bild 1: Darstellung der Justierung des Kalibriergutes. Die Abstandsmessung bezieht sich auf die Vorderfläche der Justierhilfe.

1. Beschreibung des Kalibrierguts

Es handelt sich um eine handelsübliche Deuteriumlampe, die in ein Gehäuse eingebaut wurde, das mit einer Aufnahmemöglichkeit für die Justierhilfe und für den Monitordetektor versehen ist. Auf der Oberseite des Lampengehäuses und auf der Rückseite ist die Kennzeichnung 1171 angebracht. Auf der Rückseite befindet sich zusätzlich noch eine Anschlussbuchse zur Messung von Lampenstrom und Lampenspannung.
Die zugehörige Justierhilfe ist mit der Kennzeichnung DLS-J1016-JIG versehen und auf dem Monitordetektor befindet sich die Kennzeichnung DLS-J1016-MON.

2. Messverfahren

Die spektrale Bestrahlungsstärke $E_\lambda(\lambda)$ wurde durch einen Vergleich mit der bekannten spektralen Bestrahlungsstärke einer Gruppe von Normallampen bestimmt. Bei dem Vergleich wurde ein Reflexionsnormal senkrecht zu seiner Oberfläche nacheinander vom Prüfling und von dem Vergleichsnormal bestrahlt. Die vom Reflexionsnormal innerhalb eines definierten Raumwinkels diffus reflektierte Strahlung wurde nach spektraler Aussonderung durch einen Doppel-Gittermonochromator mit einem Photomultiplier gemessen.

3. Messbedingungen

Aufstellung des Prüflings: Die in einem Lampengehäuse eingebaute Lampe wurde in senkrechter Brennstellung betrieben. Die Öffnung des Lampengehäuses zeigte in Messrichtung.

Messgeometrie: Die Lampe war so justiert, dass die waagerecht verlaufende optische Achse der Messapparatur auf die Mitte der in Strahlungsrichtung zeigenden Justierhilfe traf. Die Vorderfläche der Justierhilfe wurde senkrecht zur optischen Achse ausgerichtet. Die für die gemessene spektrale Bestrahlungsstärke maßgebende Ebene der Oberfläche des Reflexionsnormals stand in 300 mm Entfernung von der in Messrichtung zeigenden Vorderseite der Justierhilfe, gemessen etwa 15 mm unterhalb der optischen Achse (siehe Bild 1). Die für die Messung relevante bestrahlte Fläche, eine vor dem ebenen Reflexionsnormal angebrachte Blende, hatte einen Durchmesser von 10 mm.

Es wird hiermit beglaubigt, dass die Fotokopie mit der Urschrift übereinstimmt.
Braunschweig, 25.10.13
i.A. Hildy

Spektrale Bandbreite
des Monochromators: Halbwertbreite (FWHM)

$\Delta\lambda =$ 5 nm für 195 nm $\leq \lambda <$ 215 nm

$\Delta\lambda =$ 3 nm für 220 nm $\leq \lambda \leq$ 400 nm

Lampenstrom: 299,526 ± 0,008 mA Gleichstrom, jeweils 45 min vor Beginn der Messungen eingeschaltet, gemessen als Spannungsabfall über einen im Lampengehäuse eingebauten 1 Ohm Messwiderstand.
Es wurde das mitgelieferte Netzgerät (Seriennummer 09-0883200038) verwendet, das den oben angegebenen Lampenstrom fest vorgibt.

Polarität: Die Polarität wurde durch einen kodierten Stecker vorgegeben.

Lampenspannung bei der vorgegebenen Stromstärke: 79,92 ± 0,12 V (während einer Messdauer von 3 h) gemessen an der Anschlussbuchse am Lampengehäuse.

Betriebsdauer: Die Lampe wurde während der Messungen ca. 4,5 h bei der angegebenen Stromstärke betrieben.

Umgebungstemperatur: (22 ± 1) °C

Physikalisch-Technische Bundesanstalt

4. Messergebnisse

λ	$E_\lambda(\lambda)$	$u(E_\lambda)$
nm	W * m^{-2} *nm^{-1}	%
200	0,00148	5
205	0,00150	4
210	0,00144	4
215	0,00139	4
220	0,00132	4
225	0,00123	3
230	0,00115	3
235	0,00107	3
240	0,000982	3
245	0,000902	2
250	0,000828	2
255	0,000762	2
260	0,000699	2
265	0,000639	2
270	0,000586	2
275	0,000539	2
280	0,000493	2
285	0,000454	2
290	0,000417	2
295	0,000384	2
300	0,000354	3
305	0,000329	3
310	0,000305	3
315	0,000284	3
320	0,000266	3
325	0,000246	3
330	0,000231	3
335	0,000217	3
340	0,000204	3
345	0,000192	4
350	0,000181	4
355	0,000171	4
360	0,000162	4
365	0,000154	5
370	0,000147	5
375	0,000139	5
380	0,000138	6
385	0,000129	6
390	0,000124	7
395	0,000121	7
400	0,000118	7

Angegeben ist jeweils die erweiterte relative Messunsicherheit u(E), die sich aus der relativen Standardmessunsicherheit durch Multiplikation mit dem Erweiterungsfaktor $k = 2$ ergibt. Sie entspricht bei einer Normalverteilung der Abweichung vom Messwert einer Überdeckungswahrscheinlichkeit von 95 %. Die Standardmessunsicherheit ist gemäß dem „Guide to the Expression of Uncertainty in Measurement" (ISO 1995) ermittelt worden.

Es wird hiermit beglaubigt, dass die Fotokopie mit der Urschrift übereinstimmt.
Braunschweig, 15.10.13

5. Bemerkungen

- Die Messungen erfolgten im direkten Vergleich gegen 3 Transfernormale: DLS-PTB-L#01, DLS-PTB-L#02 und DLS-PTB-L#07.
- Die Kalibrierung ist rückgeführt auf einen Schwarzer Strahler als das nationale Primärnormal der PTB für spektrale Bestrahlungsstärke.

Es wird hiermit beglaubigt, dass die Fotokopie mit der Urschrift übereinstimmt.
Braunschweig, 25.10.13
i. A. Grilly

Physikalisch-Technische Bundesanstalt

Seite 6 zum Kalibrierschein vom 2013-04-15, Kalibrierzeichen: 40007-13-PTB
Page 6 of calibration certificate of 2013-04-15, calibration mark: 40007-13-PTB

Die Physikalisch-Technische Bundesanstalt (PTB) in Braunschweig und Berlin ist das nationale Metrologieinstitut und die technische Oberbehörde der Bundesrepublik Deutschland für das Messwesen. Die PTB gehört zum Geschäftsbereich des Bundesministeriums für Wirtschaft und Technologie. Sie erfüllt die Anforderungen an Kalibrier- und Prüflaboratorien auf der Grundlage der DIN EN ISO/IEC 17025.

Zentrale Aufgabe der PTB ist es, die gesetzlichen Einheiten in Übereinstimmung mit dem Internationalen Einheitensystem (SI) darzustellen, zu bewahren und weiterzugeben. Die PTB steht damit an oberster Stelle der metrologischen Hierarchie in Deutschland. Die Kalibrierscheine der PTB dokumentieren eine auf nationale Normale rückgeführte Kalibrierung.

Dieser Ergebnisbericht ist in Übereinstimmung mit den Kalibrier- und Messmöglichkeiten (CMCs), wie sie im Anhang C des gegenseitigen Abkommens (MRA) des Internationalen Komitees für Maße und Gewichte enthalten sind. Im Rahmen des MRA wird die Gültigkeit der Ergebnisberichte von allen teilnehmenden Instituten für die im Anhang C spezifizierten Messgrößen, Messbereiche und Messunsicherheiten gegenseitig anerkannt (nähere Informationen unter http://www.bipm.org).

CIPM MRA

The Physikalisch-Technische Bundesanstalt *(PTB) in Braunschweig and Berlin is the National Metrology Institute and the supreme technical authority of the Federal Republic of Germany for metrology. The PTB comes under the auspices of the Federal Ministry of Economics and Technology. It meets the requirements for calibration and testing laboratories as defined in DIN EN ISO/IEC 17025.*

The central task of PTB is to realize, to maintain and to disseminate the legal units in compliance with the International System of Units (SI). PTB thus is at the top of the metrological hierarchy in Germany. The calibration certificates issued by PTB document a calibration traceable to national measurement standards.

This certificate is consistent with the Calibration and Measurement Capabilities (CMCs) that are included in Appendix C of the Mutual Recognition Arrangement (MRA) drawn up by the International Committee for Weights and Measures (CIPM). Under the MRA, all participating institutes recognize the validity of each other's calibration and measurement certificates for the quantities, ranges and measurement uncertainties specified in Appendix C (for details, see http://www.bipm.org).

Es wird hiermit beglaubigt, dass die Fotokopie mit der Urschrift übereinstimmt.
Braunschweig, 25.10.13
i. A. Grilly

Physikalisch-Technische Bundesanstalt
Bundesallee 100
D-38116 Braunschweig
DEUTSCHLAND

Abbestraße 2-12
D-10587 Berlin
DEUTSCHLAND

Kalibrierlaboratorium für optische Strahlungsmessgrößen
Calibration laboratory for optical radiometry

GIGAHERTZ OPTIK GMBH

Einbrennzertifikat
Burn In Certificate

Gegenstand *Object*	**QH-lamp with mechanical holder**
Hersteller *Manufacturer*	**Gigahertz-Optik GmbH**
Typ *Type*	**FEL, 1000W, 120V** **Intern: F151**
Fabrikate/Serien-Nr. *Serial number*	**BN-9101-534**
Auftraggeber *Customer*	**NMISA** **Privat Bag X34 Lynnwood Ridge** **ZA-0040 Pretoria**
Auftragsnummer *Order No.*	**PO00004608 / (18133)**
Anzahl der Seiten des Einbrennzertifikats *Number of pages of the certificate*	**3**
Datum *Date*	**17-Jun-16**

Dieses Einbrennzertifikat darf nur vollständig und unverändert weiterverbreitet werden. Auszüge oder Änderungen bedürfen der Genehmigung des Kalibrierlaboratoriums der Firma Gigahertz-Optik Gesellschaft für technische Optik mbH.
Einbrennzertifikate ohne Unterschrift und Stempel haben keine Gültigkeit.

This burn in certificate may not be reproduced other than in full except with the permission of the Gigahertz-Optik GmbH.
Burn in certificates without signature and seal are not valid.

Stempel *Seal*	Stellv. Leiter des Kalibrierlaboratoriums *Deputy Head of the calibration laboratory*
	Dipl.-Ing. (FH) Stephan Fenk

• Gigahertz Optik GmbH • An der Kälberweide 12 • 82299 Türkenfeld • Tel. +49 (0)8193-93700-0 • Fax +49 (0)8193-93700-50 •

1. Beschreibung des Prüfgegenstandes:
Es handelt sich um eine selektierte Wolfram-Halogen-Glühlampe mit einem Quarzkolben, die in einem speziellen Lampenhalter für Messlampen montiert ist.
1. Description of the object:
The burn in object is a selected Tungsten-halogen-lamp with a quartz bulb. The lamp was mounted in a special lamp holder.

2. Messverfahren:
Der Strom der Lampe wird mittels Spannungsabfall über einen 100mΩ Shunt gemessen. Die Spannung wird direkt an der Lampe gemessen.
2. Measurement:
The current of the lamp was measured by a 100mΩ Shunt. The voltage was measured directly on the lamp.

3. Messbedingungen:
Aufstellung des Prüflings:
Senkrechter Brennstelle ohne Gehäuse. Die Lampe wurde nur in kaltem Zustand bewegt.
Lampenstrom:
8,0000 A Gleichstrom, Dauer der Ein- und Ausschaltvorgänge jeweils 80 Sekunden, durch Rechner gesteuert.
Polarität:
Sie wurde an den Anschlussklemmen durch Kennzeichnung („+“= rot und „-“= schwarz) vorgegeben.
Lampenspannung bei der vorgegebenen Stromstärke:
ca. 112,2V, gemessen mit separater Zuleitung an den Anschlussklemmen des Lampenhalters.

3. Conditions during burn in:
Setting up of the object:
Vertical, without housing. The lamp was only moved in cold conditions.
Current of the lamp:
8,0000 A DC, the lamp was started and ended by a current ramp, about 80 seconds, by computer.
Polarity:
It was shown on the lamp holder (“+” = red and “-“ = black).
Lamp voltage at the given current:
About 112,2V, measured with separated cable at the lamp holder.

4. Bemerkungen:
Auf der Rückseite des Lampenhalters ist die Kennzeichnung BN-9101-534 eingraviert. Die Lampe wurde 30 Stunden eingebrannt und die letzten 15 Stunden dokumentiert.
4. Remarks:
On the backside of the lamp holder, there is the designation BN-9101-534. The lamp was burned in 30 hours and the last 15 hours documented.

Current of the lamp

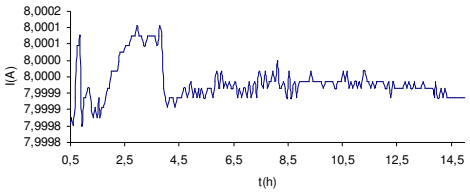

Voltage of the lamp

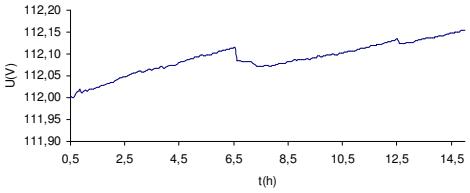

Slope of the long-term stability result

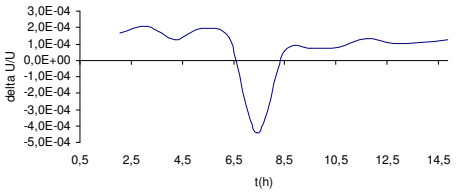

Appendix C

Publications

Proceedings of SAIP2017

Characterization of the spectral irradiance lamps at NMISA

Macdufe Mkabela[1,2*], Pieter Du Toit[1], Rheinhardt Sieberhagen[1], Walter Meyer[2]

[1] National Metrology Institute of South Africa, Private bag X34, Lynnwood Ridge, 0040, South Africa
[2]University of Pretoria, Private Bag X20, Hatfield, 0028, South Africa

E-mail: *mmkabela@nmisa.org

Abstract: This work investigates some of the uncertainty contributions to the spectral irradiance calibration of UV-C lamps. The radiometry concepts and the instrumentation used are addressed first. In ultraviolet (UV) spectroradiometry, spectral irradiance measurements have large uncertainties mainly due to a low signal-to-noise ratio (SNR) in the UV region; however other factors may also contribute to these high uncertainties. Therefore quantifying the sources of uncertainties is important to improve the accuracy of the measured results. We characterized a low pressure mercury lamp when compared to a tungsten halogen lamp when used as standards for spectral irradiance at the National Metrology Institute of South Africa (NMISA), in terms of stability, translation, and orientation. We found that the calibrations of the UV-C low pressure mercury lamps are not suitable as standard lamps for calibration of UV-C due to uncertainties introduced by orientation, translation and, instability effects of this lamp.

1. Introduction

Metrology is concerned with the accurate measurement of physical quantities and requires the determination of uncertainty of measurement. Radiometry is the field concerned with the accurate measurement of radiant energy (Q) across the entire electromagnetic spectrum (EMS), and the determination of how this energy is transferred from a source, through a medium, and to a detector [1]. Traditionally, radiometry assumes that the propagation of light can be modelled using the laws of geometric optics, and in practice radiometric measurements are limited to the optical (ultraviolet (UV), visible (VIS), and infrared (IR)) region. The International Commission on Illumination (CIE) divides the UV region into four regions (VUV, UV-C (200 nm – 280 nm), UV-B, and UV-A) based on the biological effects on microorganisms [2]. In this study we focus on the measurement of UV-C radiation of the EMS. The UV-C radiation is important because of its germicidal effectiveness on microorganisms in air and other media.

The use of radiation in the germicidal region can help combat the spread of mycobacterium tuberculosis (TB) and other microorganisms in South Africa, mainly at hospital in waiting areas and treatment rooms. This technology is referred to as air UV germicidal irradiation (UVGI) [3]. Accurate measurement of the UV-C radiation emitted by UVGI lamps is very important for the safety of staff and patients, and South African citizens in general.

The radiometric quantities of interest are introduced here. Radiometric quantities are usually wavelength dependent; the spectral quantities are radiometric quantities taken as a function of wavelength. The flux Φ emitted by the source incident on a surface per unit area dA of that surface is called irradiance E.

$$E = \frac{d\Phi}{dA}. \quad (1)$$

The measurement of spectral irradiance (measured in W/m^2/nm) of a lamp is performed with a spectroradiometer. The basic spectroradiometer consists of a monochromator, combined with a detector on the exit slit and an integrating sphere (IS) on the entrance slit. The measured result has an uncertainty associated with it, calculated using the uncertainty budget (UB). In this paper, we highlight some of the contributors to the uncertainty budget (UB) including the stability, orientation, and translation of the lamp.

2. Measurement method.

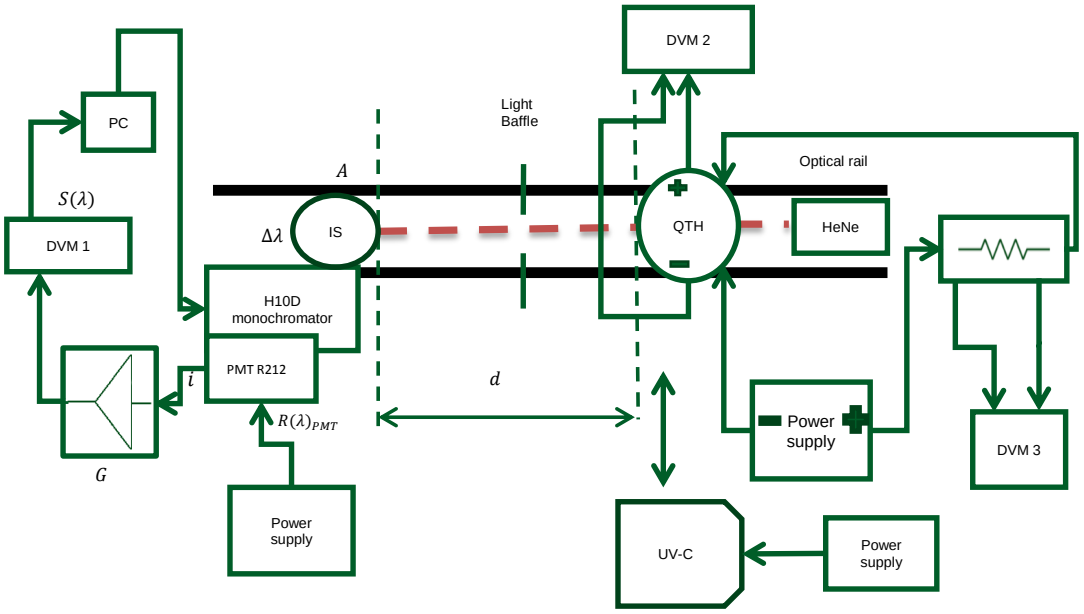

Figure 1: The measurement setup of the spectral irradiance lamp calibrations at NMISA. The setup makes use of a substitution method where one lamp is measured at a time.

The measurement setup in Figure 1 makes use of the substitution measurement method, which is a direct comparison with the value of a reference standard, having similar properties to the unit being measured (UUT) [4]. During an actual calibration, the spectral irradiance of a UUT (UV-C) is determined by a direct comparison with a calibrated spectral irradiance standard (QTH) lamp with known spectral irradiance using a spectroradiometer. During an actual calibration, the QTH standard lamp is measured at its respective position first and substituted with the UV-C lamp which is measured at a displacement position suitable for that calibration. The standard lamp is measured the second time to check repeatability. The measured voltage $S(\lambda)^{STD}$ is the measured spectral output voltage of the standard lamp and is modeled by

$$S(\lambda)^{STD} = E(\lambda)^{STD} R(\lambda) \Delta\lambda A. \quad (2)$$

Equation 2 can be explained as follows: $E(\lambda)^{STD}$ is the spectral irradiance emitted by a spectral irradiance standard lamp incident on the IS with an aperture area A, spectrally dispersed by a monochromator with a spectral bandwith $\Delta\lambda$ falling onto the photomultiplier tube (PMT) detector, and the spectroradiometer has spectral irradiance responsivity $R(\lambda)$ which is a combination of IS throughput $\rho(\lambda)$, diffraction efficiency of monochromator gratings $M(\lambda)$, PMT response $R(\lambda)_{PMT}$, and the gain G of the amplifier (which converts the current signal from the PMT into a voltage signal). Similarly the spectral output voltage of the UUT $S(\lambda)^{UUT}$ is modeled by:

$$S(\lambda)^{UUT} = E(\lambda)^{UUT} R(\lambda)\, \Delta\lambda\, A. \quad (3)$$

where $R(\lambda)$, $\Delta\lambda$, and A remain the same during calibration since $E(\lambda)^{STD}$, $S(\lambda)^{STD}$, and $S(\lambda)^{UUT}$ are known, the spectral irradiance $E(\lambda)^{UUT}$ of the UUT can be determined from equations 2 and 3 as:

$$E(\lambda)^{UUT} = \frac{S(\lambda)^{UUT}}{S(\lambda)^{STD}} E(\lambda)^{STD}. \quad (4)$$

Equation 4 is known as the measurement equation for spectral irradiance calibration.

The spectral irradiance of lamps is influenced by lamp stability, translation, and orientation. Each uncertainty contributor is evaluated using a model associated with it. The stability of lamps was monitored by two temperature controlled silicon (Si) photodiode at time *t*, and the following model was used:

$$E(\lambda) = \frac{\Phi(t)}{A} \quad (5).$$

$\Phi(t)$ is the flux incident on the area A of the Si photodiodes detector surfaces, and $E(\lambda)$ is the spectral irradiance emitted by the lamp. The uncertainties associated with translation of lamps were quantified using the inverse square law of point source model as:

$$E = \frac{I}{d^2}. \quad (6)$$

Where d is the distance from the lamp to the IS, I is the lamp intensity, and E is lamps irradiance. The inverse square law is valid only when the light source approximates a point source. A lamp approximates a point source if the distance to the lamp is at least five times greater than the largest dimension of the source [5]. The uncertainties in orientation of the lamps were quantified using $I = I_\theta cos\,\theta$ for a Lambertian distribution. θ is the angle between the optical axis and the direction of normal incidence for the spectroradiometer aperture. For a non Lambertian distribution, an alignment factor $(1-\gamma)$ is determined individually for each lamp, with γ determined from the small variations of the direction with respect to the burning position and the direction of emittance as the average of repeated alignments [6]

The spectral irradiance unit is derived from the high temperature blackbody (HTBB) radiator which employ's Plank's radiation law [7]. In the UV region, a 1000 W quartz tungsten halogen (QTH) and a 30 W deuterium lamps are generally used as standard lamps [8,9]. The QTH lamp is the most commonly used transfer standard for spectral irradiance in the wavelength region 250 nm to 2500 nm due to their good stability and ease of use [10]. The QTH lamp used here was calibrated at a specified distance (500 mm in our case) while operating at a current of approximately 8.000 A. The current was measured with a standard resistor and DVM 3 in Figure 1 using Ohm's law while the stability of the lamp was monitored by measuring the terminal voltage (normally 120 V) using DVM 2. The QTH lamp distance was realized with a rod cut and calibrated to this specific distance.

The UUT is a UV-C low pressure (LP) mercury (Hg) lamp. Between the lamps and the IS, baffles were used to minimize stray light. The IS in front of the monochromator is used to minimize the polarization of the light source by a complete depolarization of lamps and is coated internally with a reflective material ($BaSO_4$) that has a spatially uniform and uniformly diffuse reflectance [11], with the aim to combine radiant flux. The direct irradiation of the monochromator by lamps is avoided due to resultant variation in the irradiance distribution in the monochromator [2]. A double grating monochromator with a very low stray light level was used to disperse light, with a bandwidth of 4 nm. Before the start of measurements, the wavelength scale of the monochromator was confirmed to be within its calibrated uncertainty using known spectral lines from a mercury (Hg) pencil lamp.

The spectrally dispersed light was detected by the PMT detector with a spectral response from 185 nm – 650 nm, and a maximum response at 340 nm [12]. The PMT was powered by a high voltage of 700 V for all measurements in this paper. A helium neon (HeNe) laser is used to align the optical instruments (lamps, monochromator, and baffles) on the optical rail.

3. Results and discussions

The spectral output voltage stability of the QTH and the LP Hg lamps was measured with a spectroradiometer at 10 minutes interval after the lamps had been warmed-up. The low radiation output of the QTH lamp in the UV-C region, results in a low signal-to-noise ratio (SNR). As a result, the QTH lamp uncertainties were quantified in the visible region (441.5 nm and 450.5 nm) with the assumption that, the effect in orientation and translation on the output signal was the same at UV-C wavelengths. The LP Hg lamp however had a high output resulting in a significant signal around 251 nm to 255 nm as expected because of the Hg peak at 253.66 nm, and the uncertainties were quantified at 255 nm. The output stability of the two lamps was also monitored by two temperature stabilized UV-enhanced Si photodiodes at 10 minute intervals, for an independent indication of lamp stability and the results are tabulated in Table 1.

Table 1: The input electrical voltage (U) of the QTH lamp and the spectral output voltage (S) stability of both lamps.

Time [min]	t_1 (0 min)	t_2 (10 min)	t_3(20 min)	σ	U_{xi} [%]
QTH voltage (U) [V]	113.29	113.27	113.24	2.56E-02	0.02
QTH lamp current (J) [A]	8.00017	8.00022	8.00028	5.15E-05	0.001
Si -QTH (Φ) [A]	1.5174	1.5173	1.5171	8.99E-03	0.01
Si-LP Hg (Φ) [A]	0.0142	0.01419	0.01409	5.37E-01	0.5

The symbols used in Table 1 are defined as follows: t is the time in minutes at which measurements were taken, σ is the standard deviation of the measurements in Table 1, and U_{xi} is the relative uncertainties in percentage calculated by dividing the σ with the average of t_1, t_2 and t_3. U is the QTH lamp voltage measured in volts directly at DVM 2 in Figure 1 simultaneously with the QTH lamp current J measured in amperes as calculated from the voltage across DVM 3 and the standard resistor. Si-(Φ) is the output signal of the lamps monitored with the Si photodiodes detectors.

The input electrical voltage stability of the QTH lamp was measured using a four wire technique directly from DVM 2 (Figure 1) at 10 minute intervals simultaneously with the lamp time stability (measured with the spectroradiometer) and the lamp output monitored with the Si photodiodes. The time stability of the QTH standard lamp had a calculated relative uncertainty of 0.5 % compared to 3 % of the LP Hg UV-C lamp. The measured input electrical voltage of the QTH standard lamp on average was 113.27 V compared to the calibration certificate value of 113.11±0.03 V. The +0.13 V observed drift from the certificate value was speculated to be due to temperature effects of the DVM 2. The monitored lamps output of the QTH standard and LP Hg UV-C lamps with the Si photodiodes on average showed that the QTH standard lamp was more stable with a relative uncertainty of 0.01 % compared to 0.5 % of the LP Hg UV-C lamp. The Si photodiodes detectors results agreed with the time stability results, where the QTH standard lamp was in both cases more stable than the LP Hg UV-C lamp as expected.

A point source approximation was tested for both lamps (Figures 2 and 3). As expected, in both wavelengths (441.5 nm and 450.5 nm), the QTH lamp closely approximated a point source except for positions closer than 500 mm (400 mm and 300 mm). Because of the large dimensions of the LP Hg lamp it deviated from the point source approximation. We used the inverse square law of point sources Equation 6 as our model to calculate the theoretical values in Figures 2 and 3. The effect of orientation (or rotation around vertical axis) was measured at the calibrated positions of the lamps. The QTH lamp is close to symmetric; therefore, theoretically, the orientation of the QTH lamp should not have significant effect on the output signal. The difference in spectral output voltage (expressed as a percentage) produced by the lamps when displaced by 1 mm from their calibrated positions is shown in Table 2.

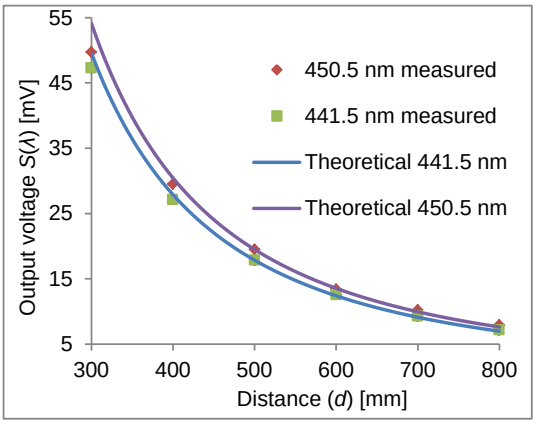

Figure 2: The point source approximation of the QTH lamp at 441.5 nm and 450.5 nm.

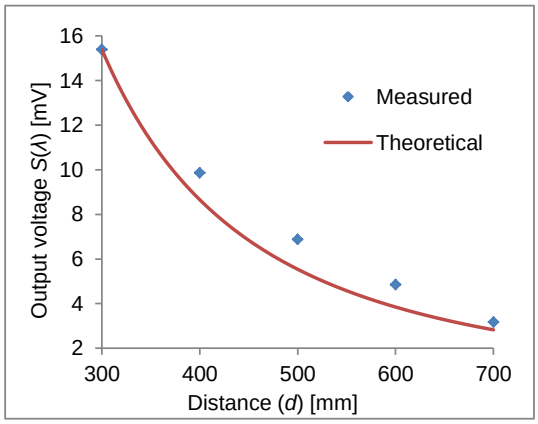

Figure 3: The point source approximation of the LP Hg lamp at 255 nm.

The 1 mm distance was chosen because with the setup at NMISA we are confident that we cannot make an error of more than 1 mm when positioning our lamps. Hence, only the effect in spectral output voltage generated by 1 mm (the worst case for each lamp) will be included in the UB. -1 mm, was when the lamps were moved closer to the spectroradiometer and +1 mm was further away from the spectroradiometer. The lamps were very sensitive to translation. For +1 mm displacement, the QTH lamp showed 0.1 % effect which was higher than 0.01 % for the LP Hg lamp

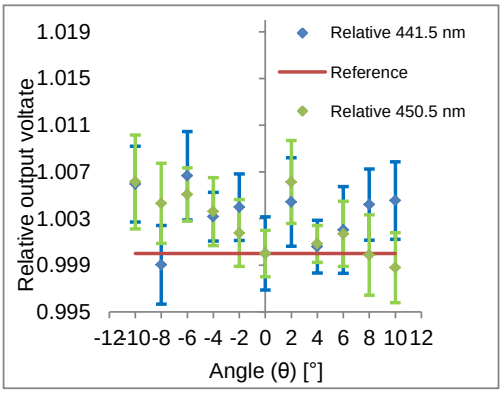

Figure 4: The orientation effect of the QTH lamp at 441.5 nm and 450.5 nm.

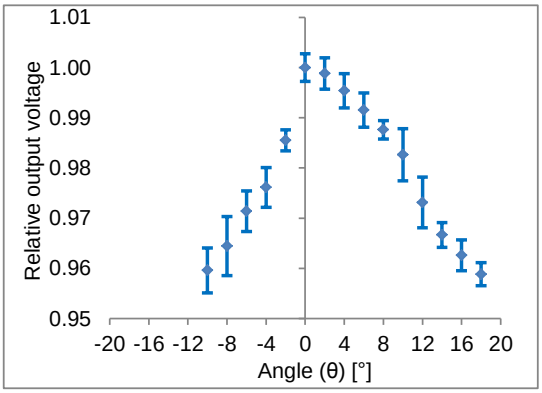

Figure 5: The angular dependence of the LP Hg lamp at 255 nm.

The LP Hg UV-C lamp had two lamp tubes mounted parallel to each other emitting light equally in all directions, but they are mounted in front of a reflector that reflects light towards the front of the lamp. Because of this, the LP Hg UV-C lamp was expected to have higher angular dependence than the QTH standard lamp. The effect of orientation of both lamps is shown graphically in Figures 4 and 5 and the calculated relative uncertainties are summarised in Table 3. As expected the QTH standard lamp had a smaller angular dependence compared to the LP Hg UV-C lamp. Furthermore, the LP Hg UV-C lamp showed an asymmetric distribution, probably due to misaligned lamp tubes or lower output from one of the lamp tubes. With the spectroradiometry setup at NMISA, we are confident that

the lamps orientation cannot be misaligned by more than 2 °, hence, only the relative uncertainties in the spectral output voltage caused by a 2 ° misalignment were included in the UB for both lamps.

Table 2: The translation effect of the QTH and LP Hg lamps.

Distance [mm]	QTH lamp 450.5 nm	LP Hg lamp 255 nm
+1	-0.07 %	-0.01 %
-1	0.9 %	0.8 %

Table 3: The orientation effect of the QTH and LP Hg lamps.

Position [°]	QTH lamp 450.5 nm	LP Hg lamp 255 nm
+2	0.4 %	-1.5 %
-2	0.6 %	-0.8 %

4. Conclusions and future work

The spectral irradiance measurement setup was characterized for translation, orientation and stability. The QTH lamp was more stable compared to the LP Hg UV-C lamp when monitored with Si photodiodes detectors. Also, the QTH lamp showed a long term drift from the lamp voltage with the lamp current very stable at 8.0002 A ± 0.0006 A. The effect of translation had a calculated relative uncertainty of 0.8 % for a 1 mm displacement from the calibrated positions for both lamps. For a 2 degrees misalignment from the optical axis, the QTH measured output signal changed by maximally 0.6 % while the LP Hg lamp changed by 1.5 %, which indicated an expected high angular dependence.

For future work, the deuterium lamp will also be characterized for translation, orientation, and stability. Due to its high spectral irradiance, the deuterium lamp is an ideal lamp to use as standard in the UV-C region. It will be investigated for use as a working standard or a primary standard. We will also test the systems temperature dependence with respect to the laboratory ambient conditions during measurements.

5. References

[1] Zalewski E F 1995 *Radiometry and Photometry Handbook of Optics* Vol **2** (Dunbury: Hughes Dunbury Optical Systems) pp 24-73
[2] CIE 1989 *International Lighting Vocabulary* (Vienna: Central Bureau of the Commission Internationale de l'Eclairage)
[3] Kowalski W 2010 *UVGI handbook: UVGI for air and surface disinfection* (New York: Springer Science & Business Media) pp 1-12
[4] Sauter G and Goodman T 2011 *Determination of measurement uncertainties in Photometry* SP1 1 (Vienna: Commission Internationale De L'Eclairage CIE Central Bureau) p 4
[5] Ryer A 1997 *The light measurement handbook* (Peabody: International Light Technologies) pp 26-7
[6] Schanda J (Ed) 2007 *Colorimetry:Understanding the CIE system* (New Jersey: John Wiley & Sons) pp 376-83
[7] Planck M 1901 On the law of distribution of energy in the normal spectrum *Annals of Physics* **4** p 553
[8] Woolliams E R, Fox N P, Cox M G, Harris P M and Harrison N J 2006 Final report on CCPR K1-a spectral irradiance from 250 nm to 2500 nm *Metrologia* **43** 1A 02003
[9] Sperfeld P 2008 Spectral irradiance 200 nm to 350 nm *Report of the CIPM key comparison CCPR-K1.b*
[10] Sanders C L and Rotter R 1984 *The Spectroradiometric Measurement of Light Sources* (Paris: Bureau central de la CIE) p 47
[11] Kostkowski H J 1997 *Reliable Spectroradiometry* (La Plata: Spectroradiometry Consulting) pp 247-9
[12] Photomultiplier Tube R212 TPMS1041E01 June 1998 Hamamatsu Photonics K K downloaded 11 March 2016 http://pdf.datasheetcatalog.com/datasheet/hamamatsu/R212.pdf

Characterization of a spectroradiometer system for ambient temperature dependence.

Author/Speaker: [*] [**]M. Mkabela

Co-authors: [*]P.J.W. du Toit, [*]R.H. Sieberhagen, [**]W.E. Meyer

[*]National Metrology Institute of South Africa

Private Bag X34, Lynnwood Ridge, 0040, South Africa

[**]University of Pretoria

Private Bag X20, Hatfield, 0028, South Africa

e-mail: mmkabela@nmisa.org

Abstract

Changes in ambient conditions, especially temperature, influence the measured output of a spectroradiometer system. At the National Metrology Institute of South Africa (NMISA), a spectroradiometer system is used for the calibration of clients' lamps and detectors. This work investigates the spectroradiometer system's measured output dependence on temperature in the UV-C spectral region. The Photometry and Radiometry laboratory at NMISA performs measurements within a (24 ± 2) °C temperature region. However, when the laboratory temperature falls outside this region it becomes necessary to correct the measured output using determined temperature coefficients. The spectroradiometer system had a calculated temperature coefficient of $-2{,}7$ %/°C for a linear temperature dependence with a coefficient of determination $R^2 = 0{,}97$.

1. Introduction

A basic spectroradiometer consists of a monochromator coupled with an integrating sphere (IS) mounted at the entrance slit and a detector at the exit slit [1]. At NMISA, a spectroradiometer is used as a transfer system in the calibration of lamps for the spectral irradiance unit measured in W/m². In the ultraviolet (UV) spectral region, 1000 W quartz tungsten halogen (QTH) lamps and 30 W deuterium (D2) lamps are used as secondary standards for spectral irradiance [2, 3]. In the UV-C spectral region (200 nm – 280 nm [4]), a low pressure (LP) mercury (Hg) lamp is used as a working standard for calibrating clients' instruments. Radiation emitted by LP Hg lamps is important in a number of applications, e.g. health care. The scope of this study is limited to radiation in the UV-C spectral region, which finds a special application in the field of air disinfection. The spectral distribution of lamps in the UV-C region used at NMISA is shown in Figure 1.

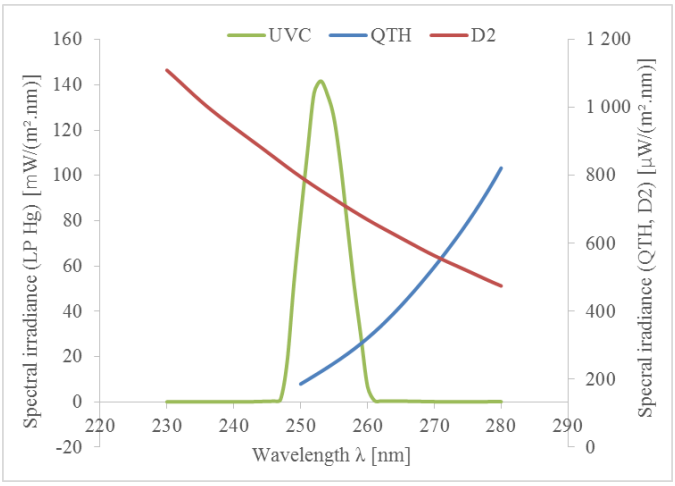

Figure 1. The spectral distributions of the QTH, D2 standards and LP Hg lamps are plotted using their spectral irradiance values [5].

Temperature changes in the laboratory during measurements of spectral irradiance may influence the measured results. Components of the spectroradiometer such as detectors and current amplifiers are susceptible to changes in ambient conditions. Any deviation from the nominal value of ambient temperature can to a first order be corrected by a linear correction function with a relative temperature coefficient [6]. A temperature coefficient α_x expresses a relation between a change in a measured output (say "Δx") and a change in ambient temperature ΔT ($\Delta T = T_2 - T_1$). The temperature coefficient is calculated from

$$\alpha_x = \frac{\Delta x}{\Delta T} \times 100 \qquad (1)$$

where

$$\Delta x = \frac{2(x_2 - x_1)}{(x_1 + x_2)}$$

is the relative change in x at temperature T_1 and T_2. For a linear temperature dependence, the linear model

$$x' = x \times (1 + \alpha_x \times \Delta T) \quad (2)$$

corrects x to obtain a value x' for a determined temperature coefficient. The associated relative measurement uncertainty of the temperature coefficient is given by

$$u^2(\alpha_{x,rel}) = \left(\frac{2x_1x_2}{x_1^2 - x_2^2}\right)^2 \left(u_{rel}^2(x_1) + u_{rel}^2(x_2)\right) + \frac{u^2(T_1) + u^2(T_2)}{(T_1 - T_2)^2} \quad (3)$$

In this study, the output measured by the system was investigated for dependence on temperature. The radiometry laboratory at NMISA performs spectral irradiance measurements in the temperature region (24 ± 2) °C. Since the laboratory ambient conditions are controlled, it is rare that the temperature changes by more than ± 5 °C during measurements. For this reason, the temperature coefficients were determined over a range (23 ± 4) °C in 2 °C steps.

2. Measurement setup

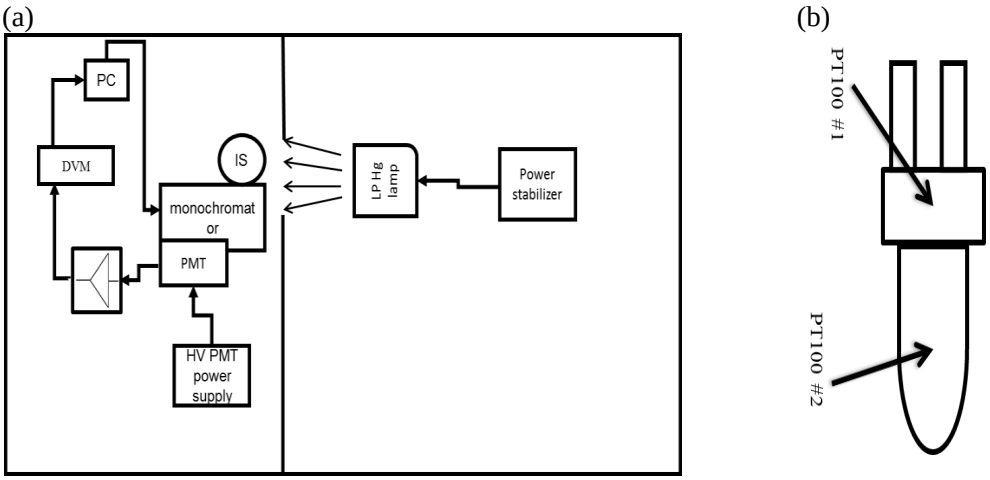

Figure 2. (a) The measurement system and lamps dependence on temperature was investigated using the setup. (b) The PT100 probes were mounted on the photomultiplier tube (PMT) detector surface to measure its temperature.

A schematic of the temperature dependence measurement setup used is shown in Figure 2.a. The whole system was placed in the room-air conditioned. The output of the measurement setup is the spectral output voltage $S(\lambda)$ measured as follows;

- The radiant flux emitted by the lamps is incident on the IS which combines and diffuses radiant flux.
- The diffused radiant flux enters the double monochromator through the entrance slit and is dispersed by the diffraction gratings.
- The dispersed radiant flux is then converted to electrical signal (photocurrent) by the PMT detector.
- The photocurrent is then converted to $S(\lambda)$ by the set gain of the amplifier. $S(\lambda)$ is measured via the digital voltmeter (DVM) which is controlled by the computer (PC). The PC has software used to control the stepper motor drive to set the positions of the gratings and to record $S(\lambda)$.

The lamp used in this experiment was a LP Hg lamp. The light output of the LP Hg lamp was monitored with a temperature-stabilized UV-enhanced Si (UV-E-Si) detector [7]. Since the UV-E-Si detector is temperature stabilized, any temperature changes in the laboratory should have negligible effect on the detector.

A double grating monochromator with a monochromator bandwidth set to 8 nm was used for all the measurements. A PMT detector was mounted at the exit slit at a 1000 V supply voltage. This ensured sufficiently high signal to noise [5]. In the UV-C region, this PMT detector has a spectral response increasing from 2,5 mA/W at 200 nm to approximately 50 mA/W at 280 nm [8]. The measurements were performed at 254 nm wavelength where $S(\lambda)$ is at its maximum (Figure 1).

The temperature of the laboratory was controlled by an air conditioner, and was allowed to stabilize overnight at each room temperature setting before measurements were performed. Two sets of measurements were performed at each air-conditioner temperature setting, approximately two hours apart to measure the short term drift. The LP Hg lamp was left switched-on between the sets because the lamp takes relatively long to warm-up. The ambient temperature was monitored with a calibrated platinum resistance thermometer (PT100)#3 probe mounted next to the monochromator to isolate it from direct air flow of the air conditioner. The temperature of the PMT detector was monitored by two calibrated PT100 probes as shown in Figure 2.b. PT100#1 measured the temperature at the base of the PMT and PT100#2 measured the temperature of its aluminium housing.

The PMT is more susceptible to ambient temperature than ordinary electronic components. Therefore, the PMT must be left for an hour or longer until the photomultiplier tube reaches the ambient temperature and its characteristics become stable. The temperature characteristics for PMT cathode sensitivity are dependent on wavelength. The temperature coefficient of cathode sensitivity varies significantly from a negative value to a positive value near the long wavelength cut-off [9]. For the photocathode material; antimony-caesium (Sb-Cs), the temperature coefficient varies from $-0{,}56$ %/°C at 200 nm to $+0{,}6$ %/°C at 650 nm.

A small amount of current; the anode dark current, flows in a photomultiplier tube detector even when it is operated in a completely dark state. The dark current greatly depends on the supply voltage. This makes it more susceptible to thermionic emissions of electrons

even at room temperatures because of the very low work functions of photocathode materials [10]. Cooling the PMT photocathode material is more effective in reducing thermionic emissions.

3. Results and discussion

Table 1. The monitored temperature readings at various laboratory locations for different room temperature settings.

Room temperature setting	**PT100#1**	**PT100#2**	**PT100#3**
[°C]	**[°C]**	**[°C]**	**[°C]**
19	22,9	21,8	21,3
21	23,8	22,7	22,1
23	24,7	23,6	23,6
25	26,4	25,7	25,6
27	27,0	26,1	25,6

The PT100#1 probe measured higher PMT detector surface temperatures than PT100#2 probe (Table 1). This was because PT100#1 probe was mounted on the warmer side (socket) of the PMT. The socket generates more electrical heat than the PMT inside the aluminium housing. The deviation of the ambient temperature measured with the PT1003# was 0 °C for a resolution of 0,1 °C. This was because the PT100#3 was isolated from the air flow of the air conditioner.

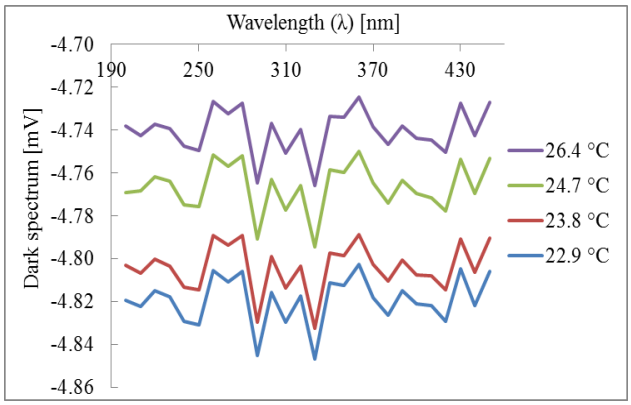

Figure 3. The measured $S(\lambda)_{dark}$ dependence on temperature.

Figure 3 shows the dependence of the measured dark spectrum $S(\lambda)_{dark}$ on temperature. The dark current of the PMT strongly depends on the photocathode type and ambient temperature. According to [9], PMT detector dark counts have a positive linear dependence on temperature. In Figure 3 it is shown that $S(\lambda)_{dark}$ was indeed higher when operated at higher temperatures. It also shows that the dark current is wavelength dependent.

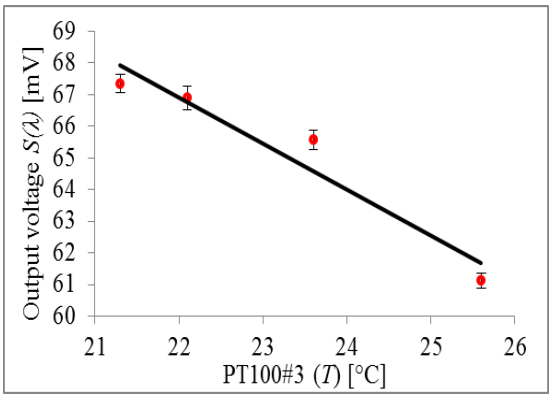

Figure 4. The measurement system apparent dependence on temperature when illuminated with the LP Hg lamp measured at 254 nm monochromator wavelength setting. The linear dependence had the linear equation: $S(\lambda) = -1{,}45\left(\frac{\text{mV}}{\text{°C}}\right) \cdot T + 99$ mV, and the coefficient of determination $R^2 = 0{,}93$. Temperature T was measured in °C.

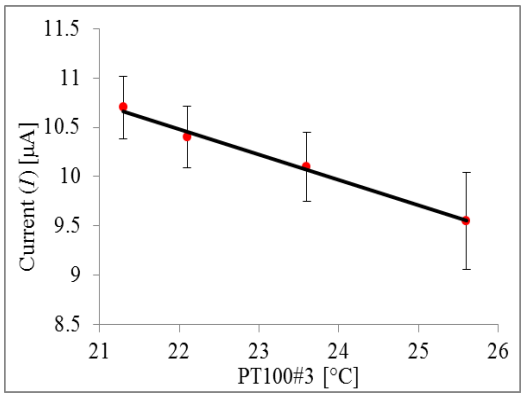

Figure 5. The current output (monitored with the UV-E-Si detector) of the LP Hg lamp dependence on ambient temperature. The linear equation was $I = -0{,}259(\frac{\mu\text{A}}{\text{°C}}) \cdot T + 16\ \mu$A with $R^2 = 0{,}99$. T was measured in °C.

The spectroradiometer seemed to have a negative linear temperature dependence as shown in Figure 4. The lamp light output was simultaneously monitored with the UV-E Si detector, and the results are shown in Figure 5. The results suggested that the lamp itself had a negative temperature dependence. Because the order of measurements were from low to high, the lamp output dependence on temperature was suspected to be caused by either one of two reasons: either the lamp output was lower at higher temperatures or was rapidly decreasing with usage time.

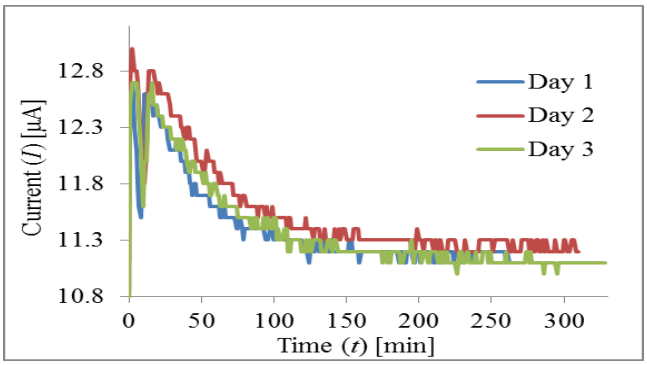

Figure 6. The reproducibility of the LP Hg lamp monitored with the UV-E-Si detector at 23 °C room temperature setting.

Further measurements at the same room temperature (Figure 6) showed that the LP Hg lamp did not decrease rapidly with usage time. This showed that the LP Hg lamp itself is sensitive to temperature changes; therefore the assumed spectroradiometer dependence is in part a lamp temperature dependence. When the lamp is started, the ballast provides high initial voltage to create the starting arc to provide proper lamp current [11]. This causes the lamp light output to first increase before it gradually drops and stabilizes as shown in Figure 6. Figure 7 shows the measurement system dependence on temperature without the lamp. The output voltages were calculated using Equation 2; where α_x were the temperature coefficients of the lamp and x, the output voltages in Figure 4. The measurement system was not sensitive to temperature compared to the measured output voltages in Figure 4 and the lamp output current in Figure 5.

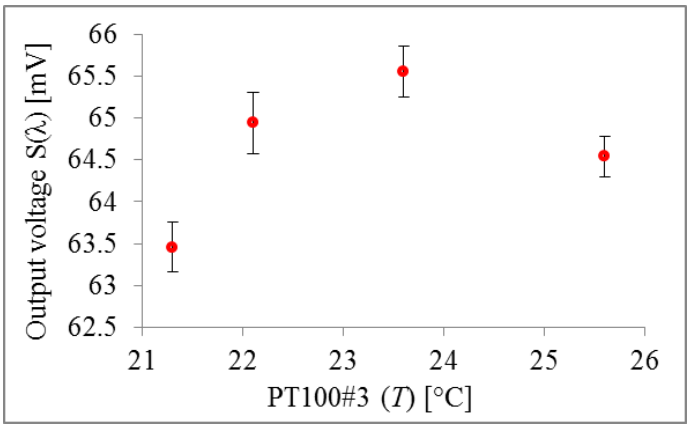

Figure 7. The temperature dependence of the measurement system without the lamp.

The calculated temperature coefficients (using Equation 1) and their uncertainties are given in Table 2. The uncertainties were calculated using Equation 3. The results showed that the temperature coefficients of the MS with the lamp were temperature dependent; decrease with increasing temperature. Since the lamp has a linear temperature dependence; Equation 2 can be used to correct $S(\lambda)$ measured outside (24 $\pm$ 2) °C temperature region using the lamp's temperature coefficients.

PT100#3 temperature	**Temperature coefficient**	
	MS + lamp	**Lamp**
[°C]	**[%/°C]**	**[%/°C]**
21,3	$-1{,}2 \pm 0{,}08$	$-2{,}5 \pm 0{,}004$
22,1	$-1{,}4 \pm 0{,}2$	$-2{,}0 \pm 0{,}01$
25,6	$-3{,}5 \pm 0{,}04$	$-2{,}4 \pm 0{,}007$

$\alpha_{S(\lambda)}$ in Table 2 taken as an average were compared to literature values given in Table 3. The large differences between the experimental and literature values could be due to the fact that literature values were determined for larger temperature differences using different techniques. The literature temperature coefficients were those of the PMTs not the measurement system or the mercury lamp. The PMT temperature coefficients were determined as an average; from +20 °C to +40 °C [13] and from −10 °C to +40 °C as an average of 23 standard PMTs [12]. The standard temperature coefficient of the PMT detector used for this experiment is approximately −0,6 %/°C in the UV-C region [9].

Table 2. The literature PMT detector temperature coefficients.

Wavelength	**Literature α**
[nm]	**[%/°C]**
200-300	−0,6 [9]
320-400	−0,7 [12]
400-800	−0,2 [13]

4. Conclusion

This study has investigated the effect of temperature on the measured spectral output voltage. When illuminated with the LP Hg lamp, the measured spectral output voltage $S(\lambda)$ had a linear dependence on temperature. The study also found that the LP Hg lamp light output was relatively higher when operated at lower temperatures. At lower temperatures, the PMT dark current is also reduced. The measurement system alone was not too sensitive to temperature compared to the lamp. For future work, the study will investigate the temperature dependence of current amplifiers.

5. References

1. H. J. Kotowski, Reliable Spectroradiometry, Spectroradiometry Consulting, La Plata, Maryland, USA, 1997.C.L.
2. E.R. Woolliams, et al, "Final report on CCPR k1-a: spectral irradiance from 250 nm to 2500 nm, Metrologia, **43**(1A), 2006.
3. P. Sperfeld, "spectral irradiance from 200 nm to 350 nm. Report of the CIPM key comparison CCPR-k1.b, 2008.
4. CIE, Ultraviolet disinfection, Publication NO:155, Commission Internationale De L'Eclairage CIE Central Bureau Kegelgasse 27 A-1030, Vienna, Austria, 2003.
5. M. Mkabela, 2018, "The development of a measuring technique for the UV-C distribution emitted from low pressure mercury lamps", Master of Science in Physics, University of Pretoria, Pretoria, South Africa [in progress].
6. CIE, Determination of measurement uncertainties in Photometry, 2011, CIE 198 SP1.1, CIE central Bureau, Kegelgassa 27, A-1030 Vienna, Austria.
7. Gooch & Housego, Enabling Photonic Technologies, Detector standards [online] Available: http://www.ghinstruments.com/products/detector-standards/ol-730-5a-and-ol-730-5c-uv-enhanced-silicon-detectors/ [2018, June 19].
8. Photomultiplier Tube R212 TPMS104E01 [online] Available: http://pdf.datasheetcatalog.com/datasheet/hamamatsu/R212.pdf, [2016, March 11].
9. Tubes, Photomultiplier Basics and applications, Hamamatsu photonics KK, Iwata city, 438–0193, 2006.
10. Photomultiplier tubes, Construction and Operating Characteristics Connections to External Circuits, [online] Available: http://sites.fas.harvard.edu/~phys191r/Bench_Notes/B4/PMT_prop.pdf, [2018, August 5].
11. K. Wladyslaw, Ultraviolet germicidal irradiation handbook: UVGI for air and surface disinfection. Springer Science & Business Media, 2010.
12. Ogio et al, "Temperature characteristics of PMTs and calibration of light sources of the telescope array influence detectors". In:31st International cosmic ray conference, Iodz, Poland, 2009.
13. A.S. Singh, and K.P. Wright, "The determination of photomultiplier temperature coefficients gain and spectral sensitivity using photon counting technique", IEEE transactions on nuclear science, **34**(1), 434-437, 1987.

References

Ashdown, Ian, & Eng, P. 2002. Photometry and radiometry. *President by heart consultants limited*.

BIPM, IEC, IFCC, ILAC, IUPAC, IUPAP, & ISO, OIML. 2008. Evaluation of measurement data—guide for the expression of uncertainty in measurement. jcgm 100: 2008. *Citado en las*, **167**.

BIPM, ISO, IEC IFCC ILAC IUPAC IUPAP, & OIML. 2008. International vocabulary of metrology - basic and general concepts and associated terms (vim). *jcgm 200:2012 (e/f)*, **2004**, 09–14.

Birch, KP, & Downs, MJ. 1993. An updated edlén equation for the refractive index of air. *Metrologia*, **30**(3), 155.

Birch, KP, & Downs, MJ. 1994. Correction to the updated edlén equation for the refractive index of air. *Metrologia*, **31**(4), 315.

Bridges, John M, & Ott, William R. 1977. Vacuum ultraviolet radiometry. 3: The argon mini-arc as a new secondary standard of spectral radiance. *Applied optics*, **16**(2), 367–376.

CDC. 1994. Centers for disease control and prevention: Guidelines for preventing the transmission of mycobacterium tuberculosis in health-care facilities. *Mmwr*, **43**(13), 1–132.

Ciddor, Philip E. 1996. Refractive index of air: new equations for the visible and near infrared. *Applied optics*, **35**(9), 1566–1573.

CIE. 1984. *The spectroradiometric measurement of light sources*. Publication N:0 63, Bureau Central De La CIE 52, Boulevard Malesherbes 75008 Paris - France.

CIE. 2003. *Ultraviolet air disinfection*. Publication No:155, COMMISSION INTERNATIONALE DE L'ECLAIRAGE CIE Central Bureau, Kegelgasse 27, A-1030 Vienna, Austria.

Czichos, Horst. 2011. Introduction to metrology and testing. *Pages 3–22 of: Springer handbook of metrology and testing*. Springer.

Duda, C Richard. 1983. Radiometric and photometric concepts based on measurement techniques. *Pages 102–111 of: Applications of optical metrology: Techniques and measurements ii*, vol. 416. International Society for Optics and Photonics.

Edlén, Bengt. 1966. The refractive index of air. *Metrologia*, **2**(2), 71.

Gardner, James L. 2003. Uncertainties in interpolated spectral data. *Journal of research of the national institute of standards and technology*, **108**(1), 69.

Gentile, Thomas R, Houston, Jeanne M, Hardis, Jonathan E, Cromer, CL, & Parr, Albert C. 1996. National institute of standards and technology high-accuracy cryogenic radiometer. *Applied optics*, **35**(7), 1056–1068.

Giacchetti, A, Stanley, RW, & Zalubas, R. 1970. Proposed secondary-standard wavelengths in the spectrum of thorium. *Josa*, **60**(4), 474–489.

Grum, F, & Becherer, Richard J. 1979. *Optical radiation measurements. volume 1-radiometry*. Vol. 1. Academic Press.

Grum, F, & Luckey, GW. 1968. Optical sphere paint and a working standard of reflectance. *Applied optics*, **7**(11), 2289–2294.

Hamamatsu, Photonics. 1998a. Photomultiplier Tube R212 TPMS1041E01 [Online]. Available: http://pdf.datasheetcatalog.com/datasheet/hamamatsu/R212.pdf [2016, March 11].

Hamamatsu, Photonics. 1998b. *Photomultiplier tubes: Construction and operating characteristics connections to external circuits*.

Hamamatsu, Photonics. 2006. Photomultiplier tubes basics and applications, 3rd edition. *Hamamatsu photonics k.k., iwata city*, 438.

Harm, Walter. 1980. *Biological effects of ultraviolet radiation*. Vol. 12. University Press, Cambridge.

Housego, Gooch &. 2018. Gooch and Housego: Enabling Photonic Technologies, Detector standards. [online]. Available: https://www.ghinstruments.com/products/detector-standards/ol-730-5a-and-ol-730-5c-uv-enhanced-silicon-detectors/ [2018, June 19].

Howarth, Preben, Redgrave, Fiona, Germany, PTB, Madsen, Søren, & Grafisk, Schultz. 2008. “metrology–in short” 3rd edition. *Euramet project*, **1011**.

Instruments, Oriel. 2015. Oriel Amplified Detectors [Online]. Available: https://www.newport.com/medias/sys_master/images/images/h65/h9c/8797226696734/Oriel-Amplified-Detectors-User-Manual.pdf [2018, June 19].

Keppy, Nicole K, & Allen, Michael. 2008. Understanding spectral bandwidth and resolution in the regulated laboratory. *Thermo fisher scientific technical note*, **51721**.

Klose, Jules Z, Bridges, John Mervin, & Ott, William R. 1987. *Radiometric standards in the vacuum ultraviolet*. Vol. 250. US Department of Commerce, National Bureau of Standards.

Kostkowski, Henry J. 1997. *Reliable spectroradiometry*. Spectroradiometry Consulting.

Kowalski, Wladyslaw. 2010. *Ultraviolet germicidal irradiation handbook: Uvgi for air and surface disinfection*. Springer Science & Business Media.

Kramida, A, Ralchenko, Yu, Reader, J., & and NIST ASD Team. 2018. NIST Atomic Spectra Database (ver. 5.5.6), [Online]. Available: `https://physics.nist.gov/asd` [2018, May 29]. National Institute of Standards and Technology, Gaithersburg, MD.

Meggers, WF, & Peters, CG. 1919. Measurements on the index of refraction of air for wave-lengths from 2218 a to 9000 a. *The astrophysical journal*, **50**, 56–71.

Meggers, William F, Corliss, Charles H, & Scribner, Bourdon F. 1961. Tables of spectral-line intensities. *Nbs monograph, washington: Us dept. of commerce, national bureau of standards,| c1961*.

Metzdorf, J, Raatz, KH, & Kaase, H. 1987. Broadband-filter detector for measuring blackbody temperature. *Photonoic measurements (photon-detectors), international measurement confederation (imeko)*, **14**, 17.

Milton, M. 2014. The Importance of Metrology for Standards, Industry and Trade [Online]. Available: https://www.bipm.org/utils/common/pdf/talks/Milton-MJT-2014-09-APMP-Symposium.pdf [2018, January 15]. BIPM.

Morrison, Sean. 2013. Resolving power of diffraction gratings.

Ogio, Shoichi, Miyauchi, Hitoshi, Matsuyama, Toshio, Ikeda, Daisuke, & Tokuno, Hisao. 2009. Temperature characteristics of pmts and calibration light sources for the telescope array fluorescence detectors. *In: 31st international cosmic ray conference, łódź, poland*.

Palmer, Christopher A, & Loewen, Erwin G. 2005. *Diffraction grating handbook*. Newport Corporation New York.

Palmer, James M, & Carroll, Lewis. 1999. Radiometry and photometry faq. *Url: http://www. optics. arizona. edu/palmer/rpfag/rpfag. htm# motivation*.

Parr, Albert C. 2001. The candela and photometric and radiometric measurements. *Journal of research of the national institute of standards and technology*, **106**(1), 151.

Planck, Max. 1901. On the law of distribution of energy in the normal spectrum. *Annalen der physik*, **4**(553), 1.

Ryer, Alex. 1997. *Light measurement handbook*. International Light Technologies.

Sanas. 2016. Certificate of Calibration for NMISA Photometry and Radiometry Metrology: Facility Accreditation Number 1611 [Online]. Available: http://www.sanas.co.za/schedules/calibration/1611-0902018.pdf [2018, September 20].

Sansonetti, Craig J, Salit, Marc L, & Reader, Joseph. 1996. Wavelengths of spectral lines in mercury pencil lamps. *Applied optics*, **35**(1), 74–77.

Saunders, RD, Ott, WR, & Bridges, JM. 1978. Spectral irradiance standard for the ultraviolet: the deuterium lamp. *Applied optics*, **17**(4), 593–600.

Saunders, Robert D, & Ott, William R. 1976. Spectral irradiance measurements: effect of uv-produced fluorescence in integrating spheres. *Applied optics*, **15**(4), 827–828.

Schanda, János. 2007. *Colorimetry: understanding the cie system*. John Wiley & Sons.

Schwarzmaier, Thomas, Baumgartner, Andreas, Gege, Peter, & Lenhard, Karim. 2013. Calibration of a monochromator using a lambdameter. *Page 888910 of: Sensors, systems, and next-generation satellites xvii*, vol. 8889. International Society for Optics and Photonics.

Singh, AS, & Wright, AG. 1987. The determination of photomultiplier temperature coefficients for gain and spectral sensitivity using the photon counting technique. *Ieee transactions on nuclear science*, **34**(1), 434–437.

Sperfeld, P, Stock, KD, Raatz, KH, Nawo, B, & Metzdorf, Jürgen. 2003. Characterization and use of deuterium lamps as transfer standards of spectral irradiance. *Metrologia*, **40**(1), S111.

Sperfeld, P, Pape, S, & Nevas, S. 2013. The spectral irradiance traceability chain at ptb. *Pages 801–804 of: Aip conference proceedings*, vol. 1531. AIP.

Sperfeld, Peter. 2008a. Final report on the cipm key comparison ccpr-k1. b: Spectral irradiance 200 nm to 350 nm. *Metrologia*, **45**(1A), 02002.

Sperfeld, Peter. 2008b. Spectral irradiance 200 nm to 350 nm. *Report of the cipm key comparison ccpr-k1. b*.

Stone Jr, Jack A, & Zimmerman, Jay H. 2001. *Index of refraction of air*. Tech. rept.

Taylor, Alma EF, *et al.* 2000. *Illumination fundamentals*. Lighting Research Center.

Walker, James H, Saunders, Robert D, Jackson, John K, & McSparren, Donald A. 1987. *Spectral irradiance calibrations*. Vol. 250. US Department of Commerce, National Bureau of Standards.

Webb, Robert B, & Tuveson, RW. 1982. Differential sensitivity to inactivation of nur and nur+ strains of escherichia coli at six selected wavelengths in the uva, uvb and uvc ranges. *Photochemistry and photobiology*, **36**(5), 525–530.

Weidner, Victor R, & Hsia, Jack J. 1981. Reflection properties of pressed polytetrafluoroethylene powder. *Josa*, **71**(7), 856–861.

Woolliams, Emma R, Fox, Nigel P, Cox, Maurice G, Harris, Peter M, & Harrison, Neil J. 2006. Final report on ccpr k1-a: spectral irradiance from 250 nm to 2500 nm. *Metrologia*, **43**(1A), 02003.

Zaidel', AN, Prokof'ev, VK, Raiskii, SM, Slavnyi, VA, & Shreider, E Ya. 1970. Tables of spectral lines. *Ifi plenum*.

Zalewski, Edward F. 1995. Radiometry and photometry. *Handbook of optics*, **2**, 24–1.